

**The selective oxidation of methane and propene  
over  $\alpha\text{-Bi}_2\text{Mo}_3\text{O}_{12}$**

By

**Jacobus Nel**

Thesis submitted in partial fulfilment  
of the requirements for the degree



**MASTER OF SCIENCE IN ENGINEERING  
(CHEMICAL ENGINEERING)**

in the Department of Process Engineering  
at the University of Stellenbosch

Supervisor

**Dr Linda Callanan**

**Stellenbosch**

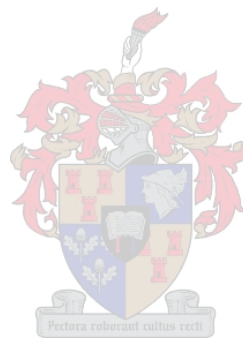
**March 2007**

# Declaration

I, the undersigned, hereby declare that the work contained in this thesis is my own original work and that I have not previously in its entirety or in part submitted it at any university for a degree.

Signature:.....

Date:.....



*Copyright©2006 Stellenbosch University*

*All rights reserved*

## Abstract

The catalytic selective oxidation of hydrocarbon molecules is the process where a selectively oxidized intermediate molecule is formed instead of the thermodynamically favoured total oxidation products, in the presence of a suitable catalyst. Examples are the selective oxidation of methane to synthesis gas at moderate temperatures, for which a catalyst is still needed and the selective oxidation of propene to acrolein over  $\alpha\text{-Bi}_2\text{Mo}_3\text{O}_{12}$ . The selective oxidation of propene over  $\alpha\text{-Bi}_2\text{Mo}_3\text{O}_{12}$  occurs via a Mars-van Krevelen mechanism where the bulk oxygen in the catalyst is inserted into the propene molecule and leaves as part of the product, while being replaced with gaseous oxygen.

From an economic perspective there is a need to produce synthesis gas from methane at low temperatures. It was seen in the literature that  $\alpha\text{-Bi}_2\text{Mo}_3\text{O}_{12}$  is a mixed metal oxide that might be capable of achieving this. The feasibility of the selective oxidation of methane to synthesis gas with  $\alpha\text{-Bi}_2\text{Mo}_3\text{O}_{12}$  was therefore investigated. However, it was found that the selective oxidation of methane over  $\alpha\text{-Bi}_2\text{Mo}_3\text{O}_{12}$  is not feasible at moderate temperatures. To circumvent the problem of producing synthesis gas at low temperatures a membrane reactor was suggested that might be able to produce synthesis gas at moderate temperatures with conventional selective methane oxidation catalysts that thermodynamically favours carbon dioxide formation at low temperatures.

No time on-stream experiments had been done previously for the selective oxidation of propene to acrolein over  $\alpha\text{-Bi}_2\text{Mo}_3\text{O}_{12}$  and several issues regarding the reoxidation of the catalyst still need to be resolved. These issues included details regarding the reoxidation process (electron transfer diagrams), the mechanism of how non-selective oxidation products form and what the reoxidation rate limiting step is during the reoxidation of the catalyst in the low temperature region.

Time on-stream experiments showed that the catalyst stayed active for at least six hours without a change in product selectivity. This indicated that the surface oxidation state of  $\alpha\text{-Bi}_2\text{Mo}_3\text{O}_{12}$  stayed the same during this period of time, which further indicated that the amount of nucleophilic and electrophilic oxygen species on the surface remained constant over the time period.

Different model equations were derived to determine the rate limiting step during the reoxidation rate limiting region (<375°C). It was found that the most likely rate limiting step at 325°C was bulk oxygen diffusion, but it could not be determined if a single or a dual site oxygen insertion was most likely to occur. At 350°C it was determined that oxygen coordination and first electron transfer to the oxygen molecule is the most likely rate limiting step, while evidence indicated that the reaction was already reduction rate limiting at 375°C. It was concluded that reaction kinetics may not be the best method to determine the definite reaction mechanism, but it can give an indication of the most likely reaction mechanism.

For the selective oxidation of propene to acrolein over  $\alpha$ -Bi<sub>2</sub>Mo<sub>3</sub>O<sub>12</sub> it is recommended that higher propene conversions are investigated. These higher conversions can be used to study the kinetics of the non-selective oxidation products. It is also recommended that spectroscopy studies are done to determine the exact species that are present during the reoxidation of the catalyst. It is further recommended that isotopic labelling and/or spectroscopic methods are used to study the reoxidation process of the selective oxidation of propene to acrolein over  $\alpha$ -Bi<sub>2</sub>Mo<sub>3</sub>O<sub>12</sub> instead of reaction kinetics.



## Opsomming

Die katalitiese selektiewe oksidasie van 'n organiese molekule is die proses waar 'n selektiewe tussen geoksideerde molekule gevorm word in plaas van die totale oksidasie produkte oor 'n geskikte katalis. Voorbeelde is die selektiewe oksidasie van metaan na sintese gas by middelmatige temperature waarvoor 'n geskikte katalis nog gevind moet word en die selektiewe oksidasie van propaan na akroliën oor  $\alpha\text{-Bi}_2\text{Mo}_3\text{O}_{12}$ . Die selektiewe oksidasie van propaan oor  $\alpha\text{-Bi}_2\text{Mo}_3\text{O}_{12}$  geskied met 'n Mars-van Krevelen meganisme waar die struktuur suurstof van die katalis in die propaan molekule gesit word en as deel van die produk die reaktor verlaat, terwyl die struktuur suurstof vervang word met suurstof van die gasfase.

Vanaf 'n ekonomiese perspektief is daar 'n behoefte om sintese gas te produseer van metaan teen lae temperature. Dit is in die literatuur gesien dat  $\alpha\text{-Bi}_2\text{Mo}_3\text{O}_{12}$  moontlik 'n geskikte katalis vir die reaksie is. Daarom is die geskiktheid van  $\alpha\text{-Bi}_2\text{Mo}_3\text{O}_{12}$  as 'n katalis vir die selektiewe oksidasie van metaan na sintese gas geondersoek in hierdie studie. Gedurende die eksperimente was dit egter bevind dat die selektiewe oksidasie van metaan oor  $\alpha\text{-Bi}_2\text{Mo}_3\text{O}_{12}$  nie lewensvatbaar by middelmatige temperature is nie. Om die probleem op te los om sintese gas by lae temperature te vorm is 'n Membraan reaktor voorgestel wat moontlik sintese gas by middelmatige temperature kan produseer met 'n konvensionele metaan selektiewe oksidasie katalis, wat totale oksidasie by lae temperature termodinamies bevoordeel.

Geen tyd aan-lyn eksperimente was al voorheen gedoen vir die selektiewe oksidasie van propaan na akroliën oor  $\alpha\text{-Bi}_2\text{Mo}_3\text{O}_{12}$  nie en 'n paar sake aangaande die reoksidasië van die katalis was nog onbeantwoord. Hierdie sake sluit in die besonderhede van die reoksidasië proses (elektron oordrag diagram), die meganisme hoe nie-selektiewe oksidasie produkte vorm en wat die reoksidasië reaksie snelheid beheerende stap is, in die lae temperatuur gebied.

Die tyd aan-lyn eksperimente het gewys dat die katalis aktief bly vir ten minste ses ure sonder verlies in produk selektiwiteit. Dit het aangedui dat die oppervlak oksidasie toestand van  $\alpha\text{-Bi}_2\text{Mo}_3\text{O}_{12}$  dieselfde gebly het oor hierdie tydperk, wat verder aangedui het dat die aantal nukleofiliese en elektrofiliese suurstof spesies dieselfde gebly het.

Verskillende model vergelykings is afgelei om die reaksie snelheid beperkende stap gedurende die reoksidasië beperkende gebied (<375°C) te bepaal. Dit is bevind dat die mees waarskynlike reaksie snelheid beperkende stap by 325°C die suurstof diffusie in die katalis kristal struktuur was, maar dit kon nie bepaal word of die suurstof met 'n enkel of 'n dubbel suurstof oop ruimte ingevoeg word nie. By 350°C is dit bepaal dat suurstof koördinasië en eerste elektron oordrag na die suurstof molekule die mees waarskynlike reaksie beherende stap was, terwyl alle bewyse gedui het daarop dat die reaksie al reeds reduksie beherend was by 375°C. Die gevolgtrekking is ook gemaak dat reaksie kinetika moontlik nie die beste metode is om die definitiewe reaksie meganisme van 'n reaksie te bepaal nie, maar dit kan wel 'n aanduiding gee van die mees waarskynlike reaksie meganisme.

Vir die selektiewe oksidasië van propeen na akrolien oor  $\alpha\text{-Bi}_2\text{Mo}_3\text{O}_{12}$  word dit aanbeveel dat 'n hoër propeen omsetting ondersoek word. Hierdie hoër propeen omsettings kan gebruik word om die kinetika van die nie-selektiewe oksidasië produkte te ondersoek. Dit word ook aanbeveel dat isotoop merking en/of spektroskopiese studies gedoen word om die reoksidasië proses te ondersoek, in plaas van reaksie kinetika.



# Acknowledgments

The author would like to acknowledge the following people:

- Dr. Linda Callanan for guidance and insights into Heterogeneous Catalysis
- The workshop personnel: Mr. Anton Cordier, Mr. Howard Koopman, Mr. Jannie Barnard for helping with the modifications of the reactor rig
- Me. Julianna Steyl and Me. Fransien Kampfer for helping with the order of equipment
- Dr. Remy Buchner at iThemba labs for doing XRD analysis and Me. Hanneli Botha for doing the BET analysis
- The rest of the personnel at the Process Engineering Department at the University of Stellenbosch for technical support and the alleviation of administrative strain
- Personnel at UCT Catalytic Research Unit for courses in Catalysis and Analytic methods
- Mr. LJ du Preez for carrying out the differential reactor setup experiments
- Friends and family for moral support
- Marlé Janse van Rensburg



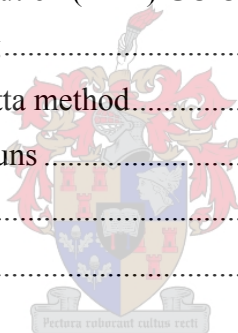
# Table of Content

Declaration .....	ii
Abstract .....	iii
Opsomming .....	v
Acknowledgments .....	vii
Table of Content .....	viii
Chapter 1 Introduction .....	1
Chapter 2 Literature Review .....	3
2.1 Selective Mixed Metal Oxide Oxidation Catalysts .....	3
2.1.1 Bismuth Molybdate .....	4
2.1.1.1 Different Phases of Bismuth Molybdate .....	4
2.1.1.2 $\alpha$ -Bismuth Molybdate Crystal Structure .....	5
2.1.1.3 General reaction mechanism of bismuth molybdate .....	7
2.1.1.4 Bismuth molybdate as a catalyst for the selective oxidation of methane .....	8
2.1.1.5 Bismuth molybdate as a catalyst for the selective oxidation of propene .....	10
2.1.2 Preparation .....	10
2.2 Selective oxidation of methane to carbon monoxide .....	10
2.2.1 Background on the selective oxidation of methane .....	11
2.2.1.1 Possible reactions occurring .....	11
2.2.1.2 Effect of different parameters on the thermodynamic equilibrium .....	13
2.2.1.3 Pathway of product formation .....	14
2.2.1.4 Possible kinetic models for the catalytic selective oxidation of methane .....	15
2.2.1.5 Activation of methane .....	16
2.2.2 Catalyst Used For the Selective Oxidation of Methane to Synthesis Gas .....	19
2.3 Selective oxidation of Propene to Acrolein .....	21
2.3.1 Reaction and catalyst used .....	21
2.3.2 Reaction mechanism .....	22
2.3.2.1 Reoxidation mechanism and redox cycle .....	26
2.3.3 Mars van Krevelen reaction mechanism for the selective oxidation propene to acrolein over $\alpha$ -Bismuth molybdates .....	29
2.3.3.1 Reported reaction orders for the selective oxidation of propene to acrolein over $\alpha$ -Bismuth molybdate .....	31
2.4 Conclusions from Literature .....	32



Chapter 3 Experimental design .....	33
3.1 Experimental Setup .....	33
3.1.1 Reactor rig .....	33
3.1.2 Procedure for conducting experiments on reactor rig .....	34
3.1.3 Ampoule sampling .....	35
3.1.4 Micro-reactor .....	35
3.1.5 Gas analysis .....	36
3.2 Preparation of $\alpha$ -Bismuth Molybdate .....	37
3.3 Experiments .....	38
3.3.1 Preliminary experiments .....	38
3.3.2 Methane .....	40
3.3.3 Propene .....	40
3.3.3.1 External mass transfer limitations .....	40
3.3.3.2 Internal mass transfer limitations .....	41
3.3.3.3 Kinetic experiments of the selective oxidation of propene to acrolein .....	42
3.4 Calculation of products from GC data .....	43
Chapter 4 Preliminary results and the selective oxidation of methane .....	46
4.1 Preliminary experimental work .....	46
4.1.1 Micro-reactors .....	46
4.1.1.1 Residence time distribution (RTD) .....	46
4.1.1.2 Reactivity of blank reactors .....	47
4.1.2 Catalyst characterisation .....	48
4.2 Results for the selective oxidation of methane with $\alpha$ -Bismuth molybdate .....	49
4.3 Possible methods for circumventing the problem of methane activation .....	49
Chapter 5 Selective oxidation of propene .....	52
5.1 Mass Transfer Limitations .....	52
5.1.1 External mass transfer limitations .....	52
5.1.2 Internal mass transfer limitations .....	54
5.2 Effect of reaction conditions on the reaction of Propene to Acrolein over $\alpha$ -Bismuth molybdate .....	55
5.2.1 Effect of time on-steam on the selective oxidation of propene to acrolein over $\alpha$ -Bismuth molybdate .....	55
5.2.2 Effect of propene to oxygen feed ratio and the reaction temperature on the selective oxidation of propene to acrolein over $\alpha$ -Bismuth molybdate .....	57

5.2.3 Effect of the WHSV (Weight hourly space velocity) .....	61
5.3 Reproducibility and experimental error of the experiments.....	67
Chapter 6 Modelling of experimental data.....	71
6.1 Power rate law for propene conversion.....	71
6.2 Reoxidation of $\alpha$ -Bismuth molybdate during the selective oxidation of propene to acrolein.....	76
6.2.1 Electron transfer mechanism during catalyst reoxidation.....	76
6.2.2 Rate determining step during reoxidation reaction .....	79
6.3 Differential reactor setup.....	87
Chapter 7 Conclusions and recommendations .....	90
References .....	93
Appendix A: Calibrations of Mass flow controllers (MFC) .....	99
Appendix B: Response factor for carbon dioxide .....	101
Appendix C: Operating the Oven.....	102
Appendix D: Residence Time Distribution (RTD) GC Output.....	103
Appendix E: Data used for modelling.....	107
Appendix F: Fourth-order Runge-Kutta method.....	108
Appendix G: GC Data of Reaction Runs .....	109
Appendix H: Nomenclature .....	117
Appendix I: List of Abbreviations .....	118



## Chapter 1 Introduction

In any reaction between a hydrocarbon reactant and oxygen, the total oxidation products water and carbon dioxide, are thermodynamically favoured. To add value to some organic reactants, it is sometimes necessary to only partially oxidize the product and to achieve this a selective oxidation catalyst is required that provides an alternative route that prevents the thermodynamically favoured total oxidation reaction. Mixed metal oxides are catalysts that have been seen to be applicable for these types of reactions.

Mixed metal oxides usually produce these selective oxidation products with the Mars-van Krevelen mechanism [Bettahar *et al.* 1996]. This is a redox mechanism where the oxygen in the catalyst takes part in the reaction and exits as part of the product molecule. The mechanism is a redox reaction because the catalyst is oxidized and reduced at two different sites on its surface at the same time. The catalyst is reduced by the insertion of the lattice oxygen into the organic reactant and is reoxidized by gaseous oxygen. It is also known that the lattice oxygen of the catalyst can diffuse through the bulk of the catalyst.

The most commonly used process in the industry to produce synthesis gas from methane currently is steam reforming [Hurtado *et al.* 2004]. For steam reforming large gas fired furnaces containing a large number of parallel reactor tubes are required [De Groote *et al.* 1995]. An alternative process for the production of synthesis gas is the partial oxidation of methane. The advantages of this partial oxidation process are the more favourable H<sub>2</sub> and CO ratio of the synthesis gas and the milder exothermic properties of the reaction. For example, the carbon monoxide of the steam reformer is too low for methanol synthesis for which a H<sub>2</sub>/(CO + CO<sub>2</sub>) ratio of 2 is required [De Groote *et al.* 1995]. The catalytic conversion of methane also occurs at lower temperatures with less energy consumption than with thermal incineration, which is necessary for steam reforming.

It might be possible to achieve the catalytic partial oxidation of methane at lower temperature using mixed metal oxides. Mixed metal oxides have not being extensively studied but some success was seen in the literature. In this study the feasibility of the catalytic oxidation of methane with  $\alpha$ -Bismuth molybdate was studied by using different reaction conditions. The results of these studies as well as suggestions for further research are described in Chapter 4.

## Chapter 1 Introduction

The rest of the study focused on the selective oxidation of propene to acrolein in the low temperature region. This is a reaction which also follows a Mars- van Krevelen mechanism but at milder conditions. The selective oxidation of propene over bismuth molybdates is different in the high and the low temperature region. At low temperatures ( $<375\text{ }^{\circ}\text{C}$ ) the reaction is rate limited by the reoxidation of the catalyst while at high temperatures the reaction is rate limited by the abstraction of hydrogen from the propene molecule. Some questions regarding the reoxidation of the catalyst still remained unanswered. Therefore time on-stream and kinetic experiments were done to investigate the reoxidation mechanism of the catalyst. This investigation of the reoxidation mechanism was done using reaction kinetic equations. The results of the selective oxidation of propene experiments are given in Chapter 5, while the modelling of the reoxidation rate limiting region data can be seen in Chapter 6.

The aim of the first part of the study was thus to investigate the feasibility of  $\alpha$ -Bismuth molybdate as a catalyst for the selective oxidation of methane at temperatures below  $500^{\circ}\text{C}$ . And the aim of the second part of the study was to answer questions regarding the reoxidation mechanism of  $\alpha$ -Bismuth molybdate by studying the selective oxidation of propene to acrolein.

The experiments for the selective oxidation of methane and propene were conducted in the same reactor rig that is described in Chapter 3. The different experiments, the sampling method as well as how the samples were analyzed are also described in Chapter 3.

## Chapter 2 Literature Review

### 2.1 Selective Mixed Metal Oxide Oxidation Catalysts

A selective oxidation catalyst should provide an alternative pathway for the formation of the partially oxidized product and not the thermodynamically favoured total oxidation products. According to Bettahar *et al.* [1996], the C-H bond strength of hydrocarbons is stronger than the intermediate partial oxidized products and leads to a tendency for total oxidation. This strong C-H bond strength leads to a low activity of saturated hydrocarbons like alkanes. To activate these reactants, reaction conditions (high activation temperature) are required that are sometimes destructive to the stability of partially oxidized hydrocarbon products. According to Keulks, 1970, the metal-oxygen bond of the mixed metal oxide selective oxidation catalyst should be of intermediate strength, because the lattice oxygen acts as a reactant in the reaction. The bond strength should be such that the oxygen can be removed with the formation of the product and that the catalyst can rapidly be regenerated by gaseous oxygen. Another aspect of a selective oxidation catalyst is that the product should have a weak interaction with the catalyst surface. This weak interaction will lead to a fast desorption and prevent the full oxidation reaction [Van Vuuren, 2004].

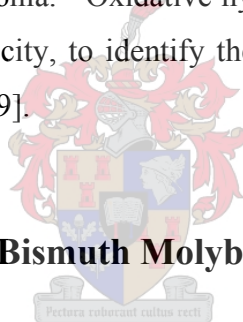
Very little research has been done on the selective oxidation of methane to synthesis gas over mixed metal oxides. Catalytic partial oxidation of methane to synthesis gas has been observed as a side product over mixed metal oxides, while studying the oxidative conversion of methane to methanol, formaldehyde, methyl formate, hydrocarbons and oxidative coupling of methane [Zhu *et al.*, 2004]. Tsyganok *et al.* [2004] also showed that the amount of noble metal can be reduced significantly, without a decrease in catalytic activity or selectivity in synthesis gas product, by supporting the metal on a Mg-Al mixed metal oxide for combined partial oxidation and dry reforming of methane. Because of the favourable properties of mixed metal oxides it may be possible to find a mixed metal oxide catalyst that will give a high methane conversion and high synthesis gas selectivity at relative low temperatures.

Mixed metal oxides like magnesium vanadates, vanadia bismuth molybdates, vanadia antimony, etc. have been used extensively as catalyst for selective oxidation of light alkanes and light olefins to produce different selective oxidation products [Bettahar *et al.*, 1996].

### 2.1.1 Bismuth Molybdate

Multicomponent bismuth molybdate catalysts of the form  $M_x^{2+}M_y^{3+}Bi_zMo_wO_n$  (where  $M^{2+}$  refers to  $Co^{2+}$ ,  $Ni^{2+}$ ,  $Mg^{2+}$  and  $M^{3+}$  to  $Fe^{3+}$ ,  $Al^{3+}$ , etc.), with traces of phosphorus and potassium, are the most widely used metal oxide catalysts [Bettahar *et al.* 1996]. These bismuth molybdate catalysts are well known for their ability to catalyze the selective oxidation and ammoxidation reactions of alkenes. Although these complex multicomponent bismuth molybdate catalysts are used industrially, most research has focused on the simpler binary  $Bi_2O_3$ - $MoO_3$  systems [Yanina and Smith 2002]. This study will also focus on these simpler binary systems.

The activity and selectivity of the bismuth molybdate catalyst is determined by the  $Bi_2O_3$  and  $MoO_3$ , since the individual compounds and their mixtures have different catalytic properties than the 50wt%  $Bi_9PMo_{12}O_{52}$  / 50wt%  $SiO_2$  catalyst that is used for the synthesis of acrylonitrile from propene and ammonia. Oxidative hydrogenation of 1-butene to butadiene was also used, because of its simplicity, to identify these active compounds in the bismuth molybdate catalysts [Gates *et al.* 1979].



#### 2.1.1.1 Different Phases of Bismuth Molybdate

According to Gates, *et al.*, 1979, it was found that the bismuth molybdate catalyst with a Bi/Mo ratio in the range of 2:1 and 2:3 has a high activity combined with a good selectivity. In this Bi/Mo range of 2:1 and 2:3 three compounds are found, with one of the compounds occurring in two modifications [Gates *et al.* 1979]:

- $Bi_2Mo_3O_{12}$  ( $\alpha$ , 2:3 ratio)
- $Bi_2Mo_2O_9$  ( $\beta$ , 1:1 ratio)
- $Bi_2MoO_6$  ( $\gamma$  {koechlinite} and  $\gamma'$ , 2:1 ratio)

The  $\alpha$  phase is very stable and has a melting point near  $700^\circ C$ . The  $\beta$  phase is unsuitable for oxidation reactions and is only stable between  $550^\circ C$  and  $670^\circ C$ . Below  $550^\circ C$  this  $\beta$  phase decays slowly into the  $\alpha$  and the  $\gamma$  phases and at temperatures above  $670^\circ C$  it decays into the  $\alpha$  and the  $\gamma'$  phases. The  $\gamma$  has an x-ray diagram similar to koechlinite and is metastable. At

temperatures higher than 660°C an irreversible transition of the  $\gamma$  phase into the  $\gamma'$  occurs [Gates *et al.* 1979].

$\alpha$ -Bismuth molybdate was chosen for this research because of its stability, high activity and its good selectivity towards acrolein during the selective oxidation of propene to acrolein.

### 2.1.1.2 $\alpha$ -Bismuth Molybdate Crystal Structure

The different bismuth molybdates are best understood if the symmetry of the oxygen surrounding the  $\text{Mo}^{6+}$  and  $\text{Bi}^{3+}$  is explained. The  $\text{Mo}^{6+}$  has various oxygen coordinations, which are distorted so strongly that it is hard to decide whether the surrounding is better described as tetrahedral or octahedral. The oxygen polyhedral can be linked as corner sharing or by edge sharing (See Figures 2-3 and 2-4). The lattice is flexible towards reduction and does not collapse with the removal of oxygen from the lattice, but restructuring occurs to make it more spacious [Gates *et al.* 1979].

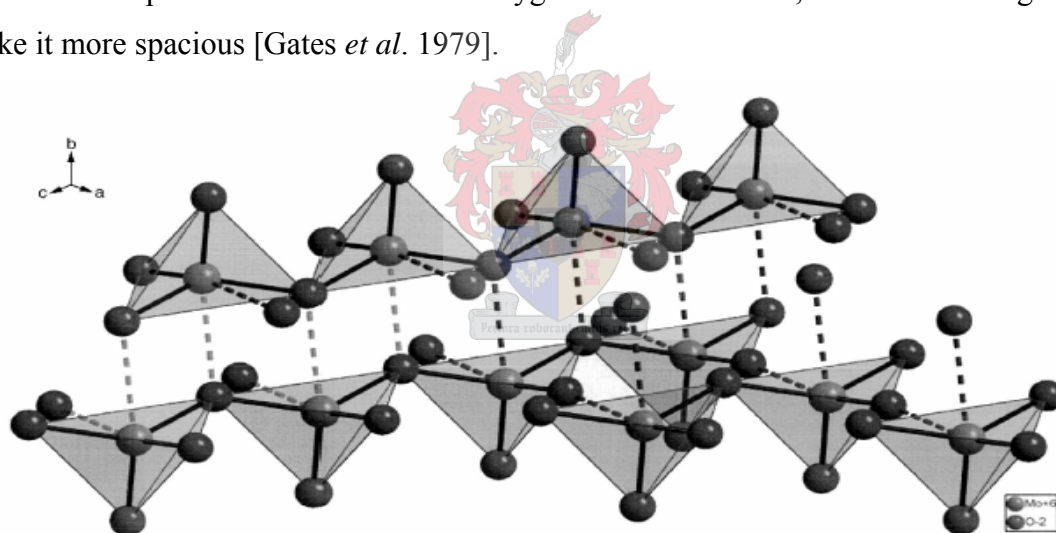
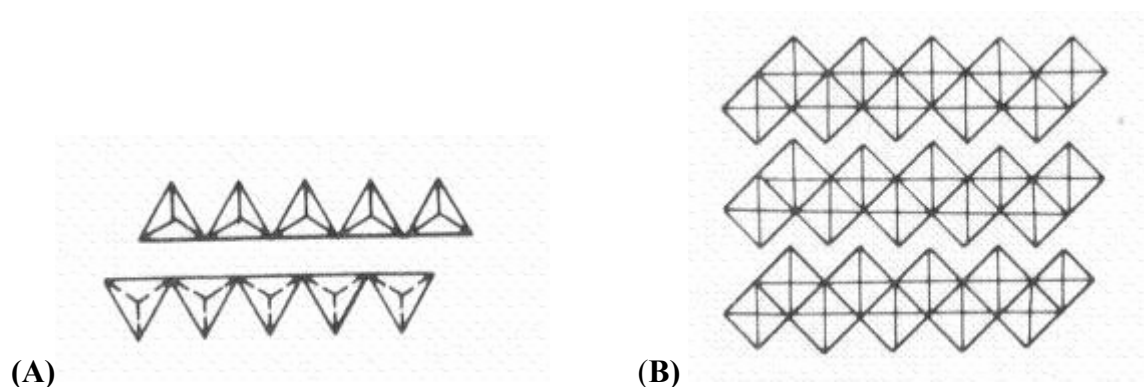


**Figure 2-1:** Drawing of the  $\text{MoO}_3$  crystal lattice showing the distorted tetrahedral oxygen coordination sphere around  $\text{Mo}^{6+}$  [Mestl *et al.* 2000].





## Chapter 2 Literature Review

**Figure 2-2:** MoO<sub>3</sub> represented as (A) infinite chains of corner-shared tetrahedra and (B) as sheets formed from octahedra sharing edges with two adjacent octahedra (in the plane) and corners with two others (above and below plane) [Gates *et al.* 1979].

The crystal chemistry of Bi<sup>3+</sup> is complex and has two different oxygen surroundings described below [Gates *et al.*, 1979] (See Figure 2-5):

1. Derived from a cubic eightfold surrounding by removing the two oxygen atoms at opposite corners to form a special type of 6 surrounding.
2. Bi<sup>3+</sup> can also be connected to oxygen layers arranged in a square pattern, where the Bi<sup>3+</sup> ions are placed above and below the centre of the square oxygen arrangement.

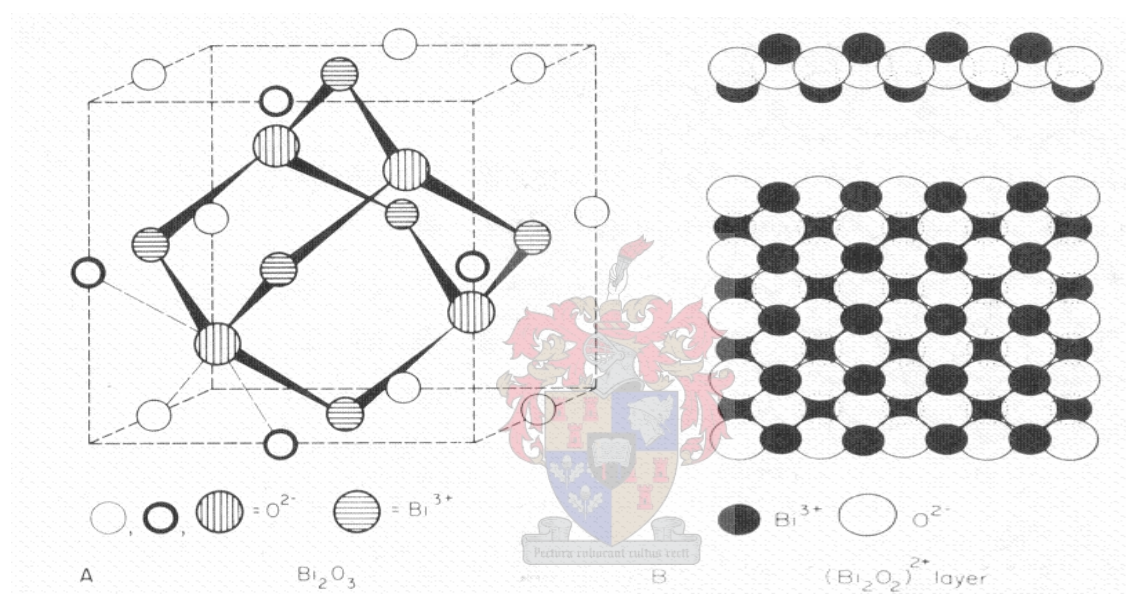


**Figure 2-3:** Different structures of Bi<sup>3+</sup> oxides [Gates *et al.* 1979]. A) Distorted Scheelite crystal structure B) Bi and Mo layers

The crystal structure of Bi<sub>2</sub>Mo<sub>3</sub>O<sub>12</sub> can be viewed as a distorted Scheelite with ordered Bi vacancies. The structure has three different Mo sites, each of which is coordinated by five O atoms. In each case, four of the Mo-O bonds are short (1.68 to 1.91 Å), while the fifth bond is longer (>2.13 Å). There are two Bi sites, each having four close O neighbours (at distances of 2.12 to 2.34 Å) and four that are further away (2.61 to 2.94 Å). The Bi and Mo are concentrated in layers parallel to (010) plane that intersect b at approximately 1/8, 3/8, 5/8 and 7/8 (figure 2.4 a). Adjacent layers are bridged and held together by metal-oxygen, primary Bi-O, bonds.



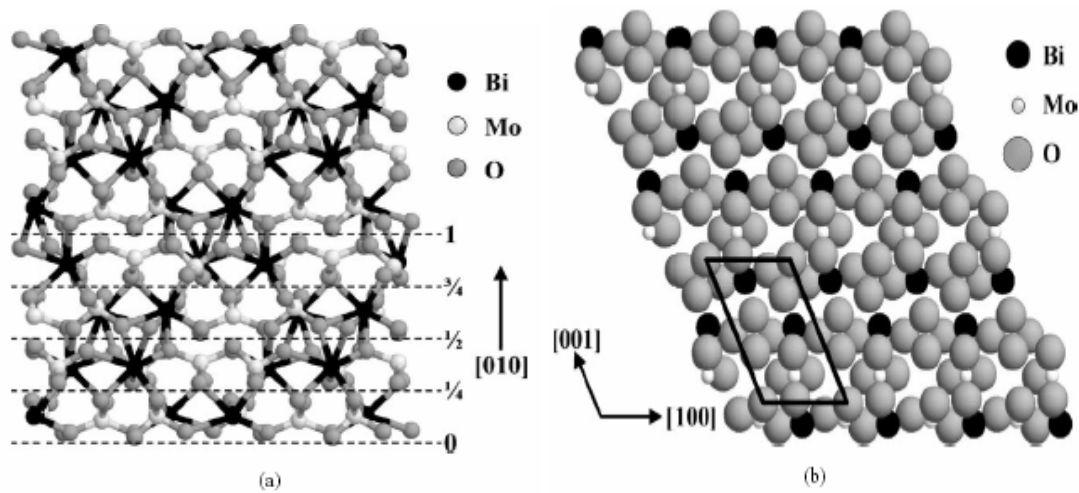


**Figure 2-4:** Layers of  $\text{Bi}_2\text{Mo}_3\text{O}_{12}$  [Yanina and Smith 2002] a) [010] Plane b) [001] and [100] planes

### 2.1.1.3 General reaction mechanism of bismuth molybdate

It is agreed that oxidation reactions on  $\alpha$ -bismuth molybdate follow the Mars-van Krevelen mechanism based on a redox cycle of the oxide surfaces, the diffusion of bulk oxide ions to the surface and the reoxidation of the catalyst with gaseous oxygen. The sites for the adsorption and oxidation of the organic reactant and the chemisorption and dissociation of the gaseous oxygen are spatially and structurally distinct from each other.

According to a study done by Ayame *et al.* [2002] it was observed by XPS that during the reduction of bismuth molybdate the  $\text{Mo}^{6+}$  is reduced to  $\text{Mo}^{5+}$  and  $\text{Mo}^{4+}$ , and that no reduction of the bismuth species occurs. The results indicated that the oxygen bridge between the  $\text{Bi}^{3+}$  and the  $\text{Mo}^{6+}$  is more active and mobile than the oxide ions doubly bonded to  $\text{Mo}^{6+}$ . It also indicated that the surface reduction was accompanied by diffusion of the lattice ions from the catalyst bulk to the surface of the catalyst. Finally it was seen that reoxidation incorporated lattice oxide into bulk oxide ion vacancies and to the doubly bonded oxide ion vacancies on the  $\text{Mo}^{4+}$  through the bulk.

#### **2.1.1.4 Bismuth molybdate as a catalyst for the selective oxidation of methane**

Bismuth molybdate has not been studied as a catalyst for the selective oxidation of methane to synthesis gas or any other selective oxidation products like formaldehyde, methanol, etc. A few studies have been done on catalysts that contained molybdenum and bismuth. An example is a study that was done on the catalytic oxidation of methane over a Mo-V-Cr-Bi-Si oxide catalyst to methanol and formaldehyde [Zhang *et al.*, 2002]. The selectivity of methanol plus formaldehyde was between 70-80% at a methane conversion of 8-10%. The molybdenum oxide was regarded to favour the partial oxidation products, vanadium oxide promoted the activation of the C-H bond in methane and chrome improved the conversion of methane. Different bismuth content resulted in different TPR reduction temperatures. With suitable TPR reduction temperatures, the catalyst could oxidize methane selectively and prohibit deep oxidation of methanol so as to increase its selectivity.

Cooper *et al.* [2001] studied the suitability of MoO<sub>3</sub> as a catalyst to produce methanol from methane (See Table 2-2). In this study it was shown that methanol is quite stable over the oxides MoO<sub>3</sub>, WO<sub>3</sub>, Nb<sub>2</sub>O<sub>5</sub>, Ta<sub>2</sub>O<sub>5</sub> and Sb<sub>2</sub>O<sub>3</sub> which make it unlikely for these catalysts to produce the full oxidation products. In particular, the conversion of methanol to carbon oxides over MoO<sub>3</sub> was very low, whilst showing high selectivity towards formaldehyde. Based on this and methane/deuterium exchange studies on Ga<sub>2</sub>O<sub>3</sub> a mixture of Ga<sub>2</sub>O<sub>3</sub>/MoO<sub>3</sub> was prepared and tested for methane oxidation. The Ga<sub>2</sub>O<sub>3</sub>/MoO<sub>3</sub> catalyst produced a high catalytic yield of methanol which was greater than the comparative homogeneous gas phase reaction over a quartz chips packed reactor. The methanol yield was also higher compared with MoO<sub>3</sub> and Ga<sub>2</sub>O<sub>3</sub> alone. This was in line with the observation of the high activation of methane over Ga<sub>2</sub>O<sub>3</sub> as well as the oxygen exchange mechanism and the selective oxidation function exhibited by MoO<sub>3</sub> during methanol oxidation studies. This indicates that, by using mixtures of metal oxides, better catalysts for methane conversion can be produced.

**Table 2-1 Methane oxidation over Ga<sub>2</sub>O<sub>3</sub>/MoO<sub>3</sub> physical mixture: CH<sub>4</sub>/O<sub>2</sub>/He = 23/2/5, 25 bar, GHSV = 5000h<sup>-1</sup> [Cooper *et al.*, 2001]**

Catalyst	Temperature °C	CH <sub>4</sub> Conversion %	Selectivity %				CH <sub>3</sub> OH per pass yield
			CH <sub>3</sub> OH	CO	CO <sub>2</sub>	C <sub>2</sub> H <sub>6</sub>	
Ga <sub>2</sub> O <sub>3</sub> /MoO <sub>3</sub>	455	3.0	22	50	27	1	0.66
Ga <sub>2</sub> O <sub>3</sub>	455	1.5	3	27	68	2	0.05
MoO <sub>3</sub>	455	0.3	13	69	18	-	0.04
Quartz packing	455	0.1	-	-	100	-	0.00
Empty tube	455	8.1	29	63	7	1	2.34

The oxidation of methane to formaldehyde was also investigated over MoO<sub>x</sub>/SiO<sub>2</sub> [Ohler and Bell, 2005]. The formation of formaldehyde was found to occur largely over MoO<sub>x</sub> and only to a limited degree over SiO<sub>2</sub>. Ohler and Bell [2005] further reported that silica supported oxides of molybdenum, vanadium and iron are among the best performing heterogeneous catalysts for the selective oxidation of methane. Silica was the preferred support because other refractory supports, such as TiO<sub>2</sub> and Al<sub>2</sub>O<sub>3</sub>, burn formaldehyde at temperatures way below the activation temperature of methane. Silica is relatively inert to formaldehyde combustion compared to these supports, but decomposition still occurs at the methane oxidation temperatures. Ohler and Bell [2005] also investigated the role of silica and homogeneous reactions in this reaction system. The product distributions are displayed in Figure 2-11 for SiO<sub>2</sub> and MoO<sub>x</sub>/SiO<sub>2</sub>. These results demonstrate that the synergy effect between two oxides can increase the conversion of methane and also that CO<sub>x</sub> formation is a secondary reaction from CH<sub>2</sub>O.

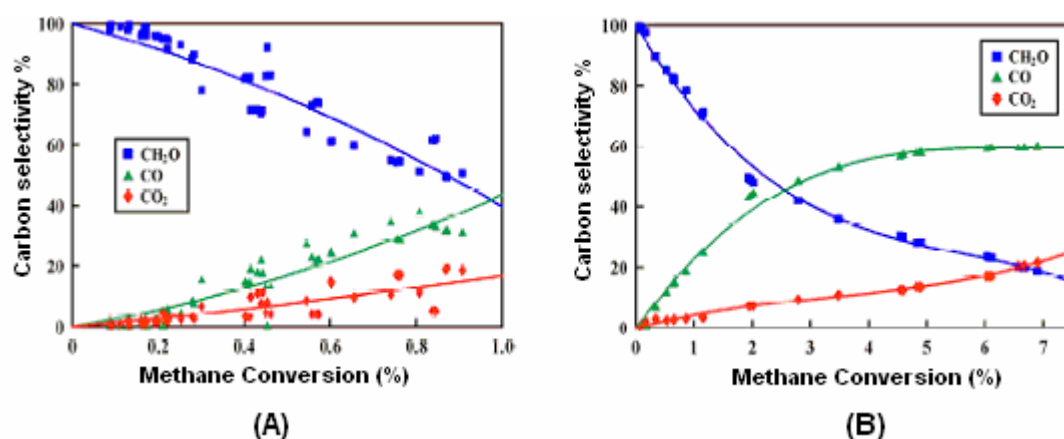


**Figure 2-5** The product distributions for (A) pure SiO<sub>2</sub> and (B) MoO<sub>x</sub>/SiO<sub>2</sub> at 873K with a 90% CH<sub>4</sub> and 10% O<sub>2</sub> feed. The CH<sub>4</sub> conversion was varied by varying the contact time. Trend lines are empirical polynomial fits. [Ohler and Bell 2005]

It is thus seen that  $\text{MoO}_3$  is able to activate methane to form selective oxidation products and that the combination of different metal oxides increase the conversion of the methane.  $\alpha$ -Bismuth molybdate might thus be a good catalyst for the conversion of methane to synthesis gas or other selective oxidation products at low temperatures.

### **2.1.1.5 Bismuth molybdate as a catalyst for the selective oxidation of propene**

Bismuth molybdate as a catalyst for the selective oxidation of propene to acrolein is discussed in section 2.2.1.

### **2.1.2 Preparation**

Bismuth molybdate is prepared by precipitation of the catalyst from mixtures of bismuth nitrate and ammonium molybdate solutions. The structure,  $\alpha$ ,  $\beta$  or  $\gamma$ , that is prepared depends on the Bi/Mo ratio, pH of the solutions, temperature and the time of interaction. After precipitation the material is calcinated at  $500^\circ\text{C}$  to form the desired phase [Gates *et al.* 1979].

## **2.2 Selective oxidation of methane to carbon monoxide**

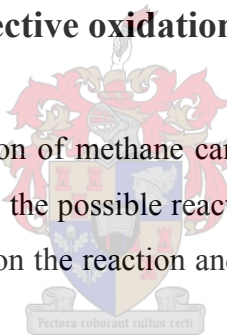
There is currently a large demand for an economic, compact, synthesis gas production technology, e.g. from methane. Such a compact technology will be useful to produce hydrogen for fuel cell vehicles in the near future. It can also be used to produce synthesis gas that can be used in the conventional internal combustion engine to create a more environmentally friendly engine start up, while the catalytic emission converter heats up to an efficient operating temperature [Schwiedernoch *et al.*, 2003]. Methane, which is the main component of natural gas, can also be converted to synthesis gas for the Fischer Tropsch process to create hydrocarbons from natural gas. New environmental policies addressed to reduce climate change also addressed the reduction of methane emission into the atmosphere which contributes to global warming [Schwiedernoch *et al.*, 2003]. This unwanted methane that is produced by coke ovens, landfills and wastewater treatment facilities can be made useful by converting it to synthesis gas.

## Chapter 2 Literature Review

There are a number of reasons why the catalytic partial oxidation of methane should be investigated. The most commonly used process in the industry to produce synthesis gas from methane currently is steam reforming [Hurtado *et al.*, 2004] that requires large gas fired furnaces. A better alternative process for the production of synthesis gas is the catalytic partial oxidation of methane. The advantages of this partial oxidation process are the more favourable H<sub>2</sub> and CO ratio of the synthesis gas and the milder exothermic properties of the reaction. For example, the carbon monoxide of the steam reformer is too low for methanol synthesis for which a H<sub>2</sub>/(CO + CO<sub>2</sub>) of 2 is required [De Groote *et al.*, 1995]. The catalytic conversion of methane also occurs at lower temperatures and therefore needs less energy than thermal incineration, which is necessary for steam reforming. Nickel, palladium, platinum and rhodium are metals that are commonly used as a partial oxidation catalyst for methane to synthesis gas at high temperatures [Hurtado *et al.*, 2004, Mallens *et al.*, 1996, De Groote *et al.*, 1995].

### 2.2.1 Background on the selective oxidation of methane

Before the catalytic selective oxidation of methane can be investigated, an understanding of this reaction is needed. This includes the possible reactions that occur during the process, the general effect of reaction conditions on the reaction and the pathway of how the products are formed.



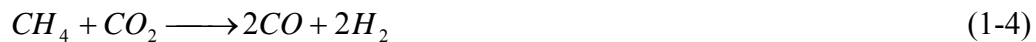
#### 2.2.1.1 Possible reactions occurring

Numerous reactions occur during the partial oxidation of methane which makes the process quite complex. These reactions have been summarized by Theron [1997] and De Groote *et al.* [1996] and are displayed below. The main methane oxidation reactions that occur during the partial oxidation reaction are the total oxidation (equation 1-1) and the selective oxidation reactions (equation 1-2):

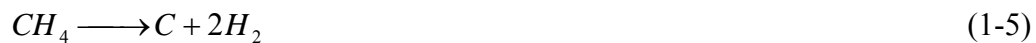


## Chapter 2 Literature Review

Some of the methane can also react with the water and the carbon dioxide that are formed by the total oxidation reaction. The reactions that occur as a result of this are known as the endothermic steam reforming reaction between water and methane (equation 1-3), and the dry reforming reaction between carbon dioxide and methane (equation 1-4). These reactions produce carbon monoxide and hydrogen in different ratios as can be seen in equations 1-3 and 1-4.



Another reaction may occur when methane dissociates on a metal surface to yield surface carbon and hydrogen with the following reaction:



More surface carbon can also be formed from carbon monoxide by the Boudouard reaction (equation 1-6) to produce carbon dioxide:

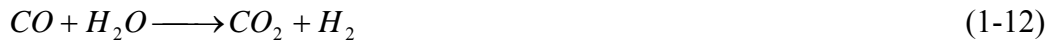


The surface carbon that is formed with reaction 1-5 and 1-6 can be removed by the reaction of the carbon with steam or oxygen to produce carbon monoxide, carbon dioxide and hydrogen:



Other possible reactions that may occur are the oxidation of the carbon monoxide (equation 1-10) and the hydrogen (equation 1-11) to produce carbon dioxide and water respectively and the water-gas shift reaction (equation 1-12):





Since there are so many possible reactions that can occur, a catalyst must be used to optimize these reactions. This catalyst must be able to produce favourable synthesis gas carbon monoxide and hydrogen ratios, while also forming as little as possible surface carbon to prevent deactivation.

### **2.2.1.2 Effect of different parameters on the thermodynamic equilibrium**

Theron [1997] investigated the thermodynamics of the partial oxidation reaction of methane by calculating the product composition at thermodynamic equilibrium by performing a Gibbs free energy minimization of all the gaseous species with the HYSIM software package.

The calculations done with the reactions from section 2.1.1.1 indicated that the major carbon containing product at low temperatures was carbon dioxide, but that carbon monoxide became the dominant product at temperatures higher than about 600°C. Complete conversion of methane to pure synthesis gas was predicted only at very high temperatures. This product distribution is in contrast with the predicted product composition for the oxidation reforming reaction (1-2) only, which indicates that pure synthesis gas will form with almost all of the methane converted at temperatures as low as 200°C. The Gibbs free energy for the oxidation reforming reaction is highly negative ( $\Delta G^\circ = -142 \text{ kJ mol}^{-1}$ ) which indicates that the reaction can occur spontaneously. Pure synthesis gas, however, has never been found at 200°C.

The effect of the  $CH_4/O_2$  feed ratio on the equilibrium was also calculated. It was found that an increase in the  $CH_4/O_2$  ratio led to a decrease in the methane conversion. The presence of less oxygen also favoured the partial oxidation reaction which resulted in higher carbon monoxide and hydrogen selectivity. The calculations further showed that the methane conversion was suppressed by higher pressure because the higher pressure shifts the steam and dry reforming reaction to the left. This also resulted in lower carbon monoxide and hydrogen selectivity.

It was also found that coking of the catalyst surface may occur when synthesis gas is manufactured at low temperatures with the catalytic selective oxidation of methane which can have a negative effect on the catalyst activity. Examples of this have been demonstrated in



## Chapter 2 Literature Review

the literature by Souza *et al.* [2005] who showed that the autothermal reaction over P/ZrO<sub>2</sub>/Al<sub>2</sub>O<sub>3</sub> is most stable above 800°C due to high resistance against coke formation at high temperatures and Sun *et al.* [2005] who showed that Ni/SiC deactivates due to carbon formation on Ni active sites.

The thermodynamics shows that the total oxidation is favoured at low temperatures for the reaction from section 2.1.1.1. A suitable catalyst is thus needed to overcome this at low temperatures and also to prevent the coking of the catalyst surface.

### 2.2.1.3 Pathway of product formation

There are two possible routes the selective oxidation of methane to synthesis gas can follow. The one is where carbon monoxide and hydrogen are formed directly and the other is where carbon dioxide and water are formed as primary products. In the second route, carbon monoxide and hydrogen are then formed via the steam- and dry reforming reactions. There is still an ongoing discussion which route is the favoured route [Theron 1997; Mallens *et al.*, 1997; Otsuka *et al.*, 1998; Wu *et al.*, 2005 and Schwiedernoch *et al.*, 2003]. There are numerous papers available that support either one or the other of these routes and are summarized by Theron [1997]. Only a few recent papers will be highlighted.

Theron [1997] concluded that by using a commercial nickel steam reforming catalyst supported on  $\alpha$ -Al<sub>2</sub>O<sub>3</sub> that the partial oxidation of methane reaction pathway consisted of a series-parallel scheme. CO, H<sub>2</sub>, CO<sub>2</sub> and H<sub>2</sub>O are all formed as primary products and that methane is also converted with steam- and carbon dioxide reforming to synthesis gas in the latter part of the catalyst bed.

Mallens *et al.* [1997] determined that the primary products that are formed in the selective oxidation of methane are CO and H<sub>2</sub> by using a rhodium oxide catalyst. This conclusion was reached because the starting point and the maximum of the CO response were observed prior to those of the CO<sub>2</sub>. Using a rhodium coated alumina monolith Schwiedernoch *et al.* [2003] concluded that a combination of the two reactions were involved in the partial oxidation of methane.



## Chapter 2 Literature Review

Another parameter that has an influence on the reaction pathway is the surface state of the catalyst. Wu *et al.* [2005] determined that CO and H<sub>2</sub> are formed directly over a reduced Ni/TiO<sub>2</sub> catalyst, while using oxidized Ni/TiO<sub>2</sub> resulted in non-selective oxidation. Zhu *et al.* [2004] showed that the pathway is also influenced by the reaction temperature by studying yttrium-stabilized zirconia.

Bruno *et al.* [2004], studied partial oxidation of methane in an annular reactor with a Rh/ $\alpha$ -Al<sub>2</sub>O<sub>3</sub> and a Rh/ZrO<sub>2</sub> catalyst. It was found that on Rh/ $\alpha$ -Al<sub>2</sub>O<sub>3</sub> the reaction followed an indirect-consecutive pathway, where carbon dioxide is formed directly and carbon monoxide is formed by the water gas shift reaction. It was also pointed out that on Rh/ZrO<sub>2</sub> a direct route to synthesis gas could not be excluded.

From these examples and other examples in literature it can be concluded that both the reaction pathways are occurring, depending on the reaction temperature, catalyst, catalyst support and surface state of the catalyst. It is important to combine the factors mentioned above and find a catalyst that follows the direct path to synthesis gas, because a catalyst that forms synthesis gas indirectly will cause huge temperature gradients in the reactor that may lead to temperature run aways [Zhu *et al.*, 2004].

### 2.2.1.4 Possible kinetic models for the catalytic selective oxidation of methane

There are three types of kinetic models described in the literature for selective oxidation reactions: Mars-van Krevelen (MVK), Langmuir-Hinshelwood (LH) and Eley-Rideal (ER). Methane can be selectively oxidized by anyone of these different kinetic models.

#### Mars-van Krevelen

Mars and Van Krevelen [1954] observed that for vanadium oxide catalyst, if adsorption of the molecules to be oxidized on the reduced part of the surface should be a reaction condition, there would be a maximum rate at a certain partial pressure of the oxygen and the organic substance. Such a maximum rate does not exist, thus they concluded that the underlying catalyst surface is the reactant for the reaction. The MVK is most often used to describe the oxidation of organic compounds over noble metals and metal oxide catalysts. According to these models, the reaction takes place through alternative oxidations and reductions of the

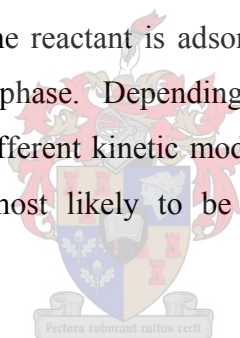
catalyst surface. The surface is oxidized by gaseous oxygen which dissociatively adsorbs on the surface and can migrate to the surface layer, the bulk and on the catalyst surface to the site where the selective oxidation occurs. The oxygen of the bulk of the catalyst takes part in the reaction because of the high mobility of the oxygen ions in the lattice. The organic reactant, i.e. propene, then reacts with the atomic oxygen on the surface in successive irreversible steps, resulting finally in the total oxidized products.

### **Langmuir-Hinshelwood**

An LH type mechanism takes place between both the reactants which are adsorbed on the catalyst surface. Due to a multi-step reaction mechanism a rate-limiting step controls the reaction. Depending on the rate-limiting step, different models can be derived if it is assumed that all the other reaction steps are at equilibrium. These models are especially appropriate when noble metals are mainly in reduced form ( $T > 500^{\circ}\text{C}$ ).

### **Eley-Rideal**

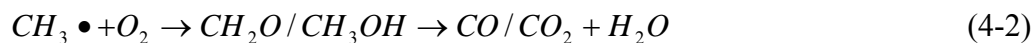
The ER mechanism occurs when one reactant is adsorbed on the surface and reacts with a second reactant which is in the gas phase. Depending on the chemisorbed reactant and the nature of the chemisorption eight different kinetic models can be derived. For the selective oxidation of methane the  $\text{O}_2$  is most likely to be adsorbed, because methane has no nucleophilic groups.



#### **2.2.1.5 Activation of methane**

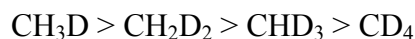
The selective activation of methane remains one of the biggest challenges facing scientists interested in design of heterogeneous catalysts [Cooper *et al.*, 2001]. The selective oxidation of methane to yield hydrocarbons containing two carbons and methanol has been studied extensively. The first oxidative coupling reaction according to Cooper *et al.* [2001] was catalysed by Lunsford with Li doped MgO. Researchers found that most oxides and oxide combinations can catalyse this type of reactions, but the  $\text{C}_2$  hydrocarbon yield in excess of 30% were extremely rare. It was later on discovered that the oxidative coupling reaction occurs homogeneously in the gas phase. The methane molecule was activated at a surface oxide site to form gas phase methyl radicals. These radicals either dimerised (equation 4-1) to form hydrocarbons or oxygenates and carbon oxides (equation 4-2).

## Chapter 2 Literature Review



It was found that the product distribution can be determined through variation of the oxygen concentrations and that the dimerisation reaction is favoured at low oxygen concentrations. However, both the formation of hydrocarbons and oxygenate products requires gas phase radical reactions which are predominant at the high reaction temperatures (>600°C) required for activation of methane on oxide surfaces. Cooper *et al.* [2001] reconsidered the problems associated with the scientific design of catalyst for the selective oxidation of methane. It was found that the most important part of methane oxidation is the activation of the molecule. Cooper proposed that the roles of defects are crucial for methane activation and investigated the activation of methane over gallium oxide and gallium oxide doped with magnesium and zinc in an attempt to increase the defect concentration. The experimental studies showed that doping Ga<sub>2</sub>O<sub>3</sub> with low levels of Zinc promoted the activity for methane oxidation and it is proposed that this is due to an increase in the defect concentration of the catalyst. Conversely, the addition of magnesium suppressed the activity. This is due to atomic relaxations resulting in cation movements towards the bulk and anion movements away from the surface. This, coupled with the larger ionic radius of the anion suggests that the simple defect free surface will favour adsorbents which can strongly interact with the anionic centres.

Hargreaves *et al.* [2002] used the H/D exchange reaction of CH<sub>4</sub> with D<sub>2</sub> to confirm that the reaction of methane occurs via an adsorbed radical intermediate. A dependence of exchange reactivity with hydrocarbon structure can be explained qualitatively by considering the order of stability of the intermediate carbanions. Before Hargreaves H/D exchange studies showed that the most active catalyst over a limited range of oxides for H/D exchange is alkaline earth oxides and La<sub>2</sub>O<sub>3</sub>, they found that the oxides Nb<sub>2</sub>O<sub>5</sub>, MoO<sub>3</sub>, SiO<sub>2</sub>, SnO<sub>2</sub>, Tb<sub>4</sub>O<sub>7</sub>, WO<sub>3</sub> and Y<sub>2</sub>O<sub>3</sub> show no detectable exchange activity even after 5 hours on line at 540°C and are therefore not able to activate the methane molecule. In accordance with its surface area, the total conversion over Al<sub>2</sub>O<sub>3</sub> was greatest in the group of oxides that showed moderate activity at 420°C. These include Al<sub>2</sub>O<sub>3</sub>, CaO, Gd<sub>2</sub>O<sub>3</sub>, La<sub>2</sub>O<sub>3</sub>, MgO, Nd<sub>2</sub>O<sub>3</sub>, Pr<sub>6</sub>O<sub>11</sub>, Sm<sub>2</sub>O<sub>3</sub>, V<sub>2</sub>O<sub>5</sub>, Yb<sub>2</sub>O<sub>3</sub> and ZrO<sub>2</sub>. CH<sub>3</sub>D was the predominant product in all cases. The Cr<sub>2</sub>O<sub>3</sub>, Ga<sub>2</sub>O<sub>3</sub> and ZnO oxides showed considerably higher conversions than the other oxides investigated over the same temperature range of 420-540°C. All possible products were observed and the relative selectivities were:



Hargreaves *et al.* [2002] could not explain why  $\text{Ga}_2\text{O}_3$  and  $\text{ZnO}$  species are most active for these exchange reactions. It was suggested that it might possibly be related to the redox behaviour, hydroxyl chemistry, alkyl formation or the catalyst structure.

One case was reported by Zhu *et al.* [2004] where methane activation is not the rate limiting step. It was found that the formation of formate on the surface of YSZ12 indicates that methane is activated and reacts with oxygen at temperatures as low as  $400^\circ\text{C}$  over YSZ12. This indicated that at low temperatures the rate limiting step of the catalytic partial oxidation of methane is not methane activation but formate decomposition. However, the activation of methane becomes the rate determining step at temperatures above  $600^\circ\text{C}$ . This should be kept in mind if one is designing a catalyst for low temperature activation of methane.

It can thus be seen that the major problem with the selective oxidation of methane at low temperatures is the activation of the methane molecule. Very little is understood about this process and it can strongly be suggested to study the redox behaviour, hydroxyl chemistry, alkyl formation and catalyst structures of the most active metal oxides mentioned by Hargreaves *et al.* [2002]. If this activation process is better understood it can be used to develop a mixed metal oxide with the correct properties to achieve selective oxidation of methane at low temperatures.

From these different cases mentioned above it might also seem that during the selective oxidation of methane the catalyst is only needed to form radical methane molecules that will react with gaseous oxygen to form the selective oxidation products. If this is the case mixed metal oxides like bismuth molybdates that oxidize hydrocarbons with a Mars van Krevelen mechanism will not be very suitable for the selective oxidation of methane. However Hurtado *et al.* [2004] showed that methane is selectively oxidized with a Mars-van-Krevelen mechanism by  $\text{Pd}/\text{Al}_2\text{O}_3$ , which indicates that methane radicals are not the only pathway towards the formation of selective oxidation products during the selective oxidation of methane.

### 2.2.2 Catalyst Used For the Selective Oxidation of Methane to Synthesis Gas

A wide range of catalysts have been studied in the past for the selective oxidation of methane as summarized by Theron [1997]. The main types of catalyst are supported metal catalysts, metal oxide catalysts and multicomponent catalysts. The most work has been done on supported metal catalysts with very little work done on metal oxide catalysts. In general, the activity of Group VIII B and VI A metals for the catalytic selective oxidative reforming reaction can be given as.



Nickel, palladium, platinum and rhodium are metals that are commonly used as a partial oxidation catalyst for methane to syngas at high temperatures [Hurtado *et al.*, 2004; Mallens *et al.*, 1996; De Groote *et al.*, 1995], but a lot of research is still being done to develop/discover new and better catalysts.

The research that is being done on the catalytic partial oxidation of methane to synthesis gas can be divided into the following six research areas, each with a few recent examples to give some background on what research is being done on the catalytic oxidation of methane:

**Plasma catalytic conversion of methane into synthesis gas:** This is a relative new field where a catalyst is placed in a plasma region to change the plasma properties to enhance the reactions. An example is Heintze *et al.* [2004] who studied the plasma catalytic conversion of methane to synthesis gas. This investigation combined the operation of a dielectric barrier discharge and an  $\alpha$ -alumina supported Ni catalyst. It was found that the catalyst was only active above 300°C, where plasma induced partial oxidation of methane is active over the entire range of 100-400°C. It was also found that pure plasma favours CO with a CO/CO<sub>2</sub> ratio of 9. It was found that the reaction takes place in the gas phase and thus that the catalyst has no effect on the reaction, which technically makes this not a catalytic partial oxidation reaction. A lot of work will still be done in this area in the future.

**Refinement of metal oxides to pure metal and synthesis gas:** This occurs when the metal oxide ore is used to catalyze methane while it is reduced to the pure metal. An example is Ebrahim *et al.* [2004] who proposed the partial oxidation of methane to refine Zn from ZnO. It was found that ZnO produces a synthesis gas with a favourable H<sub>2</sub>/CO ratio of 2.

**Environmental clean up of green house gases:** As mentioned in the beginning of the chapter environmental policies aim for lower methane emissions. Therefore research is being done to convert methane instead of flaring it. Xu *et al.* [2004], reported a method to produce low cost synthesis gas from coalmine-drained methane gas with a NiO/MgO solid solution catalyst. High activity and selectivity were found with a Ni loading in the range of 12,0 – 20,5 wt%, which can remove this methane that would otherwise be released into the atmosphere. Tri-reforming, which is a combination of CO<sub>2</sub>, H<sub>2</sub>O and O<sub>2</sub> reforming in one reactor is another method to remove green house gases that was reported by Song *et al.* [2004]. This method can be used to reduce the flue gasses from fossil fuel based power plants by using the CO<sub>2</sub> for dry reforming and oxygen from the air.

**Membrane reactors:** Is another area that is receiving great attention currently, because a membrane can remove oxygen directly from the air for the catalytic partial oxidation process, which will make expensive oxygen from air separation plants unnecessary. Karton *et al.* [2005], tried to combine oxygen separation from air with the partial oxidation and methane reforming with a Fe-, Co-, Ni- and V- containing mixed conductor ceramic membrane, but found that total oxidation dominated. Research to refine this process and overcome difficulties is an ongoing process.

**Investigation of reaction mechanism:** To improve the performance of existing catalyst it is important to understand the reaction mechanism of these complex reactions over the catalyst. An example is Guo *et al.* [2004], who prepared a BaTi<sub>1-x</sub>Ni<sub>x</sub>O<sub>3</sub> series with a sol-gel method and showed that selective oxidation of methane occur with a two step mechanism over these catalysts. It was concluded that the total combustion occurs followed by the formation of carbon monoxide and hydrogen.

**The search for more efficient catalyst and fine tuning existing catalysts:** This is probably the biggest research area, which includes all areas of research above, for the catalytic selective oxidation of methane to find more efficient catalysts and may follow a trial and error approach. This area goes hand in hand with the investigation of the reaction mechanism since the example mention above [Guo *et al.*, 2004] is very much a trial and error approach to search for a more efficient catalyst combined with a mechanism investigation. There are a lot of examples in the literature with only a few shown below:

- Wang *et al.* [2004] studied Ce-promoted catalyst and found Pt/Ce<sub>0.14</sub>Zr<sub>0.86</sub>O<sub>2</sub> is more active, stable and selective than Pt/ZrO<sub>2</sub>. It also showed promise for the autothermal reforming reaction. At temperatures as low as 500°C a H<sub>2</sub>/CO ratio of 2,5 was achieved, but with a low methane conversion of 8%.

## Chapter 2 Literature Review

- Souza *et al.* [2005], who has been studying autothermal reforming over a Pt/ZrO<sub>2</sub>/Al<sub>2</sub>O<sub>3</sub> catalyst.
- Viparelli *et al.* [2005], found that a BaZr<sub>(1-x)</sub>Rh<sub>x</sub>O<sub>3</sub> perovskite catalyst experiments with short contact times gave promising results in terms of high synthesis gas yield at low Rh loading.

The focus of this research was to investigate the feasibility of the catalytic partial oxidation of methane over  $\alpha$ -bismuth molybdate which is classified as a mixed metal oxide. Catalytic partial oxidation over mixed metal oxides is an area that has not received as much attention as supported metals. The structure of mixed metal oxides will be discussed in section 2.3.

### 2.3 Selective oxidation of Propene to Acrolein

From 1959-1962 multicomponent Bi<sub>2</sub>O<sub>3</sub>.nMoO<sub>3</sub> catalysts were developed for the SOHIO process. The SOHIO process is the selective oxidation and ammoxidation of propene to make acrolein and acrylonitrile, used in industry on a large scale. These are chemicals that are widely used and in 2000 the worldwide demand for acrylonitrile alone was estimated as 5 million tons per year [Hanna 2004]. Although the simple binary bismuth and molybdenum catalysts are no longer used in industry, an understanding of their chemistry is very applicable to current catalysis. A better understanding of this very complex reaction mechanism can be used to develop new catalysts or to improve existing catalytic processes.

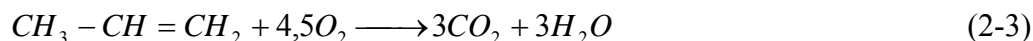
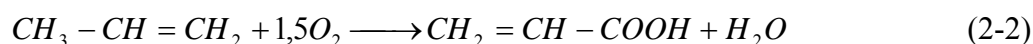
#### 2.3.1 Reaction and catalyst used

Acrolein is industrially produced by the selective insertion of an oxygen atom into the propene molecule without affecting the double bond by using a suitable catalyst (2-1).



Carbon dioxide (2-3) and acrylic acid (2-2) are the main side products that form during the reaction.





The industrial catalytic formulations for propene oxidation to acrolein are based on multicomponent metal oxides containing bismuth, molybdenum and tungsten oxides with various metals added to enhance the catalyst performance [Bettahar *et al.*, 1996]. A summary of these catalysts is given in Table 2-1.

**Table 2-2 Some active phases used in industrial catalyst for the oxidation of propene to acrolein [Bettahar *et al.*, 1996]**

Oxides	Reaction temperature (°C)	Propene conversion (%)	Acrolein selectivity (%)
Mo, Bi, Fe, Co, Ni, P, Mg	350	98	95
Mo(W)Bi Fe, Co, Ni, Si	250-450	96	90-93
Mo, Bi, Fe, Co, Ni, Sn, K	300	87	97
Bi-Mo (multicomponent)	290-350	95-99	92-96

Several studies have been done on mixed oxides based on molybdenum or antimony or on Cu<sub>2</sub>O simple oxide. Bettahar *et al.* [1996] have done a review on all these different catalysts used for the selective oxidation of propene and therefore the literature in this study is only going to focus on pure  $\alpha$ -Bismuth molybdate. Pure  $\alpha$ -Bismuth molybdate was chosen for this study because of its high activity and since the reaction is already complex for the binary mixture, no additives were added to prevent the reaction from getting more complex.

### 2.3.2 Reaction mechanism

The selective oxidation of propene to acrolein over bismuth molybdates occurs via a redox mechanism [Van Hooff, 1980]. This redox mechanism is better known as the Mars- van Krevelen mechanism which consists of two reactions. The first reaction is the reduction of the catalyst with the hydrocarbon (propene) and the second is the reoxidation reaction of the catalyst. These two reactions can be represented by the following two equations:





The electrons that are subtracted from the hydrocarbon are donated to the molybdenum atoms in the catalyst:



This has been confirmed by Ayame *et al.* [2002] who observed  $Mo^{5+}$  and  $Mo^{4+}$  cations while studying the reduction of bismuth molybdate. These electrons are then donated back to gaseous dioxygen to produce nucleophilic oxygen anions.



This section will only deal with the reduction reaction (equation 2-2) while the reoxidation reaction will be discussed in section 2.3.1.4. For 40 years a large amount of research has been done on the reaction mechanism of the selective oxidation of propene on which Hanna [2004] has done a review to determine the role of bismuth in the reaction. It was found that despite all the research that the exact mechanistic details still remain unresolved.

This controversy arises from the difficulties surrounding the complexity of the reaction mechanism. The redox reaction indicates that the reoxidation and the reduction reaction of the catalyst takes place at different sites. It is difficult to experimentally determine the exact site where and how the reactants interact with the catalyst. The catalyst performance is also highly dependent on the pre-treatment of the catalyst, the exact reaction conditions, method of preparation, purity, etc. Not only is the performance influenced by the reaction conditions, but the whole reaction mechanism is dependent on the reaction conditions. By changing a variable the whole mechanism of the reaction can change and this makes it hard to make conclusions that are correct.

Most of the intermediate components of the reaction mechanism have been determined using deuterium labelling and  $^{18}O_2$  studies. The steps for activation of propene and the formation of the acrolein can be given as:

- Initial coordination of the propene molecule
- Activation of the propene molecule to form an allylic species (H abstraction)
- Oxygen diffusion through the catalyst
- Insertion of the oxygen into the propene molecule

## Chapter 2 Literature Review

- Abstraction of the second hydrogen to form acrolein

The first step before the propene molecule can be activated is the coordination of the propene molecule on the catalyst surface. Evidence from the literature for initial coordination at a molybdenum site is stronger than that for coordination at a bismuth site [Hanna 2004]. The coordination of the propene molecule can be illustrated by Figure 2-1.

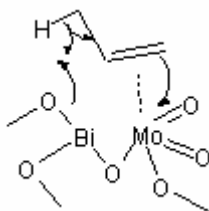


**Figure 2-6 Coordination of propene by molybdenum [Hanna, 2004]**

The hydrogen atom of an olefin on the carbon next to the double bond (alpha position) can be relatively easily removed leading to an allylic structure that is very stable [Van Hooff, 1980]. After the propene is coordinated the first step of the formation of acrolein is the formation of a symmetric allylic species. This species is formed by a combination of a redox and an acid-base step [Bettahar *et al.*, 1996]. The acid-base step is where the alpha hydrogen (proton) of the propene is removed by a basic site to form a radical. This propene radical is then oxidized to form a  $\pi$ -allyl cation on a redox active site. In the review article by Hanna [2004] it was confirmed that the  $\text{Bi}^{\text{III}}$  site is responsible for this activation of the propene molecule. Different possible mechanisms have been identified for this activation (Figure 2-2), but no experiments that have been done could distinguish between these different mechanisms. The abstraction of the hydrogen has been determined as the rate limiting step in the reaction by using isotope labelling experiments [Van Hooff, 1980]. These labelling experiments also showed that the allylic species is symmetrical and that the oxygen can be inserted on both sides of the propene molecule to form acrolein. After the proton is removed from the  $\text{CH}_3$  group and attached to a surface oxygen, the resulting carbanion binds via a  $\pi$ -bonding to a transition metal, molybdenum in this case. The  $\pi$ -bonding takes care of the equivalence of the terminal C-atoms while the interaction between the p-orbitals of the allyl and the d-orbitals of the transition metal cause the allyl to bond to the surface. The redox reaction occurs by a transfer of electrons between the transition metal and the bonded species.



high temperatures the Bi-O bond length increases which results in a decrease of the bond strength and the migration of oxygen anions thus becomes easier.

Uncertainty still remains regarding the question of whether the acrolein oxygen originates from a Bi- or a Mo-bounded oxygen [Hanna 2004]. After this oxygen has been inserted and a  $\delta$ -allylic species has formed, the second hydrogen should be abstracted to form acrolein. This step is also still unclear, but it is suggested that the same bismuth site that is responsible for the first abstraction is also responsible for the second hydrogen abstraction [Hanna 2004].

The formation of non-selective oxidation products is the result of electrophilic oxygen species and will therefore be discussed in section 2.3.1.4 together with the reoxidation of the catalyst.

### 2.3.2.1 Reoxidation mechanism and redox cycle

Since the selective oxidation of propene occurs via a redox mechanism, the catalyst needs to be reoxidized. More mechanistic studies have been done on the activation of propene and the formation of the acrolein molecule than on the reoxidation mechanism. The redox reaction occurs in a cycle that is illustrated in Figure 2-7.

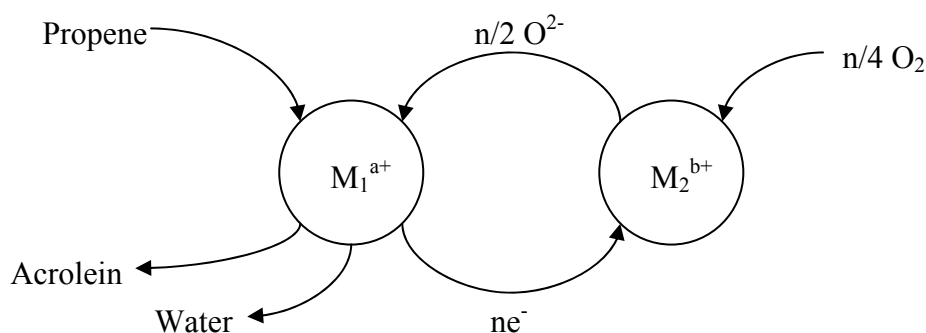


Figure 2-8 Redox cycle [Libre *et al.*, 1983]

The redox reaction occurs simultaneously at two sites. The first site ( $M_1$ ) is where the propene is oxidized to the selective oxidation product while the catalyst is reduced. The second site ( $M_2$ ) is where the reoxidation of the catalyst takes place during this process. Electrons flow from  $M_1$  to  $M_2$  while the nucleophilic oxygen anions diffuse from  $M_2$  to  $M_1$  through vacancies in the catalyst bulk [Libre *et al.*, 1983]. The precise mechanism of propene

oxidation to acrolein over bismuth molybdates has been described in section 2.2.2 and therefore will not be covered in this section again.

The reoxidation cycles for the selective oxidation and ammoxidation of propene over  $\alpha$ -Bismuth molybdate are displayed in Figure 2-8. In the figure it can be seen that the mechanism for the propene activation and acrolein formation are displayed completely, but the details of the reoxidation (from species E to A) is left out.

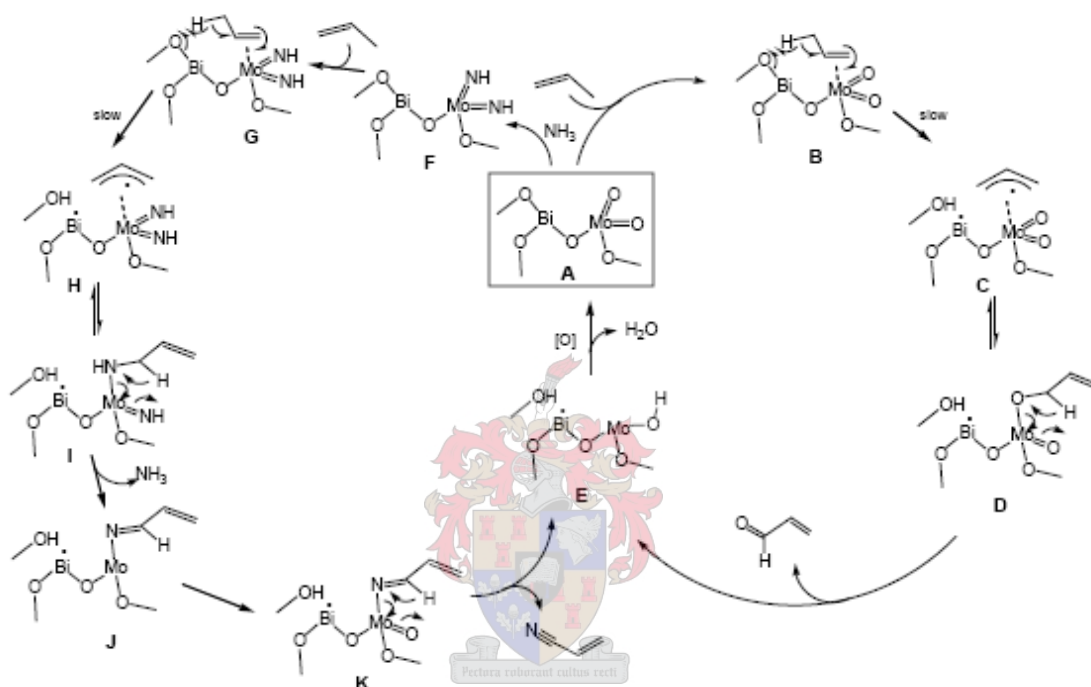


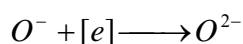
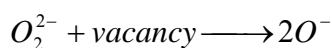
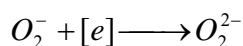
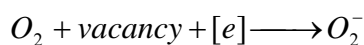
Figure 2-9 Graselli's proposed mechanism for the SOHIO process [Hanna, 2004]

The physical reoxidation of the catalyst can be divided into the adsorption of the gaseous oxygen, electron transfer to the oxygen and the diffusion of the nucleophilic oxygen anions through the catalyst bulk. It was shown by Ayame *et al.* [2002] that the site where the chemisorption and the dissociation of the oxygen molecules occur are spatially and structurally distinct from the active sites at which the adsorption and oxidation of the propene take place, which is in agreement with the model in Figure 2.7. There are not necessarily one available pathway for the reoxidation of the bismuth molybdates, but Hanna [2004] showed with spectroscopic studies that the Mo-O-Bi bridging oxygen sites are the most active sites where this reoxidation of the catalyst occurs.

During the reoxidation process different oxygen anions are involved, which are the result of electron transfer reactions. The nucleophilic oxygen anions that are responsible for the

## Chapter 2 Literature Review

selective oxidation products are not formed directly from the gaseous dioxygen molecules, but via electrophilic oxygen anions which are formed by the mentioned electron transfer reactions. These reactions were summarized by Van Hooff [1980] as four basic steps:



The electrophilic oxygen species ( $O_2^-$ ,  $O_2^{2-}$  and  $O^-$ ) formed in the steps above are responsible for the formation of the non-selective oxidation products, while the nucleophilic oxygen ( $O^{2-}$ ) are responsible for the selective oxidation products. The steps above, as well as the oxygen diffusion through the catalyst bulk, are illustrated in Figures 2-9 and 2-10 by Haber *et al.* [2000].

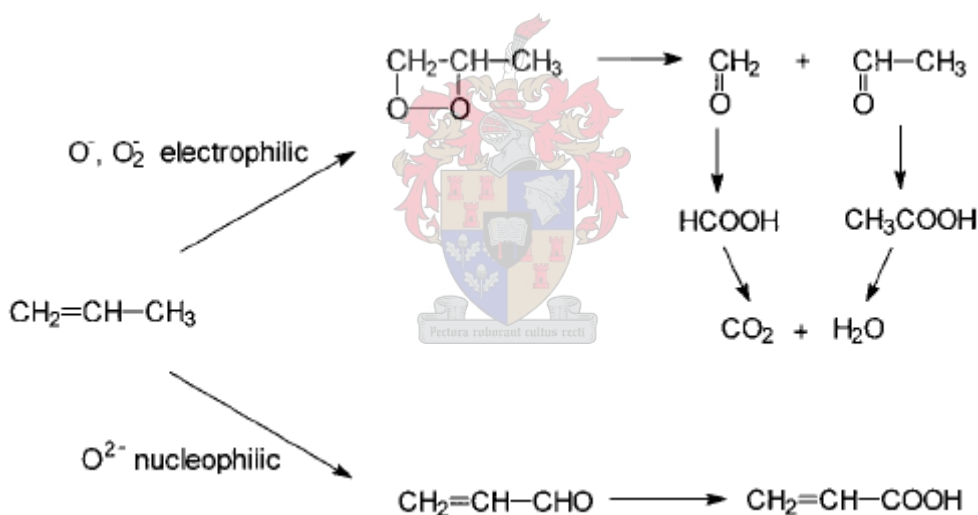


Figure 2-10 Effect nucleophilic and electrophilic oxygen attacks [Haber *et al.* 2000]

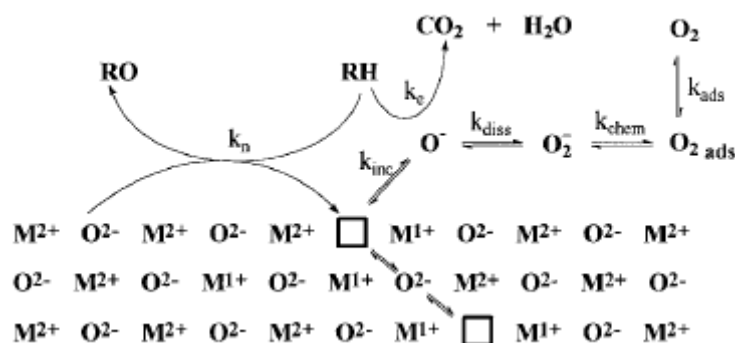


Figure 2-11 General mechanism of olefins reaction over oxide catalysts [Haber *et al.* 2000]

## Chapter 2 Literature Review

Libre *et al* [1983] found that at high temperatures the oxygen anions diffuse easier through the catalyst bulk. This was explained by a decrease of the bond strength which is the result of the Bi-O length that increases with an increase in temperature.

Magagula and Van Steen [1999] showed that these electrophilic species can be studied by time on stream experiments. They showed that there are more electrophilic species on the surface of  $\gamma$ -Bismuth molybdate at the beginning of the reaction than at steady state. It was shown that the selectivity for acrolein increased strongly with time on stream for the  $\gamma$ -Bismuth molybdate, while the activity decreased strongly. This might explain the interesting observation that was made by Graselli *et al.* [1980<sup>a</sup>] that different reoxidation energies are observed depending on the initial degree of catalyst reduction.

The general questions regarding the reoxidation of  $\alpha$ -Bismuth molybdate that arise from the literature review are:

- How exactly does the oxygen diffuse through the catalyst bulk?
- What are the details regarding the reoxidation process (electron transfer diagrams)?
- How do the non-selective oxidation products form (mechanism)?

What is the cause of the reoxidation rate limiting step during the reoxidation of the catalyst in the low temperature region?



### **2.3.3 Mars van Krevelen reaction mechanism for the selective oxidation propene to acrolein over $\alpha$ -Bismuth molybdates**

Experiments done in the past have confirmed [Keulks *et al.* 1980; Bettahar *et al.* 1996; Fansuri 2005] that the selective oxidation of propene to acrolein over bismuth molybdates occurs via the Mars-van Krevelen mechanism. During the most recent study done on pure  $\alpha$ -Bismuth molybdate by Fansuri [2005], this has been reconfirmed and the Langmuir-Hinshelwood and the Eley-Rideal mechanism were ruled out for this reaction.

The Mars-van Krevelen mechanism implies that the reaction occurs via a redox mechanism where the lattice oxygen of the catalyst is inserted into the propene, while the gaseous oxygen reoxidizes the catalyst by replacing this used lattice oxygen. According to the model the rate of propene consumption (reduction reaction) is a function of the propene partial pressure ( $P_p$ )

## Chapter 2 Literature Review

and the fraction of catalyst active sites that are filled with nucleophilic oxygen ( $\theta$ ). This can be represented by equation 2-6 [Keulks *et al.* 1980].

$$-r_p = k_p P_p^n \theta \quad (2-6)$$

The oxidation reaction can then be represented by the gaseous oxygen partial pressure ( $P_{O_2}$ ) and the fraction of the reduced catalyst active sites ( $1-\theta$ ). This is shown mathematically by equation 2-7.

$$-r_{O_2} = k_o P_{O_2}^m (1-\theta) \quad (2-7)$$

From the overall stoichiometry ( $2 \text{ Propene} + O_2 \rightarrow 2 \text{ Acrolein}$ ) the following relationship between the rates of propene and oxygen consumption can be deduced:

$$r_p = 2r_{O_2} \quad (2-8)$$

Technically this is not correct because side products like carbon dioxide, acrylic acid, etc. form, which will affect the overall reaction rates. However, since these side products are formed in lower amounts, it was assumed that equation 2-8 applies. By substituting equation 2-6 and 2-7 into equation 2-8 the surface coverage  $\theta$  can be determined (equation 2-9).

$$\theta = \frac{2k_o P_{O_2}^m / k_p P_p^n}{1 + (2k_o P_{O_2}^m / k_p P_p^n)} \quad (2-9)$$

Equation 2-9 can now be substituted back into equation 2-6 and simplified to get an expression for the rate of propene consumption (equation 2-10).

$$-r_p = \frac{1}{\frac{k_p}{2k_o P_{O_2}^m} + \frac{1}{P_p^n}} \quad (2-10)$$



### 2.3.3.1 Reported reaction orders for the selective oxidation of propene to acrolein over $\alpha$ -Bismuth molybdate

From equation 2-11 and 2-12 it can thus be concluded that the rate of propene consumption is the only parameter that needs to be studied to get an understanding of the reoxidation and reduction process of bismuth molybdates. However, nowhere in the literature the reaction orders for propene and oxygen are given for the conversion of propene for the selective oxidation of propene to acrolein over pure  $\alpha$ -Bi<sub>2</sub>Mo<sub>3</sub>O<sub>12</sub>. The only activation energy (120 kJ/mol) and reaction orders for propene conversion in the reoxidation limited region that were found were that of an industrial multicomponent bismuth molybdate [Redlinghöfer *et al* 2003]. The reaction orders at the different temperatures can be seen in Table 2-3.

**Table 2-3 Reaction orders for propene conversion over an industrial multicomponent bismuth molybdate [Redlinghöfer *et al* 2003]**

Temperature [°C]	$n_{\text{propene}}$	$n_{\text{oxygen}}$
330	0.00	0.86
350	0.00	0.93
360	0.96	0.49
370	0.92	0.00

Keulks *et al.* [1980] reported the propene and oxygen reaction orders for acrolein and carbon dioxide formation. These reaction orders can be seen in Table 2-4. Keulks *et al.* [1980] stated that the reaction order of oxygen at low temperatures was determined to be zero, because it was failed to examine low oxygen partial pressures. These low partial pressures should be examined.

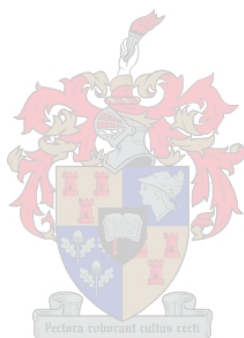
**Table 2-4 Reaction orders for acrolein and carbon dioxide formation over  $\alpha$ -Bi<sub>2</sub>Mo<sub>3</sub>O<sub>12</sub> [Keulks *et al* 1980]**

Temperature [°C]	Acrolein formation		Carbon dioxide formation	
	$n_{\text{propene}}$	$n_{\text{oxygen}}$	$n_{\text{propene}}$	$n_{\text{oxygen}}$
325	0.0	0.0	0.0	0.4
350	0.0	0.0	0.0	0.4
375	0.7	0.0	0.7	0.4

## 2.4 Conclusions from Literature

From the literature it was seen that there is a need for an economic low temperature synthesis gas production unit. The catalytic partial oxidation of methane is a possible way to achieve this economic synthesis gas production at low temperatures. The literature also showed that the selective oxidation of methane over mixed metal oxides has received very little attention, but that it might be possible to produce synthesis gas from methane with  $\alpha$ -Bismuth molybdate.

In the literature it was also seen that some questions regarding the reoxidation of bismuth molybdates during selective oxidation reactions are still unanswered.



## Chapter 3 Experimental design

In this chapter the experimental setup that was used is described together with the limitations of the experiments. The different experiments that were conducted as well as the analytical techniques are also described.

### 3.1 Experimental Setup

#### 3.1.1 Reactor rig

A schematic diagram of the reaction apparatus used, including mass flow controllers, control valves, pressure gauges, an ampoule sampler with a septum and micro-reactors suspended in an oven is shown in Figure 3.1. The rig can support up to five micro-reactors in series which can be used to give an indication what happens at different points in the catalyst bed. Three-way valves were installed to enable the rig to operate between one and five of these reactors. There was also a four-way valve that could be used to bypass the reactors and let the reactants vent into the atmosphere, while helium flowed through the catalyst bed. All the tubing upstream of the reactors was constructed from 1/8" stainless steel tubing to reduce the pressure drop across the tubing. The tubing after the reactors was constructed from 1/16" stainless steel which ensures turbulent flow and reduces the hold-up and therefore limited homogeneous reactions in the product stream. Since acrolein is a solid at room temperature, the tubing down stream of the reactors was heated with heating wire to prevent the condensation of the products in this tubing. The feed to the reactors was controlled by four calibrated mass flow controllers that could control the reactants very accurately. (The calibration of these mass flow controllers can be seen in appendix A) An ampoule sampling point was installed in the product stream, which made it possible to take a small sample of the product stream at any time interval without disturbing the reaction upstream. The rest of the product stream was vented to the atmosphere after it was bubbled through a water and nitric acid solution to dissolve the acrolein.

The feed stream consisted of helium, oxygen, ethane and methane or propene. The helium was used to dilute the feed and to control the partial pressures of the reactants (oxygen, propene or methane) during the reaction. Nitrogen or argon could also be used for this

## Chapter 3 Experimental design

purpose, but helium was chosen because the helium was also used as the carrier gas in the gas chromatograph. A known amount of ethane was added to the feed stream after the reactors to act as an internal standard. This internal standard was used to determine the exact amount of each compound in the product stream.

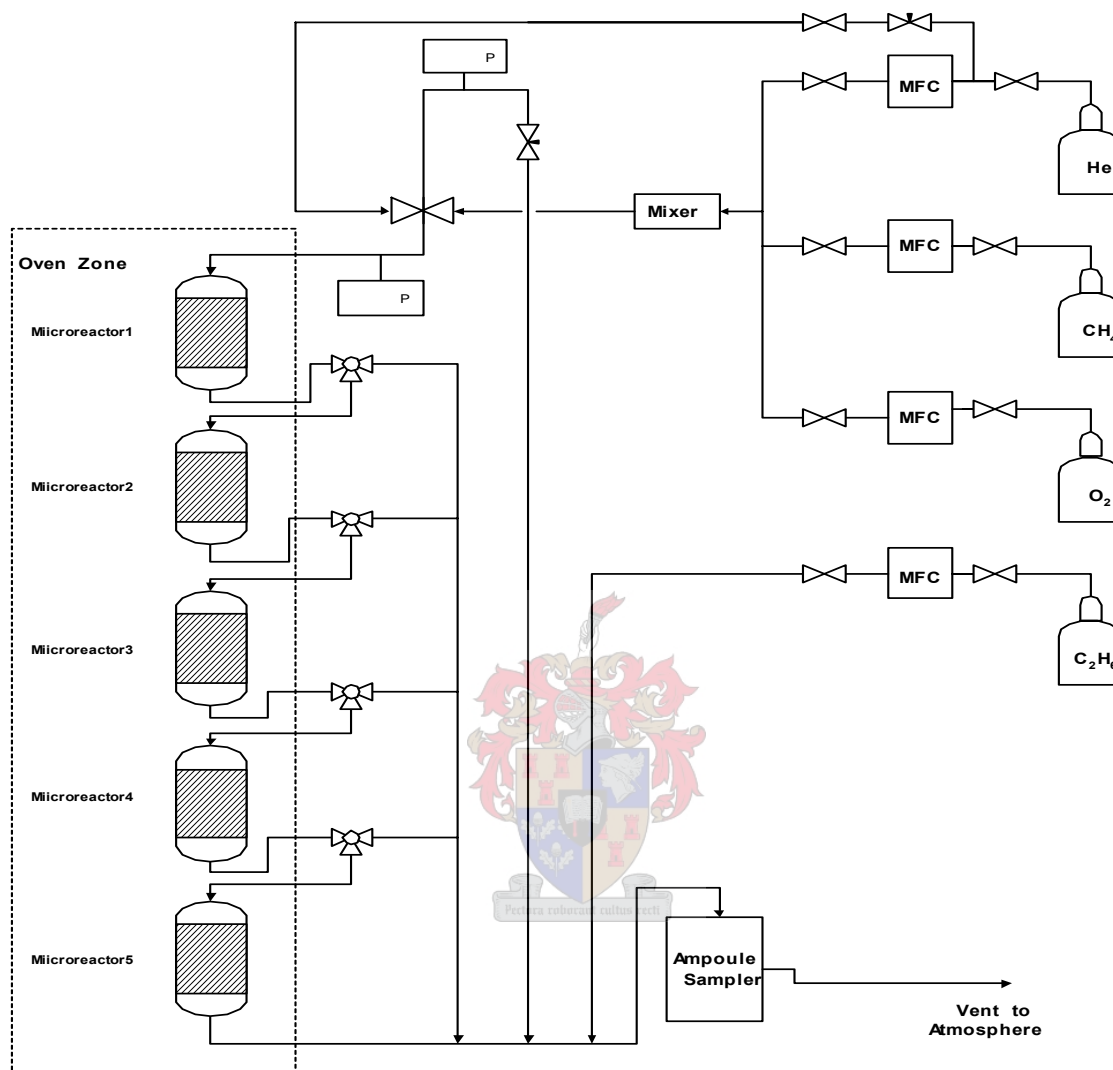


Figure 3-1: Flow diagram of the reactor rig

### 3.1.2 Procedure for conducting experiments on reactor rig

The first step in conducting a reaction run was to calculate the catalyst mass that had to be used for each run to achieve the desired weight hourly space velocity (WHSV). The flow rate of the propene was kept constant and therefore the mass of catalyst was changed to change the WHSV. This was done to ensure that the partial pressures of the reactant streams did not change for different WHSV. While the oven was heating up pure oxygen was passed over the catalyst to ensure that the catalyst was fully oxidized when the reaction was started.

After the oven had reached the desired temperatures the four-way valve was used for the feed stream to bypass the reactors while helium purged the catalyst bed. This made it possible to set the mass flow controllers to the desired set points before the reaction was started, which was necessary to conduct short time transient kinetic experiments. The helium in the balance line which was used to purge the catalyst bed was controlled with a needle valve. Pressure gauges were mounted before the reactors and in the balance line to see if there was a pressure difference across the catalyst bed and to check that the pressure drop over the reactor and bypass lines was the same. This difference was reduced by turning the needle valve in the balance line before the four-way valve was turned to start the reaction. Sampling was done at short time intervals using evacuated glass ampoules.

### 3.1.3 Ampoule sampling

An ampoule is an evacuated glass tube with a very thin tip. In the product stream leaving the reactors an ampoule sampling unit was mounted. This ampoule sampling unit consisted of a rubber septum through which the ampoule tip was passed and a metal fork which could be turned to break the tip of the ampoule. The metal piece of the ampoule sampling unit was turned at the reaction time when the sample was wanted. This broke the thin tip of the ampoule which sucked a small sample of the product stream into the ampoule. The ampoule tip was then resealed and the ampoule kept for later analysis. This type of sampling was chosen because the gas chromatograph used for the analyses took 20 minutes to analyze one sample which made on-stream analyzes for transient kinetics, where sampling should be done over small time intervals (30s), impossible.

### 3.1.4 Micro-reactor

Van Vuuren [2004] evaluated two types of reactors, namely glass and metal reactors. Glass reactors were initially chosen because of their transparency and their formability. A layer of catalyst particles were distributed uniformly on a fine sinter frit to ensure even reaction rate and a low pressure drop. The metal reactor was made from stainless steel 316. The reactor was packed with a layer of glass wool, followed by a layer of silicon carbide particles on which the catalyst was placed. Van Vuuren [2004] found that the metal reactor gave much

## Chapter 3 Experimental design

better results than the glass reactor since it was catalytically inactive for the selective oxidation of propene to acrolein. The metal reactor was also found to be more robust and easier to work with. For this reason a similar stainless steel micro-reactor was constructed and tested before and after the stainless steel was treated with pickling gel as mentioned by Van Vuuren [2004].

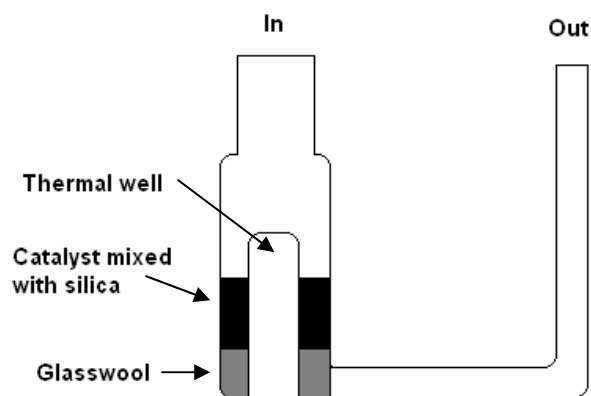


Figure 3-2: Schematic of micro-reactor used

However it was found that a blank metal reactor gave high conversions for propene and no conversion for methane. The conversion of propene to carbon oxides over stainless steel has been reported at 360°C by Fansuri [2005]. These stainless steel reactors were used for the selective oxidation studies for methane, but glass reactors were used for the propene reactions. These glass reactors did not have sinter glass like the ones used by Van Vuuren [2004] and the internal volume was also smaller to reduce the homogenous reactions observed by Van Vuuren. The catalyst particles were mixed with quartz in the mass ratio 1:5 for all the reactions and were placed in the glass reactor on top of a piece of glasswool to prevent the particles from being blown out of the reactors. A thermocouple was inserted into a thermo well inside the catalyst bed to measure the temperature of the bed more accurately.

It was decided to use the glass reactors for the propene reactions because they are much cheaper than the stainless steel reactors and because the propene conversions are lower in the glass reactors.

### 3.1.5 Gas analysis

The samples gathered by using the ampoule sampling technique was analyzed using a Varian CP-3380 gas chromatograph (GC) fitted with an ampoule breaker. After the ampoule

## Chapter 3 Experimental design

containing a sample was placed in the ampoule breaker the air was purged out of the ampoule breaker with helium. The gas chromatograph was then given time to stabilize (drifting in TCD voltage output stopped) which took 35 minutes. After 35 minutes, the ampoule was broken with a metal rod that slides down and crushes the ampoule in the ampoule breaker, releasing the sample. The analysis then took 20 minutes to complete.

The GC was fitted with two columns and two analysers. The analyzers that were used were a TCD and a FID. The column for the FID was a Supelco. custom column 031 92004; Packed with 80/100 Tenax TA in a 6 ft x 1/8 inch stainless steel column. The TCD was fitted with a 6 m stainless steel column with an internal diameter of 2 mm packed with Hayesep D with a mesh range of 80/100. The temperature program for the GC oven started at 70°C and held for a minute before it ramped at 7°C/min to 180°C where it was held for 10 minutes.

The more accurate FID was used to analyze most components, but the TCD was needed to detect compounds, e.g. CO<sub>2</sub>, which do not show up on the FID.

### 3.2 Preparation of $\alpha$ -Bismuth Molybdate

The catalyst was prepared by the coprecipitation method which was developed by Keulks *et al.* [1974]. This method was developed specifically to enable researchers to reproduce pure  $\alpha$ -Bismuth molybdate for research purposes. A summary of the method can be given as follows:

- 15,895g (NH<sub>4</sub>)<sub>6</sub>Mo<sub>7</sub>O<sub>24</sub>·4H<sub>2</sub>O was dissolved in 200mL distilled water
- The solution was acidified to a pH of 1,5 by slowly adding concentrated nitric acid while the solution was vigorously stirred
- A white precipitate formed which was allowed to stand for an hour
- 29,102g Bi(NO<sub>3</sub>)<sub>3</sub>·5H<sub>2</sub>O were dissolved in 55mL 55wt% nitric acid
- After dissolution, 1075mL distilled water were added
- The bismuth nitrate solution was added very slowly (over approximately 4 hours) to the aged molybdate solution while the solution was continuously stirred with an electric stirrer
- The pH of the molybdate solution was kept at 1,5 by back titrating with concentrated ammonium hydroxide

## Chapter 3 Experimental design

- After the addition of the bismuth nitrate was finished the precipitate and the mother liquor were allowed to stand for 20 hours
- The solution was then filtered and the precipitate was collected in a crucible
- The crucible was placed in an oven and the precipitate was dried for 2 hours at 115°C
- The precipitate was then calcined at 200°C for 5 hours and then at 375°C for 9 hours

## 3.3 Experiments

### 3.3.1 Preliminary experiments

Before the experiments were conducted preliminary experiments had to be conducted to ensure that the experiments were as accurate as possible. These experiments included calibration of the mass flow controllers and thermocouples, determining of the GC response factors, reactor residence time distribution, blank reactor runs and catalyst characterisation.

The calibration of the mass flow controllers was done with a bubble flow meter and a stop watch while the thermocouple was calibrated using a water bath on a heating plate and a thermometer. The results for these calibrations can be seen in appendices A and C respectively. The calculation of the different response factors is explained in section 3.4, while the results can be seen in appendices B.

Blank reactor runs were done to determine the degree of homogeneous propene and methane reactions that occurs in the different micro reactors. The blank reactor runs were done over a temperature range of 25 to 400°C for the metal and the glass reactors, which were filled with the same amount of silica that was used for the actual reactions with catalyst. Runs were also done without a reactor in the heating zone to determine the homogeneous reactions in the reactor rig tubing. The different runs that were conducted are displayed in Table 3-1.



## Chapter 3 Experimental design

**Table 3-1 Blank reactor runs with Hydrocarbon:Oxygen:Helium = 1:2:7; Hydrocarbon flow rate = 0.24 mmole/min; Quartz inside reactor = 0.4 g**

Hydrocarbon	Temperature [°C]	Type of reactor
Methane	25	Metal
Methane	400	Metal
Propene	325	Glass
Propene	350	Glass
Propene	375	Glass

The residence time distribution of the glass reactors were determined to calculate if the flow through the reactors was plug flow at the chosen reaction conditions. Plug flow is required when reaction kinetics of a catalytic reaction are studied to insure that the kinetic data determined by the reactions are correct. The residence time distribution studies were done by using propene as a step input through the micro reactor used for the experiments. The reactor exit was connected to the TCD of the GC to measure the propene distribution that came out of the reactor versus the time. This distribution was determined at room temperature and at 400°C for two flow rates (Table 3-2). This was done to get an indication of the effect of the flow rate and the temperature on the flow of the reactants through the reactor. A step input was also done without a reactor by connecting the reactor input directly with the tubing that was connected to the TCD to determine the residence time in the system.

**Table 3-2 Conditions for which the RTDs were determined**

Flow rate [ml/s]	Temperature [°C]	Reactor
60	27	Glass
75	27	Glass
60	340	Glass
75	340	Glass
60	27	No Reactor
75	27	No Reactor

From the RTD data the nature of the flow of the reactor was calculated. The calculations are explained in appendix D and discussed in section 4.1.1.1.

The catalyst was also characterized to ensure that the catalyst that was prepared was  $\alpha$ -Bismuth molybdate. The catalyst phase was determined using X-ray diffraction (XRD). To understand the mass transfer results the surface area of the catalyst and the porosity of the catalyst particles was measured using BET.

### 3.3.2 Methane

Since the selective oxidation of methane over alpha bismuth molybdate has never been attempted before, a range of reaction conditions were examined to determine if the reaction is possible at atmospheric pressures. These reaction conditions are displayed in Table 3-3.

**Table 3-3 Experiments done to determine if methane can be activated by  $\alpha$ -Bismuth molybdate**

Reaction no.	CH <sub>4</sub> /O <sub>2</sub> /He Ratio	Catalyst Mass [g]	Temp. [°C]	WHSV [g <sub>m</sub> /(g <sub>cat</sub> ·h)]
1	1/1/11	0.100	321	1.88
2	1/1/4	0.052	423	10.34
3	1/2/4	0.120	452	4.50
4	1/2/2	0.570	466	1.00
5	1/2/1	0.300	433	2.00
6	1/2/1	0.300	499	2.00

### 3.3.3 Propene

#### 3.3.3.1 External mass transfer limitations

Kinetic experiments must be done at a linear velocity where external mass transfer limitations across the boundary layer do not occur. Therefore tests (Table 3-4) were done at different linear velocities through the catalyst bed. The linear velocity was changed by increasing the reactant mass flow rate and the mass of catalyst proportionally to keep the WHSV the same. If there are no mass transfer limitations, the rate of reaction will be the same for the different linear velocities of reactants through the catalyst bed. The tests were done at a WHSV of 3 g<sub>Propene</sub>/(g<sub>cat</sub>·h) and a temperature of 325°C. 325°C was chosen because this is the lowest temperature where the kinetic experiments were done and it was assumed that at the lowest temperature the diffusion coefficient for the boundary layer will be the lowest [Fogler 1999]. Therefore if there are no mass transfer limitations at this temperature there will be no mass transfer limitations at higher temperatures. For the experiments in Table 3-4, samples were taken before the run was started, at 5, 10, 20, 40, 60, 90 and at 120 minutes.

**Table 3-4 External mass transfer limitation experiments**

Sequence	Catalyst Mass [g]	Bed pressure [bar]	Temp. [°C]	MFC C <sub>3</sub> H <sub>6</sub> [mmol/min]	MFC O <sub>2</sub> [mmol/min]	MFC He [mmol/min]
Run 26	0.204	1.45	325	0.238	0.476	1.663
Run 27	0.249	1.55	325	0.298	0.595	2.081
Run 29	0.154	1.35	325	0.179	0.357	1.250

### 3.3.3.2 Internal mass transfer limitations

To test for internal mass transfer limitations the rate of reaction for different particle sizes must be the same. Different catalyst particle sizes were obtained by sieving the catalyst with a particle sieve. Because of a limited amount of catalyst only a small amount of catalyst was sieved and therefore only a small mass of catalyst could be packed into the reactor. The particle size fractions were particles between 150 – 250  $\mu\text{m}$  and smaller than 150  $\mu\text{m}$ . Runs were done with these different sizes for a WHSV of 3  $\text{g}_{\text{Propene}}/(\text{g}_{\text{cat}}\cdot\text{h})$  and a temperature of 325°C (Table 3-5). 325°C was chosen for the same reason as for the external mass transfer limitations. For the experiments in Table 3-5, samples were taken before the run was started, at 10, 40, 60 and at 90 minutes.

**Table 3-5 Internal mass transfer limitation experiments**

Sequence	Catalyst Mass [g]	Bed Pressure [bar]	Temp. [°C]	MFC C <sub>3</sub> H <sub>6</sub> [mmol/min]	MFC O <sub>2</sub> [mmol/min]	MFC He [mmol/min]	Particle size ( $\mu\text{m}$ )
Run 30	0.154	1.39	325	0.179	0.357	1.250	150-250
Run 31	0.155	1.39	325	0.179	0.357	1.250	<150

Run 31 was repeated twice to see if the smaller particles deactivated by losing their lattice structure during regeneration. Between the repeat runs, the catalyst was reoxidized with pure oxygen.

### 3.3.3.3 Kinetic experiments of the selective oxidation of propene to acrolein

It was decided to only investigate the low temperature region of the selective oxidation of propene to acrolein where the reoxidation reaction is the rate limiting reaction. A three by three factorial design (Tables 3-6 and 3-7) was used with the propene to oxygen partial pressure ratio and the temperature as the two factors. 325, 350 and 375°C were chosen as the three temperature levels and 0.5, 0.75 and 1.00 were chosen as the propene to oxygen ratios. The partial pressure ratio was changed by keeping the flow rate of propene constant and changing the oxygen flow rate. The helium flow rate was also changed to keep the total molar flow rate the same for all reactions and in this way keeping the partial pressure of propene constant. The experiments were carried out in random order; the sequence is shown in Tables 3-6 and 3-7, to avoid biased data.

No transient study of the selective oxidation of propene has been carried out before and therefore it is not known what happens during the start up of the catalytic reaction. In order to see what happens in the first hour and a half fourteen samples were taken for each run. The first sample was taken while bypassing the reactor, before the run was started to calculate the carbon balance of each sample. The other samples were taken at: 2, 4, 6, 8, 10, 12, 15, 17, 20, 35, 45, 60 and 90 minutes.

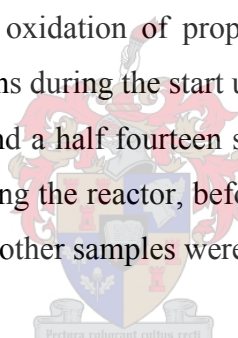


**Table 3-6 Transient kinetic experiments for a WHSV of 3 g<sub>Propene</sub>/(g<sub>cat</sub>.h)**

Number	Temp	Ratio o/p	Sequence	MFC C <sub>3</sub> H <sub>6</sub> [mmol/min]	MFC O <sub>2</sub> [mmol/min]	MFC He [mmol/min]
1	325	1	Run 38	0.239	0.238	1.905
2	325	1.333	Run 46	0.239	0.319	1.826
3	325	2	Run 42	0.239	0.476	1.663
4	350	1	Run 44	0.239	0.238	1.905
5	350	1.333	Run 47	0.239	0.319	1.826
6	350	2	Run 36	0.239	0.476	1.663
7	375	1	Run 43	0.239	0.238	1.905
8	375	1.333	Run 45	0.239	0.319	1.826
9	375	2	Run 37	0.239	0.476	1.663

Since the kinetic studies were carried out under reaction conditions where the propene conversions were too high (>5%) to qualify as differential reactor data more WHSV data were needed to model this data. Therefore reactions were also done with a WHSV of 2 and 5 g<sub>Propene</sub>/(g<sub>cat</sub>.h) for each of the reaction conditions at steady state conditions. The WHSV was changed by changing the mass of catalyst in the reactor to keep the partial pressures of the

## Chapter 3 Experimental design

reactants in the feed stream the same as in the transient kinetic studies. A sample was taken before each run and two samples were taken at each reaction condition at steady state. Based on the transient kinetic studies it was assumed that steady state was reached after 30 minutes.

**Table 3-7 Experiments for different WHSV of 2 and 5 g<sub>Propene</sub>/(g<sub>cat</sub>·h)**

Number	Temp	Ratio o/p	Sequence	MFC C <sub>3</sub> H <sub>6</sub> [mmol/min]	MFC O <sub>2</sub> [mmol/min]	MFC He [mmol/min]	WHSV g <sub>Propene</sub> /(g <sub>cat</sub> ·h)	Catalyst Mass [g]
10	325	1	Run 51	0.239	0.238	1.905	2	0.3
	325	1.333		0.239	0.319	1.826		
	325	2		0.239	0.476	1.663		
11	325	1	Run 54	0.239	0.238	1.905	5	0.15
	325	1.333		0.239	0.319	1.826		
	325	2		0.239	0.476	1.663		
12	350	1	Run 50	0.239	0.238	1.905	2	0.3
	350	1.333		0.239	0.319	1.826		
	350	2		0.239	0.476	1.663		
13	350	1	Run 55	0.239	0.238	1.905	5	0.15
	350	1.333		0.239	0.319	1.826		
	350	2		0.239	0.476	1.663		
14	375	1	Run 52	0.239	0.238	1.905	2	0.3
	375	1.333		0.239	0.319	1.826		
	375	2		0.239	0.476	1.663		
15	375	1	Run 53	0.239	0.238	1.905	5	0.15
	375	1.333		0.239	0.319	1.826		
	375	2		0.239	0.476	1.663		

### 3.4 Calculation of products from GC data

The gas samples were analyzed using a gas chromatograph. The amount of propene in the product stream was determined by looking at the peak sizes of the ethane (internal standard) and the propene. The ratio of these two peaks was multiplied with a response factor to determine the molar ratio of the two compounds and because the amount of ethane in the sample was known, the amount of propene could be calculated (see equation 3-1). The response factor (RSF) was determined by analyzing a number of different binary mixture samples with known amounts of propene and ethane (see appendix B).

$$n_{\text{Propene}} = \text{RSF} \cdot \frac{\text{Area}_{\text{Propene}}}{\text{Area}_{\text{Ethane}}} \cdot n_{\text{Ethane}} \quad (3-1)$$

The carbon dioxide, acrylic acid and acrolein concentrations were determined in the same way. The response factor for carbon dioxide was also determined using a known amount of

### Chapter 3 Experimental design

carbon dioxide (appendices B), but the response factors for acrylic acid and acrolein were determined theoretically due to the instability of these molecules. The correction factor for an area measured with an FID can be calculated with equation 3-2 [UCT class notes].

$$f_{0,i} = \frac{N_{Ci}}{N_{C(No\ O)} + 0,55.N_{C(O)}} \quad (3-2)$$

With:  $f_{0,i}$  : Area correction factor for organic compound i  
 $N_{Ci}$  : Number of carbon in molecule  
 $N_{C(O)}$  : Number of carbon connected to 1 oxygen with 1 single bond  
 $N_{C(No\ O)}$  : Number of carbon not connected to oxygen

It should be noted that the correction factor calculated with equation 3-2 is carbon based and therefore the amount of carbon in the molecules must be used to determine the amount of acrolein and acrylic acid. Equation 3-1 thus becomes equation 3-3 to determine the amount of acrolein and acrylic acid.

$$3n_{Acrolein} = RSF \cdot \frac{Area_{Acrolein}}{Area_{Ethane}} \cdot 2n_{Ethane} \quad (3-3)$$



With the response factor calculated with equation 3-4 (calculate  $f_{0,acrolein}$  and  $f_{0,ethane}$  by substitution of the relative values into equation 3-2):

$$RSF = \frac{f_{0,acrolein}}{f_{0,ethane}} = f_{0,acrolein} \quad (3-4)$$

**Table 3-8 Response factors for different compounds**

Compound	Response factor (RSF)
Propene (TCD)	0.692
Propene (FID)	0,628
Carbon dioxide	1,317
Acrolein (carbon based)	1,500
Acrylic Acid (carbon based)	1,500

### Chapter 3 Experimental design

Since the detector could not pick up the oxygen and the water in the sample these two compounds were calculated using a mass balance. For this mass balance it was assumed that all the hydrogen atoms that were removed from the propene molecule reacts with oxygen to form water. From this assumption Table 3-9 can be derived:

**Table 3-9 Mass balance for propene conversion**

Reactant	Product	H released	O <sub>2</sub> consumed
Propene	Acrolein	2	0,5
Propene	3 CO <sub>2</sub>	6	4,5
Propene	Acrylic acid	2	1,5

Using the mass balance in Table 3-9 equations can be derived to calculate the amount of oxygen (3-6) consumed and water (3-5) that were present in the sample.

$$n_{H_2O} = n_{Acrolein} + 3n_{CO_2} + n_{Acrylicacid} \quad (3-5)$$

$$n_{O_2} = n_{Acrolein} + 1,5n_{CO_2} + 1,5n_{Acrylicacid} \quad (3-6)$$

The carbon balances of the experiments were calculated with equation 3-7.

$$Carbon\ balance\ (\%) = 100 - \frac{100x(3n_{C_3H_8, Bypass} - 3n_{C_3H_8, exit} - n_{CO_2} - 3n_{Acrolein} - 3n_{Acrylicacid})}{3n_{C_3H_8, Bypass}} \quad (3-7)$$

The selectivity for all the products was determined with equation 3-8.

$$Selectivity_x = 100 \frac{Mole\ Carbon\ in\ x\ produced}{Mole\ Carbon\ in\ Propene\ converted} \quad (3-8)$$

x in equation 3-8 can be acrylic acid, acrolein or carbon dioxide.

## Chapter 4 Preliminary results and the selective oxidation of methane

The results for the methane selective oxidation experiments are discussed in this chapter together with the preliminary results of the experimental work. Suggestions are also made as to what needs to be studied in the future to find a catalyst that can produce synthesis gas at low temperatures from methane.

### 4.1 Preliminary experimental work

#### 4.1.1 Micro-reactors

##### 4.1.1.1 Residence time distribution (RTD)

Kinetic experiments must be performed in a plug flow reactor to ensure that the parameters that are determined with the experimental data are correct. Therefore the reactors that were used for the experiments were tested for plug flow behaviour. To test for plug flow behaviour the reciprocals of the Peclet numbers for the different flow conditions were required.

The calculations of the mean residence time and variance that were required to determine the Peclet number are explained in Appendices D and the results for the different flow conditions are displayed in Table 4-1.

**Table 4-1 The mean residence time, variance and reciprocal of the Peclet number calculated for the glass reactor at 27 and 340°C with a flow rate of 60 and 75ml/s.**

RTD no	Flow rate [ml/s]	Temp [°C]	$t_m$ [s]	$\delta^2$	$1/Pe_r$
1	60	27	0.988	0.126	0.069
2	75	27	0.968	0.098	0.055
3	75	340	0.991	0.098	0.053
4	60	340	1.034	0.141	0.071

According to Fogler [1999] pure plug flow reactors will have a reciprocal of the Peclet number equal to 0, while total mixed flow reactors will have a reciprocal of the Peclet number



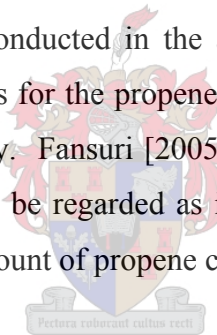
Chapter 4 Preliminary results and the selective oxidation of methane

equal to infinity. Table 4-1 showed that the values of the reciprocals for the flow conditions during the experiments were between 0.053 and 0.071. These values indicated that there was an intermediate amount of dispersion in the reactors just as was expected, because no real reactor will ever show pure plug flow conditions. The results also indicated that with an increase in the flow rate, the flow through the reactor came closer to plug flow. It was also seen that the temperature had no effect on the dispersion of the flow through the reactor.

According to Fogler [1999] a large amount of dispersion only occurs for a reciprocal of the Peclet number larger than 0,2. It can therefore be assumed that under the reaction conditions (325 to 375°C, Propene flow rate of 60ml/s) that were used for the kinetic experiments the reactor behaved as a plug flow reactor.

#### 4.1.1.2 Reactivity of blank reactors

Kinetic experiments must also be conducted in the absence of homogenous reactions and therefore the reactivity of the reactors for the propene and methane in the glass and stainless steel reactors were tested respectively. Fansuri [2005] found that for the selective oxidation of propene, quartz glass reactors can be regarded as inert at temperatures below 390°C, but did not give an indication of what amount of propene converted can be regarded as inert.



For this study the mean propene conversions for blank glass reactors with quartz particles were found to be: 1,54% at 325°C; 2,79% at 350°C and 4,63% at 375°C for a WHSV of  $3 \frac{\text{g}_{\text{Propene}}}{(\text{g}_{\text{cat}} \cdot \text{h})}$ , while no methane conversion occurred in the stainless steel reactor. Since the WHSV was changed by changing the mass of catalyst in the reactor and not by changing the reactant flow rates, the amount of homogeneous reactions can be assumed to stay the same for all the WHSV reactions that were performed. This assumption can be justified by the fact that the homogenous reactions are a function of the residence time and the temperature in the reactor.

From these results and the propene conversions (appendix E) it was determined that the homogenous reactions accounted between 13 to 36% of the propene conversion during the kinetic experiments for propene. For this reason it can not be assumed that the glass reactors were inert. To determine the conversions of the heterogeneous reactions the conversions

caused by the homogeneous reaction were subtracted from the conversions that were measured for the catalytic reactions.

### 4.1.2 Catalyst characterisation

BET analysis showed that the surface area of the catalyst that was prepared was 3,5 m<sup>2</sup>/g, while Fansuri [2005] prepared  $\alpha$ -Bismuth molybdate with a surface area of 3,2 m<sup>2</sup>/g. This was more than twice the surface area of the  $\alpha$ -Bismuth molybdate that was prepared originally by Keulks *et al* [1980] which had a surface area of 1,6 m<sup>2</sup>/g. The differences in surface areas can be explained by the particle size of the catalyst that was prepared, which depended on the degree of grinding the catalyst particles underwent. Results for the same catalyst with different surface areas can be compared if the calculations are based on the reaction rate per unit surface area. The BET analysis also showed that the catalyst had no micropores.

An XRD done by iThemba labs confirmed that the prepared catalyst was  $\alpha$ -Bismuth molybdate (see Figure 4-1).

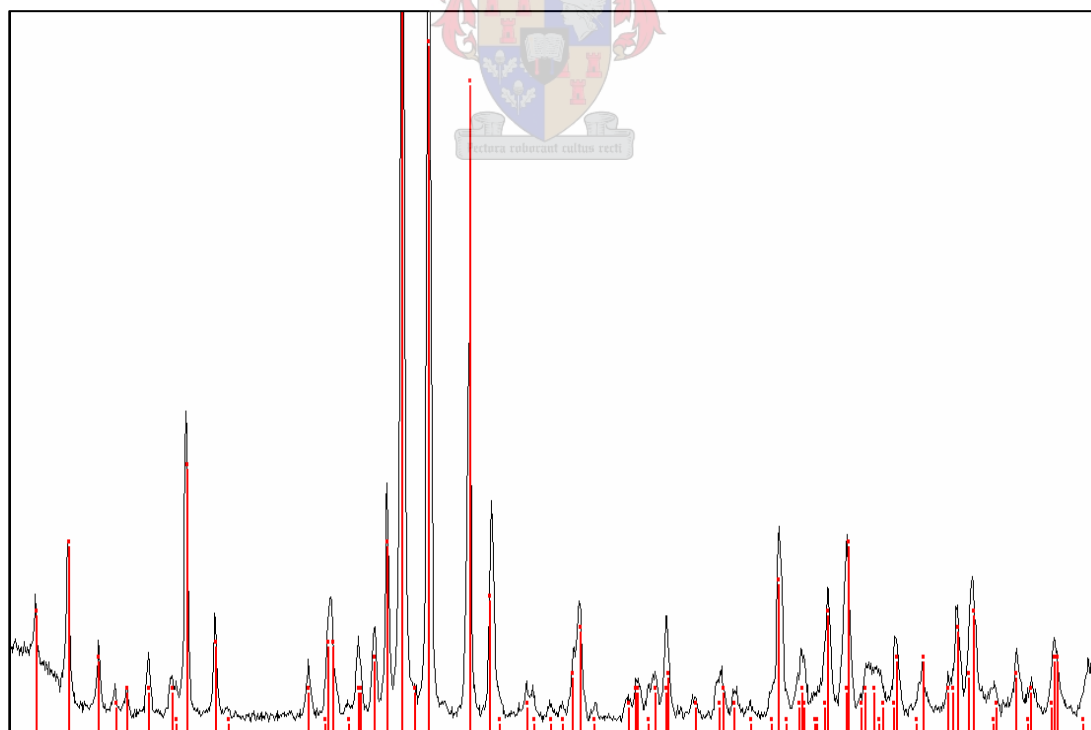


Figure 4-1 XRD of catalyst prepared (Vertical lines are the expected peaks for  $\alpha$ -Bismuth molybdate)

## 4.2 Results for the selective oxidation of methane with $\alpha$ -Bismuth molybdate

For each reaction in Table 3.3 (see Section 3.3.2) seven samples were taken at different time intervals to see if some of the methane was converted. No products and no conversion were observed over the temperature range 321 – 499 °C, for a WHSV ranging from 1,88 to 10,38  $\text{g}_{\text{methane}}/(\text{g}_{\text{cat}}\cdot\text{h})$  at atmospheric pressure. The experiments conducted in this range gave no conversion that could be detected by the GC. Cooper and Bell [2001] reported a methane conversion of 0,3% over  $\text{MoO}_3$  at a temperature of 455°C and a pressure of 15 bar. This conversion is however very small and would not be detectable with a conventional GC. From the experiments that were conducted in this study it can be said that a methane bismuth molybdate system within the range of conditions that were examined depends on the analysis equipment used.

## 4.3 Possible methods for circumventing the problem of methane activation

To overcome the problem with the activation of methane at low temperatures a new catalyst must be found. A good place to start will be to study the chemistry behind the activation of methane by  $\text{Ga}_2\text{O}_3/\text{MoO}_3$  and use the results to search for a more active catalyst. Another option is to add an alkali metal like lithium to bismuth molybdate to see if it enables the catalyst to activate methane and form selective oxidation products. The idea with the insertion of the alkali metal is to increase the basic function of bismuth molybdate.

Djaidja *et al.* [2000] showed that several factors influence the oxidative transformation of methane reaction on nickel based catalysts. This includes reaction conditions, nature of the support, nickel composition and the presence of metal additives. The reaction was favoured by Ce and Sm supports, low nickel composition, Li additive at a low reaction temperature (723K). On the other hand a La support, Ba additive and high reaction temperature enhanced the partial oxidation of methane activity. These were the result from modification of the reducibility or acid-base surface properties by changing the surface chemical composition of the catalyst. This showed that additives are very important in heterogeneous catalysis and supported the suggestion that adding alkali metals to bismuth molybdates might be able to

## Chapter 4 Preliminary results and the selective oxidation of methane

activate methane. Further studies should thus be conducted on the effect of different additives on the selective oxidation of methane. The best catalyst to use to study these additives will probably be  $\text{Ga}_2\text{O}_3/\text{MoO}_3$ . Studies can also be done to see if by supporting bismuth molybdate (or any other mixed metal oxides) on different supports have a positive affect on the activation of methane.

Basile *et al.* [2001] studied synthesis gas production by the partial oxidation of methane with pure oxygen. It was proposed that the process can be made more economic by using air in a membrane reactor in which the membrane is perm selective to oxygen. Pure hydrogen can also be produced by using dense palladium as a membrane which enables hydrogen product to permeate out through the membrane, shifting the conversion to values higher than thermodynamic equilibrium values. Hydrogen is the only molecule that is allowed to permeate through these dense palladium membranes. By removal of the hydrogen through the membrane the reaction gave a higher methane conversion. A conventional reactor was compared with different membrane reactors for the partial oxidation of methane. A Nickel catalyst supported on alumina was placed inside the membrane reactor. It was found that with the best membrane reactor configuration that a methane conversion of 56.2% can be obtained at 450°C and 45.3% at 400°C. The hydrogen selectivity at these conversions were found to be 46% at 450°C and 34% at 400°C.

In this work it is suggested that a possible solution is to design a new kind of membrane reactor using a dense palladium membrane as mentioned above and use the product stream that has been stripped of the hydrogen as the sweep gas. The hydrogen stripped gas pressure must be lowered before it can be used as a sweep gas and therefore the gas must be expanded in an expansion chamber. See Figure 4-2. It might be possible to produce synthesis gas this way at low temperatures by using conventional catalyst for which total oxidation is thermodynamically favoured at low temperatures.

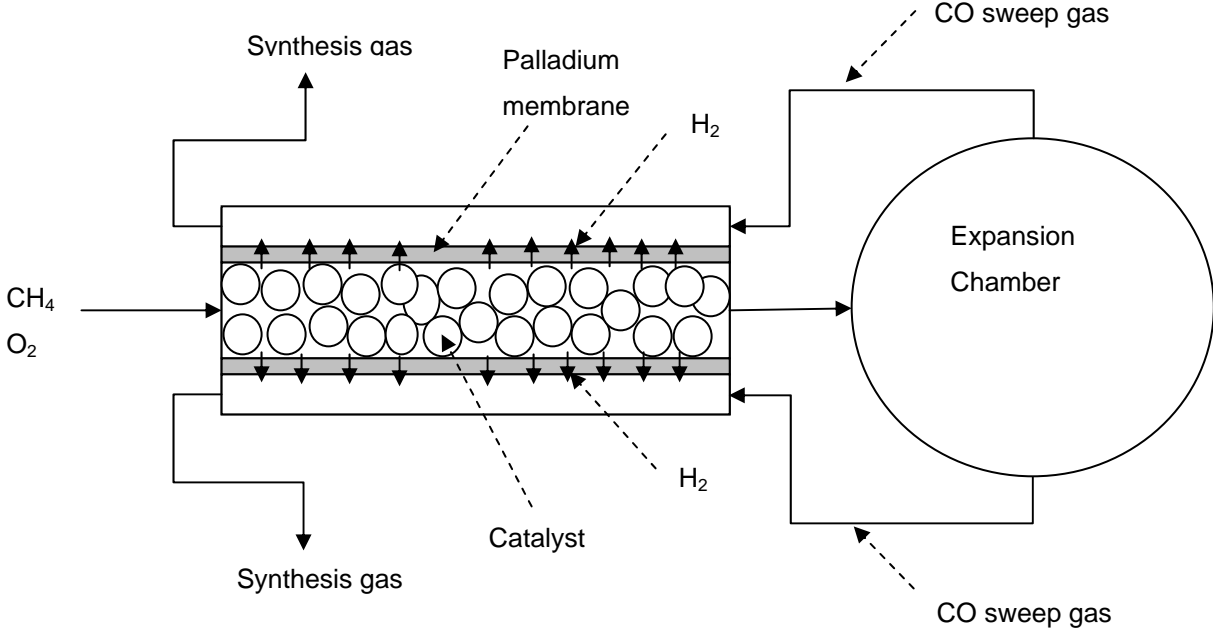


Figure 4-2 Diagram of proposed membrane reactor to produce synthesis gas



## Chapter 5 Selective oxidation of propene

In the most recent paper on the kinetics of propene to acrolein [Redlingshöfer *et al.* 2003] and a PhD thesis that was submitted in 2005 [Fansuri 2005] a lot of papers are referenced where the kinetics of bismuth molybdates had been studied. The only kinetics, however, that were investigated for the selective oxidation of propene to acrolein over pure  $\alpha$ - $\text{Bi}_2\text{Mo}_3\text{O}_{12}$  were done by Keulks *et al.* [1980] and Fansuri [2005].

### 5.1 Mass Transfer Limitations

Before any kinetic experiment could be done, experiments had to be performed to test for any mass transfer limitations. The kinetics done by Keulks *et al.* [1980] and Fansuri [2005] did not mention that they investigated if there were any mass transfer limitations. Two kinds of mass transfer limitations can occur: External and internal.

#### 5.1.1 External mass transfer limitations

External mass transfer limitations occur when the reaction rate is limited because the reactant diffuses slower across the boundary layer that forms around the external catalyst surface, than the reactant molecule takes to react. This can be tested by changing the linear superficial flow rate of the reactants through the catalyst bed which will change the thickness of the boundary layer on the catalyst surface. The WHSV of the reactants needs to stay the same when the linear flow rate is changed to ensure the concentrations of the reactants are the same to ensure the same reaction conditions. If no external mass transfer limitation exists, the rate of reaction will be independent of the linear velocities for a given WHSV.

Three different linear flow rates were chosen and the experiments were done at 325°C. The diffusion of the reactant across the boundary layer can be given with equation 5-1 for a differential reactor [Fogler 1999].

$$W_{\text{reactant}} = -D_{AB} \cdot \frac{dC_{\text{reactant}}}{dz} \quad (5-1)$$

## Chapter 5 Selective oxidation of propene

With:  $W_{reactant}$  : Molar flux of reactant, mol/(dm<sup>2</sup>.s)  
 $D_{AB}$  : Diffusivity, dm<sup>2</sup>/s  
 $\frac{dC_{reactant}}{dz}$  : Concentration profile, in the radial direction, of reactant across the boundary layer, mol/dm<sup>4</sup>

The diffusivity increases with an increase in temperature [Fogler 1999] and therefore the diffusion will be slower at lower temperatures. The lowest temperature at which the kinetic experiments would be done (325°C) was thus chosen to test for mass transfer limitations. The reasoning behind this was that at higher temperatures the diffusion will increase and if there are no mass transfer limitations at the lowest temperature there will be no mass transfer limitations at the higher temperatures.

The results of the external mass transfer limitation experiments are given in Figure 5-1. Since all the propene conversions were smaller than 9,27% it was assumed that the reactor can be treated as a differential reactor. The rate of reactions was thus calculated with the differential reactor design equation (Equation 5-2) [Fogler 1999].

$$-r_{Pr\text{opene}} = \frac{F_{Pr\text{opene},0} \cdot X}{W} \quad (5-2)$$

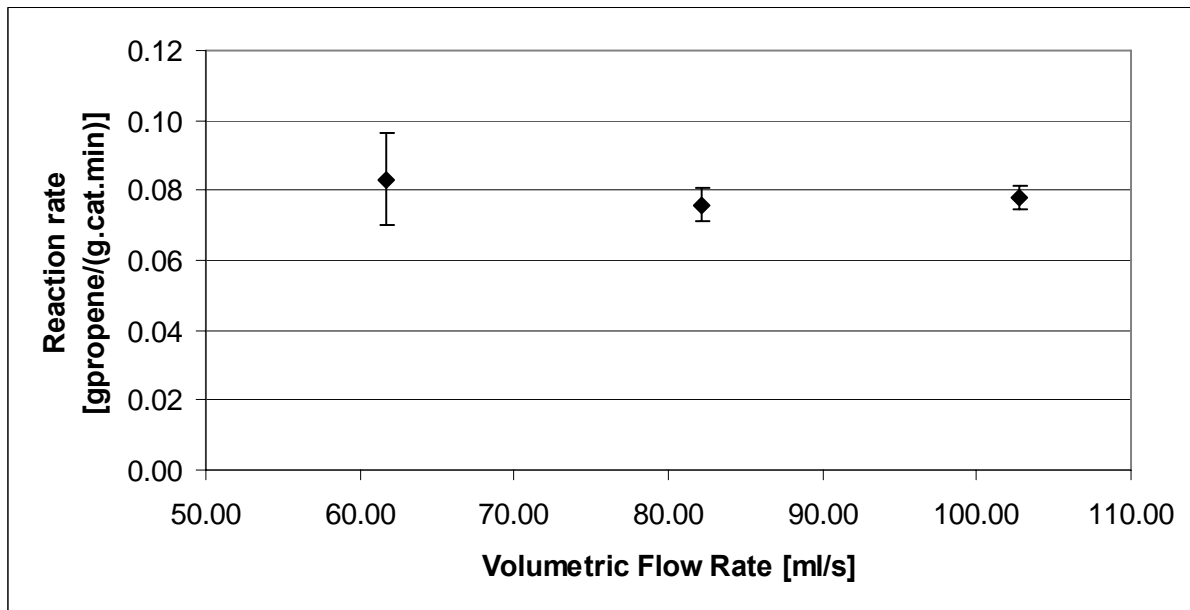
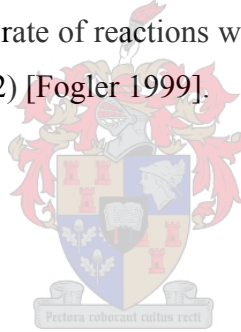


Figure 5-1 Effect of linear velocity through reactor on rate of reaction at a temperature of 325°C (WHSV = 3 g<sub>Propene</sub>/(g<sub>cat</sub>·h) and Propene/Oxygen/Helium = 1/2/7)

From Figure 5-1 it can be concluded that there are no external mass transfer limitations in the region where the kinetic experiment were conducted. The difference in the rate of reaction at different linear velocities can be ascribed to experimental error.

### 5.1.2 Internal mass transfer limitations

Internal mass transfer limitations occur when the reactant diffuses slower through the micropores of the catalyst than the reactant takes to react at the active site on the catalyst surface in the pores. The BET surface area measurement that was done to determine if there were micropores in the catalyst showed that there were none.

The fact that there are no micropores indicated that there would be no internal mass transfer limitations. A test was performed to determine if there was an influence of the particle size on the rate of reaction (Figure 5-2). With the reaction only occurring on the external surface, it would be expected that the reaction rate would increase with decreasing particle size. The reverse of this was seen with the experiments that were conducted on the different particle sizes.

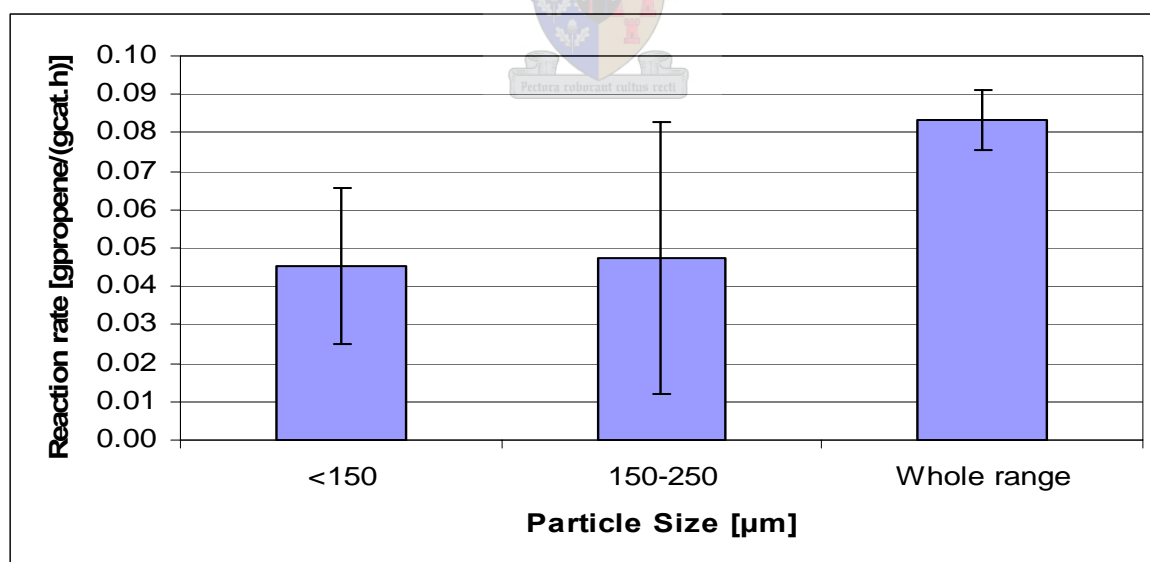


Figure 5-2 Effect of particle size distribution on rate of reaction at a temperature of 325°C (WHSV = 3  $\text{g}_{\text{Propene}}/(\text{g}_{\text{cat}}\cdot\text{h})$  and Propene/Oxygen/Helium = 1/2/7)

If one looks at the Mars-van Krevelen mechanism (Section 2.4.1), according to which this reaction takes place, this phenomenon can be explained. Van Hooff [1980] mentioned that by using  $^{18}\text{O}$ -enriched oxygen and propene over bismuth molybdates the product initially



contained mostly  $^{16}\text{O}$  and that only after almost all of the catalyst bulk oxygen has been exchanged that the feed  $^{18}\text{O}$  and the  $^{18}\text{O}$  in the product comes in equal ratios. This indicates that one needs a bulk “reservoir” of oxygen anions that takes place in the reaction. The results of experiments conducted by Han *et al.* [1998] also showed that a minimum particle size is required for bismuth molybdate catalyst which can provide sufficient lattice oxide ions during the catalytic redox cycle. However, this minimum particle size required must still be determined. This argument is in agreement with the results found here where the rate is higher for larger particles.

## **5.2 Effect of reaction conditions on the reaction of Propene to Acrolein over $\alpha$ -Bismuth molybdate**

### **5.2.1 Effect of time on-stream on the selective oxidation of propene to acrolein over $\alpha$ -Bismuth molybdate**

The time on-stream behaviour of the selective oxidation of propene to acrolein over  $\alpha$ -Bismuth molybdate was investigated. This investigation was done over a temperature range from 325 to 375°C and a propene to oxygen feed ratio range from 0,5 to 1,0. For each reaction done, with the different reaction conditions, 14 samples were taken over a period of 90 minutes using the evacuated ampoule sampling method described in section 3.1.3.

The results for the propene conversion for the selective oxidation of propene to acrolein over  $\alpha$ -Bismuth molybdate for a time on-stream of 90 minutes are given in Figure 5-3 while the results for the acrolein selectivity are given in Figure 5-4. These results showed that there is no loss in activity of the  $\alpha$ -Bismuth molybdate catalyst or any change in the selectivity towards acrolein for the first 90 minutes on stream. Du Preez [2006] did further experiments that showed that the reaction did not show any loss in activity for the first 6 hours.

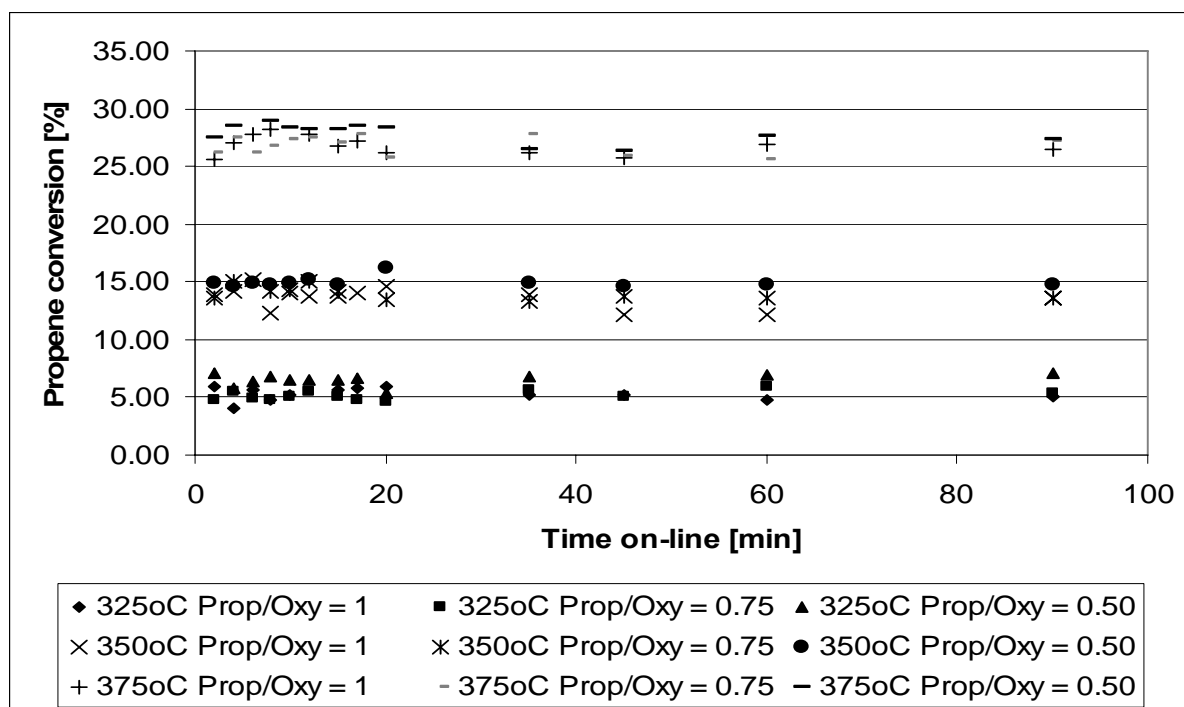


Figure 5-3 The propene conversion over  $\alpha$ -Bismuth molybdate as a function of time on-line (At 325, 350 and 375°C; Propene to Oxygen feed ratios of 0.50, 0.75 and 1.00;  $P_{Total} = 1.45$ ;  $WHSV = 3 \text{ g}_{Propene}/(\text{g}_{cat}\cdot\text{h})$ )

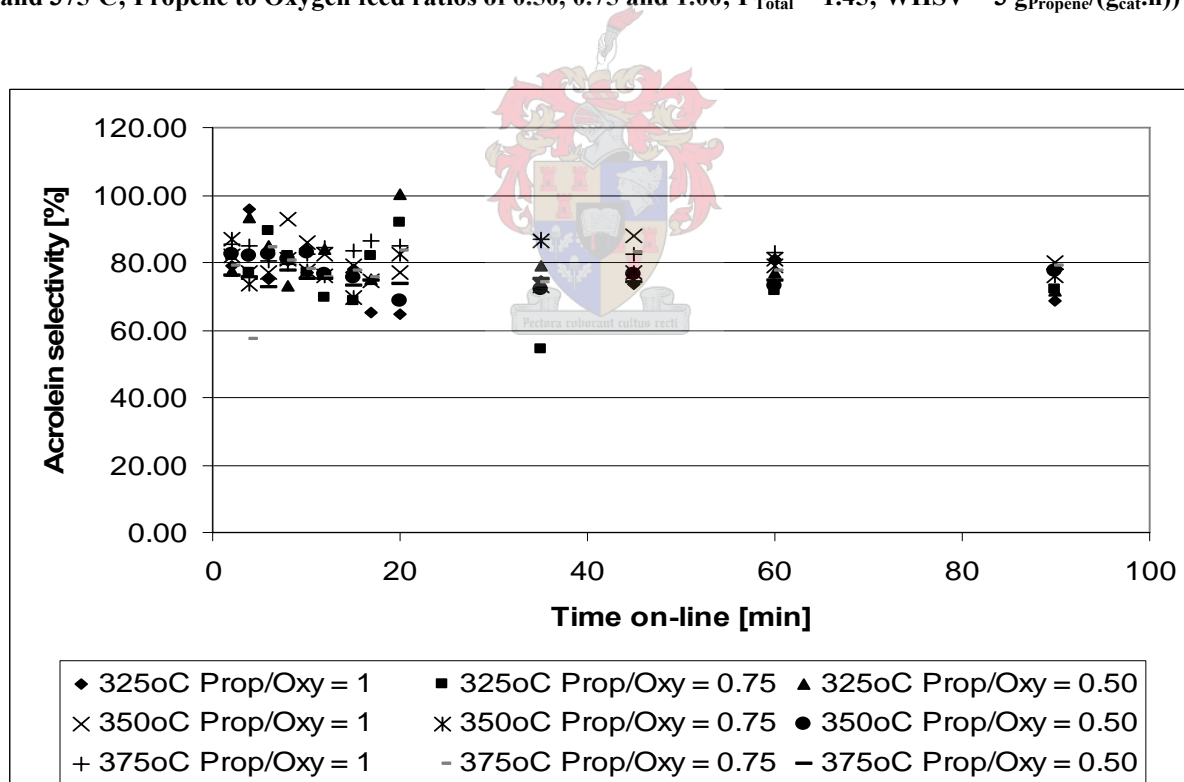


Figure 5-4 The acrolein selectivity of the reaction between oxygen and propene over  $\alpha$ -Bismuth molybdate as a function of time on-line (At 325, 350 and 375°C; Propene to Oxygen feed ratios of 0.50, 0.75 and 1.00;  $P_{Total} = 1.45$ ;  $WHSV = 3 \text{ g}_{Propene}/(\text{g}_{cat}\cdot\text{h})$ )

## Chapter 5 Selective oxidation of propene

It was seen in section 2.3.1.4 that Magagula and Van Steen [1999] did similar time on-stream experiments for the selective oxidation of propene to acrolein, but using  $\gamma$ -Bismuth molybdate instead of  $\alpha$ -Bismuth molybdate. It was shown that the selectivity for acrolein increased strongly with time on stream for the  $\gamma$ -Bismuth molybdate, while the activity decreased strongly. This indicated that the catalyst surface contained more electrophilic oxygen species at the beginning of the reaction than at steady state.

For  $\alpha$ -Bismuth molybdate this was not the case as was seen in Figures 5-3 and 5-4, which showed that the activity and the selectivity of the catalyst stayed stable over the first 90 minutes on-stream. This indicated that the surface oxidation state of  $\alpha$ -Bismuth molybdate stayed the same during this period of time, which further indicated that the amount of nucleophilic and electrophilic oxygen species on the surface stayed the same over the time period. It might thus be concluded that the reaction reached steady state almost immediately.

### 5.2.2 Effect of propene to oxygen feed ratio and the reaction temperature on the selective oxidation of propene to acrolein over $\alpha$ -Bismuth molybdate

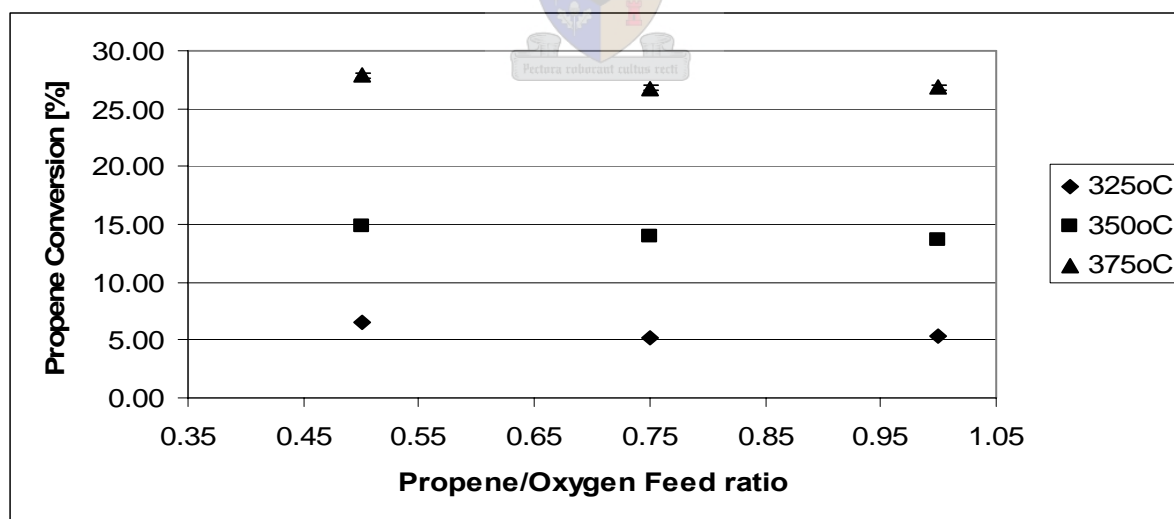


Figure 5-5 The propene conversion as a function of the propene to oxygen feed ratio (At 325, 350 and 375°C; A Propene to Oxygen feed ratios of 0.50 , 0.75 and 1.00;  $P_{\text{Total}} = 1.45$ ;  $\text{WHSV} = 3 \text{ g}_{\text{Propene}}/(\text{g}_{\text{cat}}\cdot\text{h})$ )

In Figure 5-5 the effect of the propene to oxygen feed ratio (P/O) on the propene conversion is demonstrated. The results showed that there is no change in the propene conversion for a propene to oxygen feed ratio higher than 0,75, but for a feed ratio below 0,75 the propene

## Chapter 5 Selective oxidation of propene

conversion increased slightly. This pattern was repeated for all three temperatures that were investigated as can be seen in Figure 5-5. The differences between the propene conversions for the propene to oxygen feed ratios of 0,75 and 0,50 were 21,15% for 325°C, 6,33% for 350°C and 3,84% for 375°C respectively. All these differences were higher than the 3,80% experimental error with a 95% confidence level that was determined in section 5.3. The fact that the differences in conversions were larger than the experimental error indicated that the propene to oxygen feed ratio really had an effect on the propene conversion. The reason why the propene conversion increases with decreasing propene to oxygen feed ratios might be the fact that there is less oxygen to prevent the propene from reaching propene activation sites.

The results from Figure 5-5 were in agreement with the observations made by Al'kaeva *et al.* [1995] and Redlingshöfer *et al.* [2002] that the rate of propene conversion increased at low temperatures (330 and 350°C) for a higher oxygen content over bismuth molybdates. It was also observed by Al'kaeva *et al.* [1995] that with an increase in temperature the effect of the propene to oxygen ratio on the propene conversion decreased.

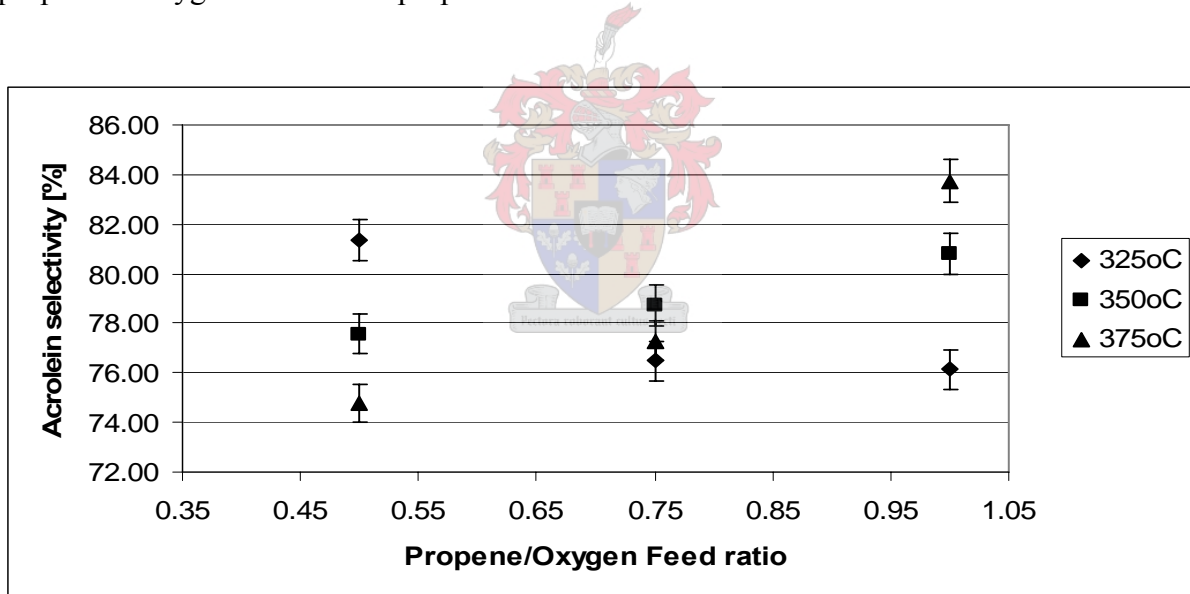


Figure 5-6 The acrolein selectivity as a function of the propene to oxygen feed ratio (At 325, 350 and 375°C; A Propene to Oxygen feed ratios of 0.50 , 0.75 and 1.00;  $P_{Total} = 1.45$ ;  $WHSV = 3 \text{ g}_{Propene}/(\text{g}_{cat}\cdot\text{h})$ )

In Figure 5-6 the acrolein selectivity of the selective oxidation of propene to acrolein over  $\alpha$ -Bismuth molybdate is demonstrated; for the temperature range of 325 to 375°C and a propene to oxygen range of 0,5 to 1,0. The results showed that the acrolein selectivity did not follow a general trend in the region where the experiments were conducted. Figure 5-6 shows that the acrolein selectivity increased with an increase in propene to oxygen feed ratio at 350 and 375°C, while it decreased at 325°C. It was also seen that the increase in the acrolein

## Chapter 5 Selective oxidation of propene

selectivity was more rapid at 375°C than at 350°C for an increase in propene to oxygen feed ratio. This inversion in the trends of the selectivity between temperatures below 350°C and above 375°C might be the result of the reaction mechanism change explained in Section 6.2.2.

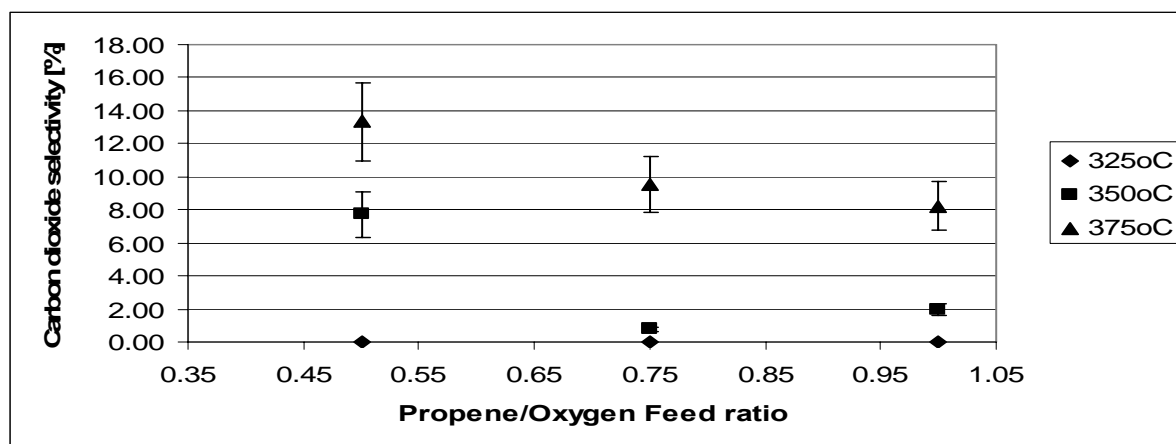


Figure 5-7 The carbon dioxide selectivity as a function of the propene to oxygen feed ratio (At 325, 350 and 375°C; A Propene to Oxygen feed ratios of 0.50 , 0.75 and 1.00;  $P_{\text{Total}} = 1.45$ ;  $\text{WHSV} = 3 \text{ g}_{\text{Propene}}/(\text{g}_{\text{cat}}\cdot\text{h})$ )

The carbon dioxide selectivity for the selective oxidation of propene to acrolein over  $\alpha$ -Bismuth molybdate is shown in Figure 5-7. No carbon dioxide was observed below 350°C while the selectivity increased rapidly from 350 to 375°C. The selectivity towards carbon dioxide decreased with an increase in propene to oxygen feed ratio. This indicated that the catalyst had more electrophilic oxygen species on the catalyst surface in an oxygen rich environment resulting in more non-selective oxidation products.

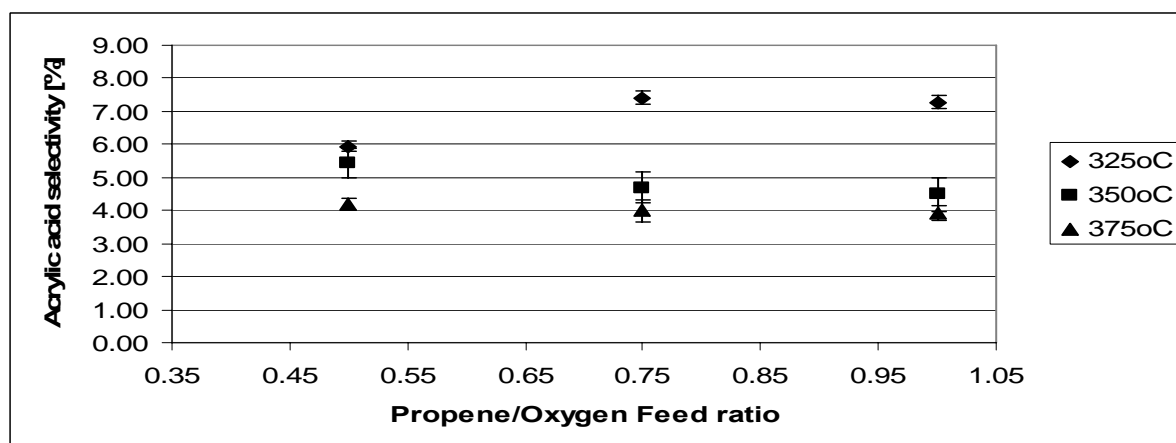


Figure 5-8 The acrylic acid selectivity as a function of the propene to oxygen feed ratio (At 325, 350 and 375°C; A Propene to Oxygen feed ratios of 0.50 , 0.75 and 1.00;  $P_{\text{Total}} = 1.45$ ;  $\text{WHSV} = 3 \text{ g}_{\text{Propene}}/(\text{g}_{\text{cat}}\cdot\text{h})$ )

## Chapter 5 Selective oxidation of propene

Figure 5-8 illustrates the effect of the propene to oxygen feed ratio and the reaction temperature on the acrylic acid selectivity for the selective oxidation of propene to acrolein reaction. In general the acrylic acid selectivity decreased with an increase in temperature. At 325°C the selectivity of acrylic acid increased with an increase in the propene to oxygen feed ratio, while it decreased at 350 and 375°C. The influence of the propene to oxygen feed ratio on the difference between the acrylic acid selectivity at 350 and 350°C also decreased significantly from that at 325°C. This might also be explained by the change in the reaction mechanism caused by an increase in reaction temperature as discussed in Section 6.2.2.

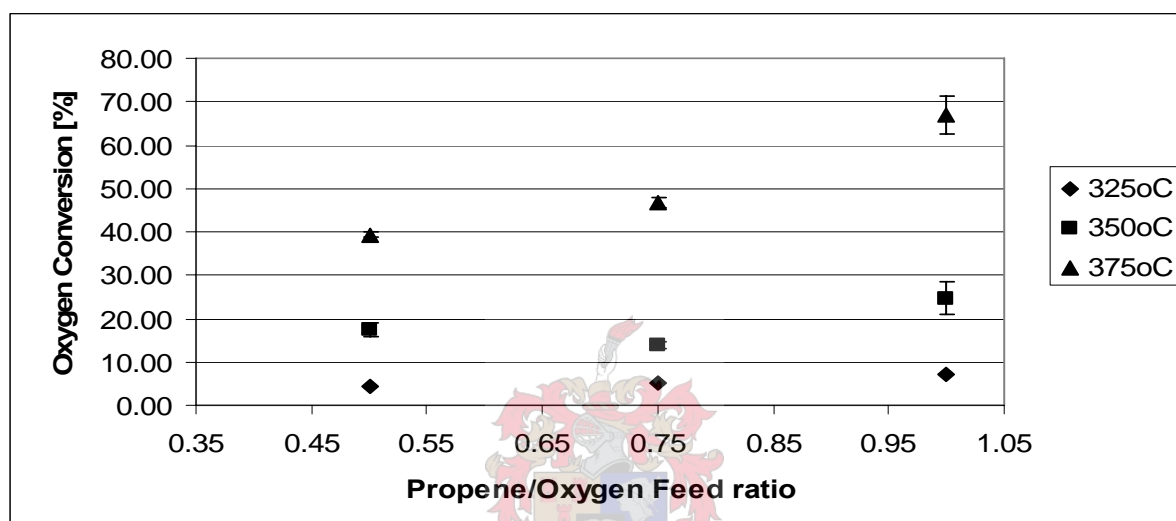


Figure 5-9 The oxygen conversion as a function of the propene to oxygen feed ratio (At 325, 350 and 375°C; A Propene to Oxygen feed ratios of 0.50, 0.75 and 1.00;  $P_{\text{Total}} = 1.45$ ;  $WHSV = 3 \text{ g}_{\text{Propene}}/(\text{g}_{\text{cat}} \cdot \text{h})$ )

Figure 5-9 shows the oxygen conversion as a function of the propene to oxygen feed ratio at 325, 350 and 375°C. The oxygen conversion increased with temperature and with propene to oxygen feed ratio. It can also be seen that the effect of the increase in the propene to oxygen region was more for 375°C than for 325 and 350°C. The fact that more oxygen was converted at higher propene to oxygen feed ratios can be explained by the fact that the percentage of the oxygen converted, will increase when less oxygen is fed for propene conversions in the same order of magnitude. The average carbon balances of all the different reactions were calculated between 97,0 and 99,4%.

In general it seemed as if the behaviour of the reaction was similar for 350°C and 375°C while it changed at 325°C. It is well know that there is a reaction mechanism change between the high and low temperature region [Keulks *et al.* 1980, Redlinghöfer *et al.* 2002], but from the acrolein, carbon dioxide and acrylic acid selectivity for this study it seemed as if there was

also a change in the reaction mechanism between the temperatures in the low temperature region. This will be investigated further in chapter 6.

### 5.2.3 Effect of the WHSV (Weight hourly space velocity)

The effect of the WHSV on the selective oxidation reaction of propene to acrolein over  $\alpha$ -Bismuth molybdate has also been investigated. Due to the large amount of experimental data and to aid in the clarity of discussion the data was split into three groups according to the propene to oxygen feed ratio and plotted on to separate graphs as can be seen in Figures 5-11 to 5-14.

Figures 5-10 and 5-11 illustrate the effect of the WHSV on the propene and oxygen conversion over a temperature range of 325 to 375°C and a propene to oxygen feed ratio range of 0,5 to 1,0. The effect of the WHSV on the propene and oxygen conversion was as expected and decreased with an increase of the WHSV for all the temperatures and feed ratios that were investigated. This was because the reactant had longer contact time with the catalyst resulting in higher conversions of the oxygen and the propene.

The general trend for the change in the selectivity of the acrolein was that it decreased with an increase of the WHSV (Figure 5-12). This indicated that the catalyst surface contained more electrophilic oxygen species at higher WHSVs. This can be explained by the fact that at low WHSVs the catalyst gets more time for the conversion of the gaseous oxygen to nucleophilic oxygen via electrophilic oxygen species.

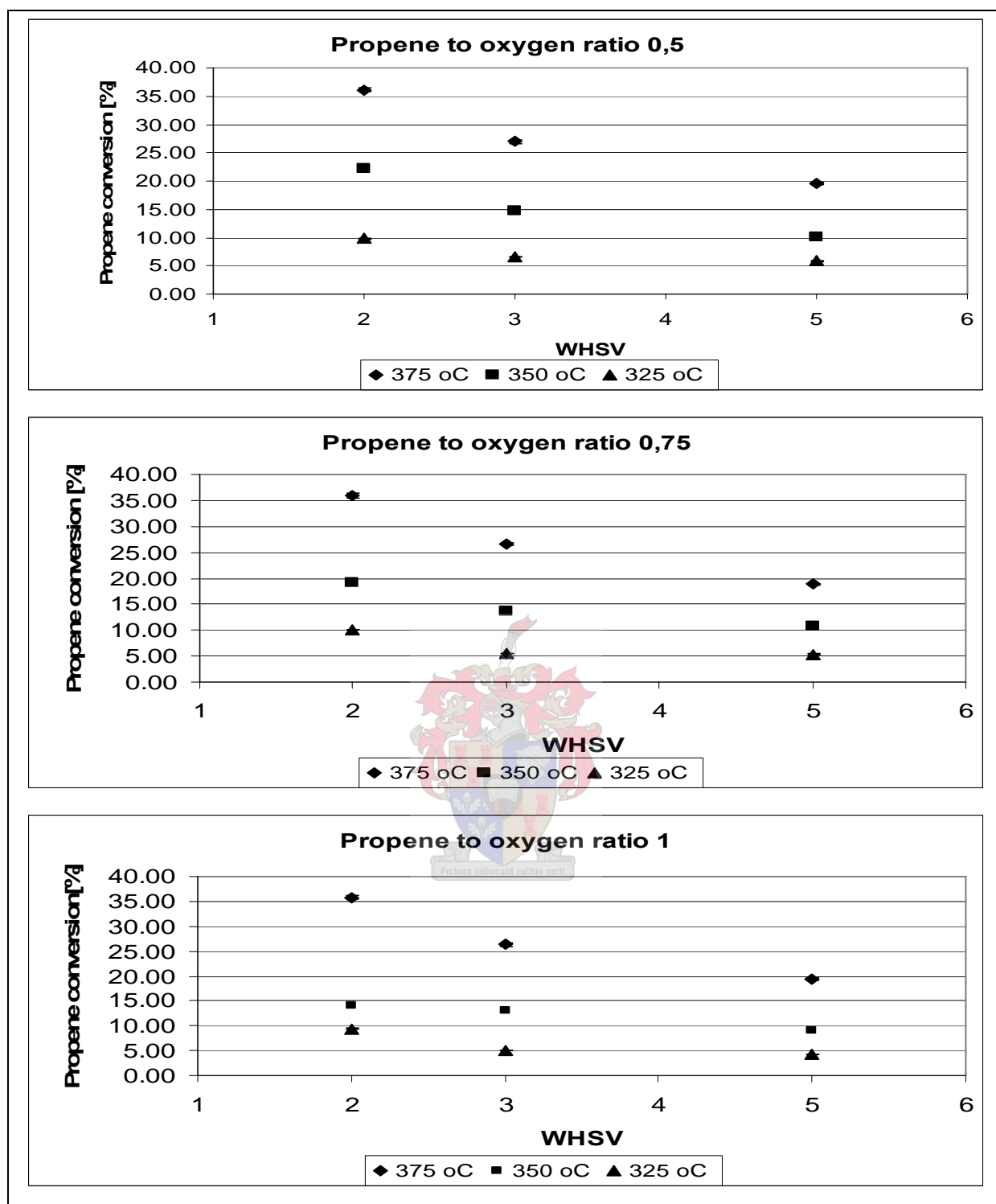


Figure 5-10 Effect of WHSV ( $\text{g}_{\text{Propene}}/(\text{g}_{\text{cat}}\cdot\text{h})$ ) on propene conversion for the selective oxidation of propene to acrolein over  $\alpha$ -Bismuth molybdate (Temperatures = 325, 350 and 375°C and Propene to oxygen feed ratios = 0,50; 0,75 and 1,00)



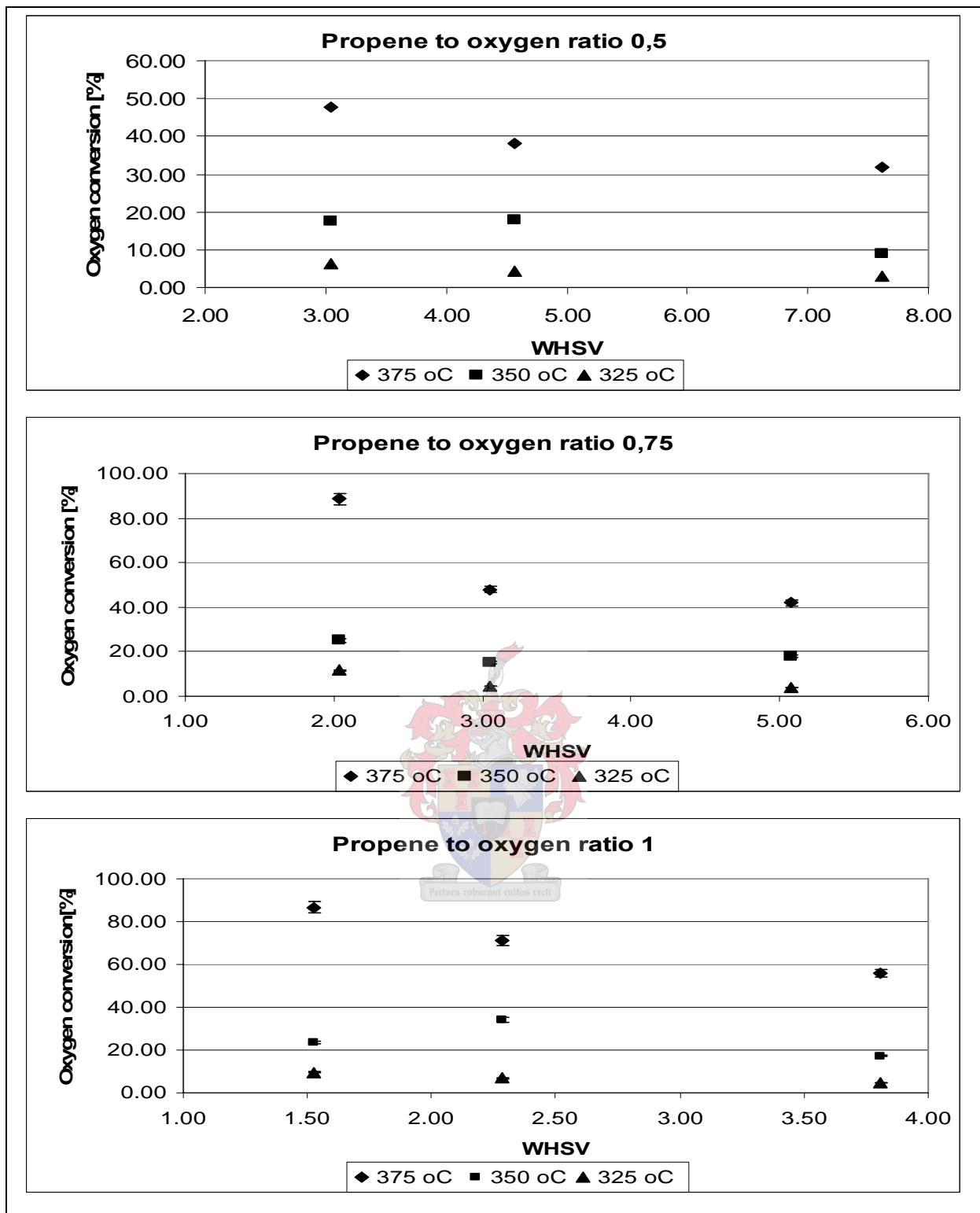


Figure 5-11 Effect of WHSV ( $\text{g}_{\text{Oxygen}}/(\text{g}_{\text{cat}}\cdot\text{h})$ ) on oxygen conversion for the selective oxidation of propene to acrolein over  $\alpha$ -Bismuth molybdate (Temperatures = 325, 350 and 375°C and Propene to oxygen feed ratios = 0,50; 0,75 and 1,00)

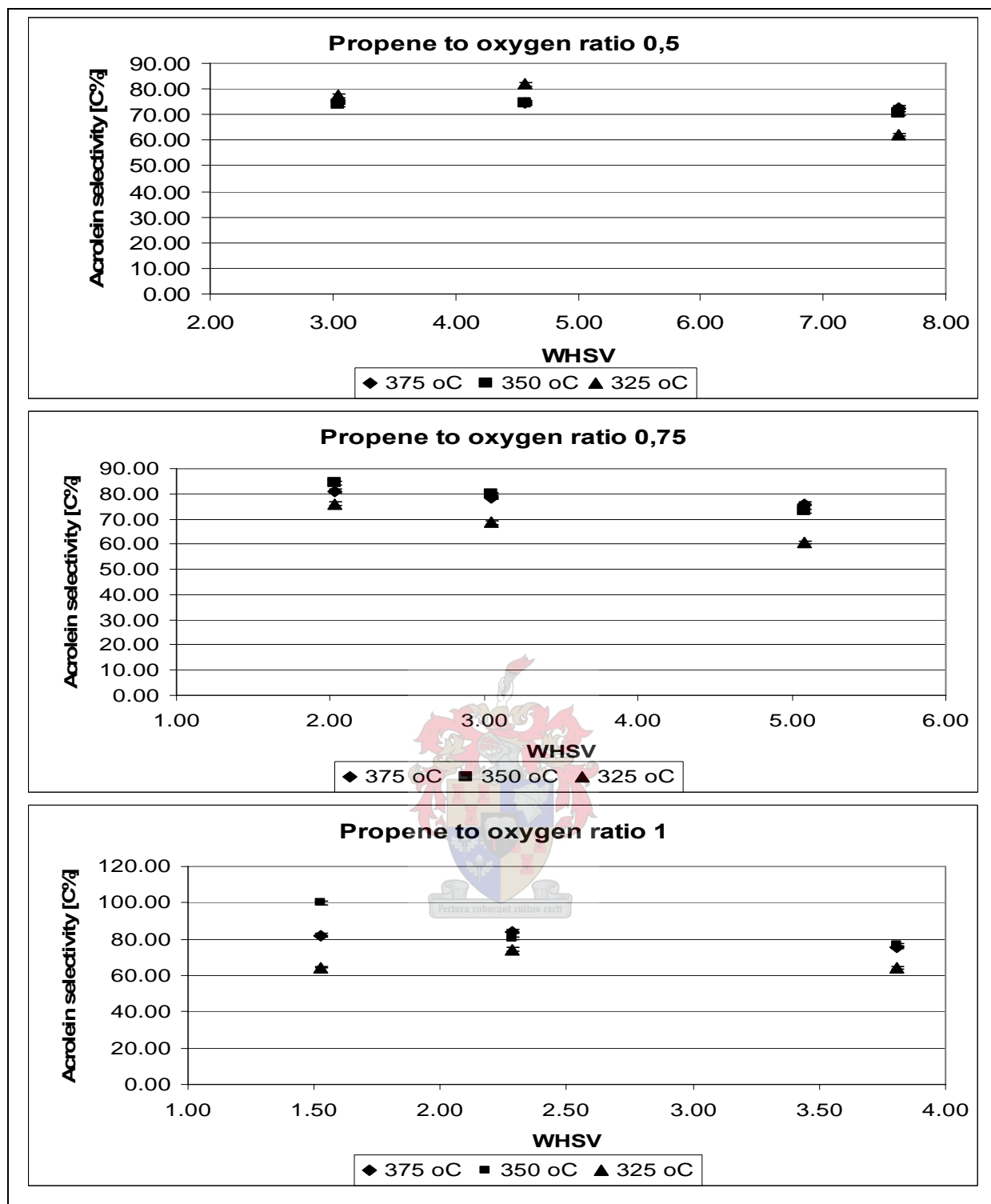


Figure 5-12 Effect of WHSV ( $\text{g}_{\text{Propene}}/(\text{g}_{\text{cat}}\cdot\text{h})$ ) on acrolein selectivity for the selective oxidation of propene to acrolein over  $\alpha$ -Bismuth molybdate (Temperatures = 325, 350 and 375°C and Propene to oxygen feed ratios = 0,50; 0,75 and 1,00)

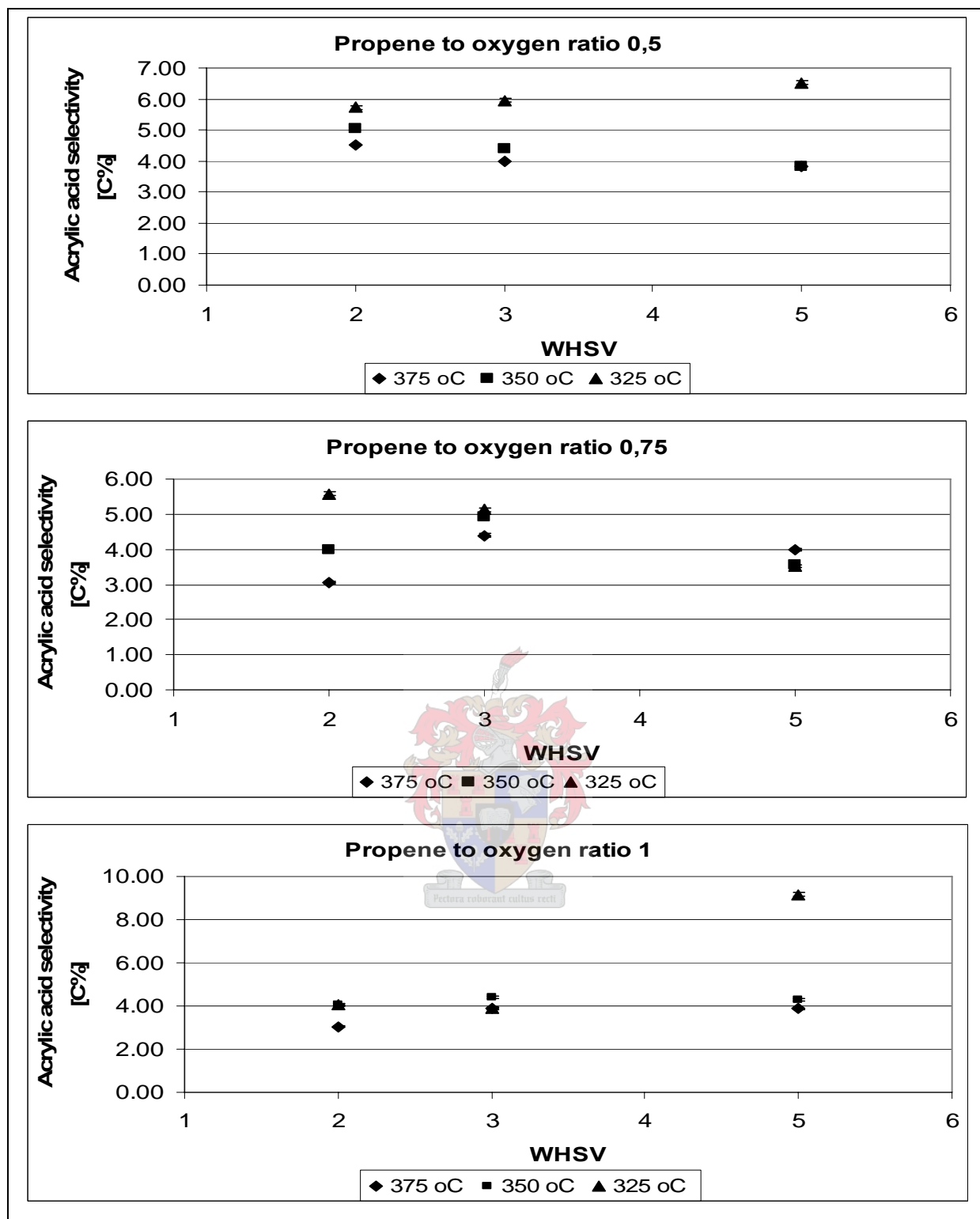


Figure 5-13 Effect of WHSV ( $\text{g}_{\text{Propene}}/(\text{g}_{\text{cat}}.\text{h})$ ) on acrylic acid selectivity for the selective oxidation of propene to acrolein over  $\alpha$ -Bismuth molybdate (Temperatures = 325, 350 and 375°C and Propene to oxygen feed ratios = 0,50; 0,75 and 1,00)

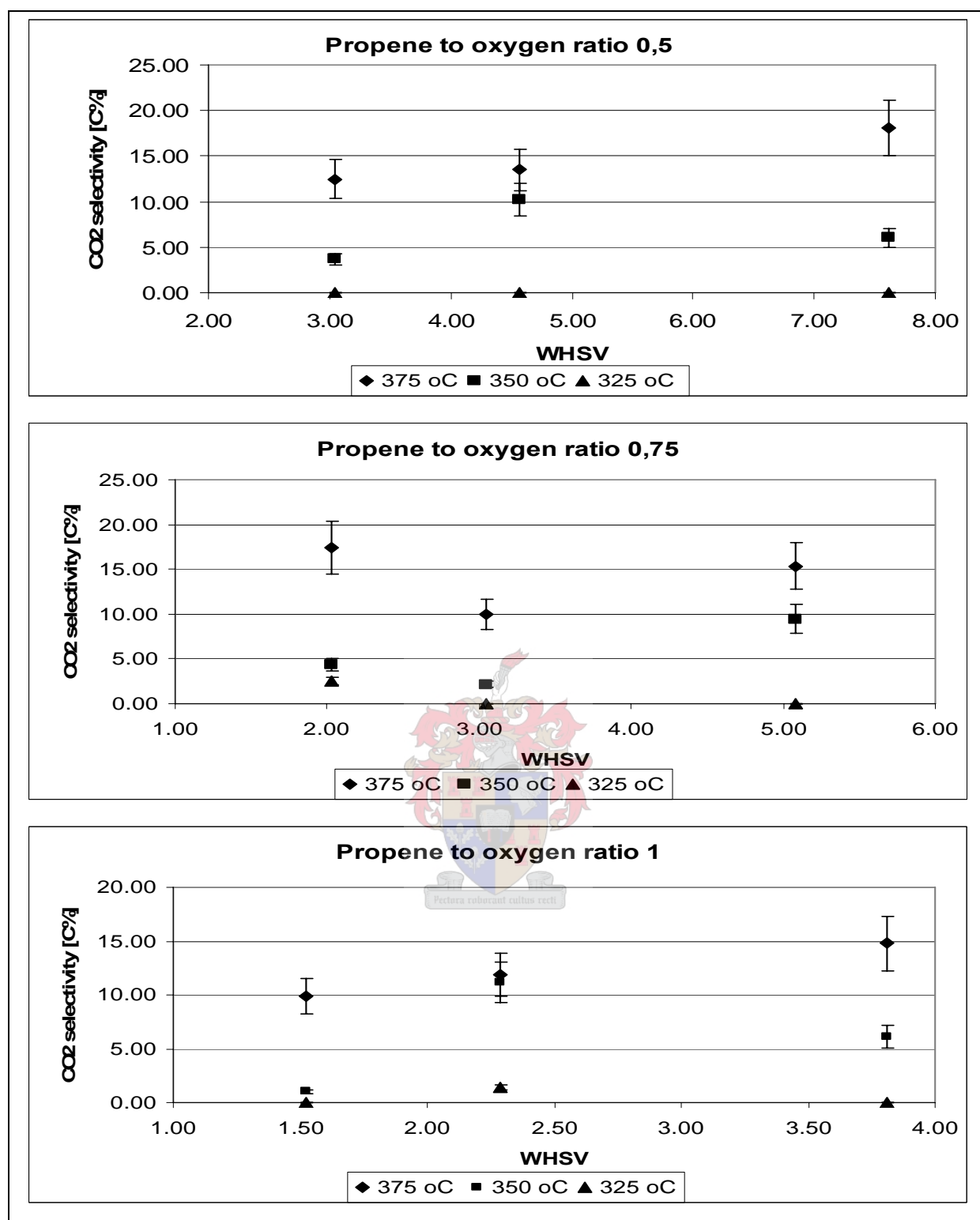


Figure 5-14 Effect of WHSV ( $\text{g}_{\text{Propene}}/(\text{g}_{\text{cat}}\cdot\text{h})$ ) on carbon dioxide selectivity for the selective oxidation of propene to acrolein over  $\alpha$ -Bismuth molybdate (Temperatures = 325, 350 and 375°C and Propene to oxygen feed ratios = 0,50; 0,75 and 1,00)

Figures 5-13 and 5-14, however, showed no general trends in the acrylic acid and carbon dioxide selectivity with an increase in the WHSV. The fact that no general trend can be observed from Figures 5-13 and 5-14 might be a change in the reaction mechanism (See Section 6.2.2). To determine the trend for each temperature more WHSV experiments need to

be conducted. The carbon balances for all the WHSV experiments were between 97,5 and 102,7%.

### 5.3 Reproducibility and experimental error of the experiments

The reaction at 350°C with the propene to oxygen feed ratio of 0,75 and a WHSV of 3  $\text{g}_{\text{Propene}}/(\text{g}_{\text{cat}}\cdot\text{h})$  was repeated three times to determine the reproducibility of the experimental data. The results of these reactions are compared and displayed in Figure 5-15 to 5-19.

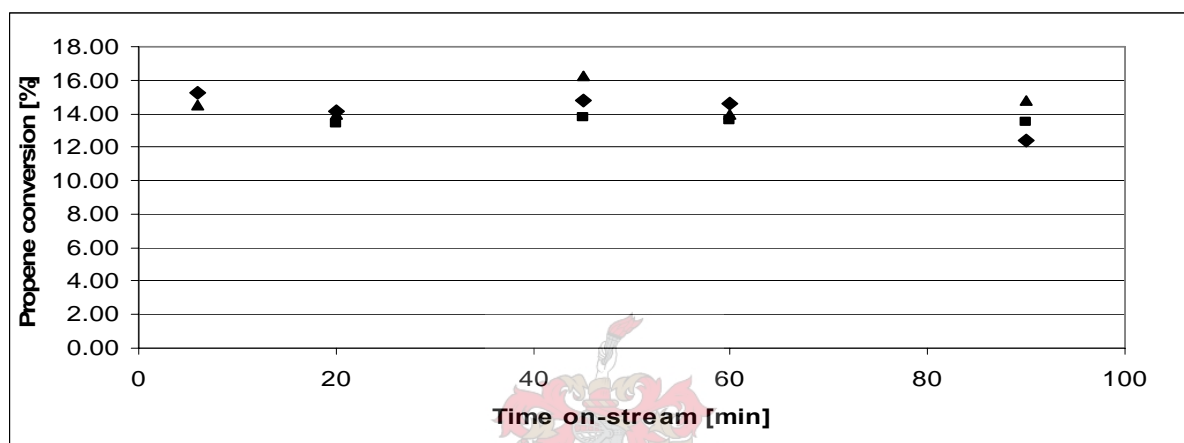


**Figure 5-15 Reproducibility of propene conversion with time on-stream (350°C, WHSV = 3  $\text{g}_{\text{Propene}}/(\text{g}_{\text{cat}}\cdot\text{h})$ , Propene/Oxygen/Helium = 1/2/7 and  $P_{\text{Total}}=1,45$  bar)**

The mean value for the propene conversion at 350°C with a propene to oxygen ratio of 0,75 was calculated from the different data points displayed in Figure 5-15 for the three different reaction runs. The mean propene conversion was calculated as  $14,2 \pm 0,5\%$  for a 95% confidence level. The absolute confidence level (95%) of 0,5% was calculated using MS Excel. This indicated that if the propene conversion was reproducible the experimental error in the propene conversion would have been 3,8%. Since the three repeats in Figure 5-15 showed no apparent pattern for each repeat it was assumed that the propene conversion for the experiments was reproducible with a experimental error of 3,8%.

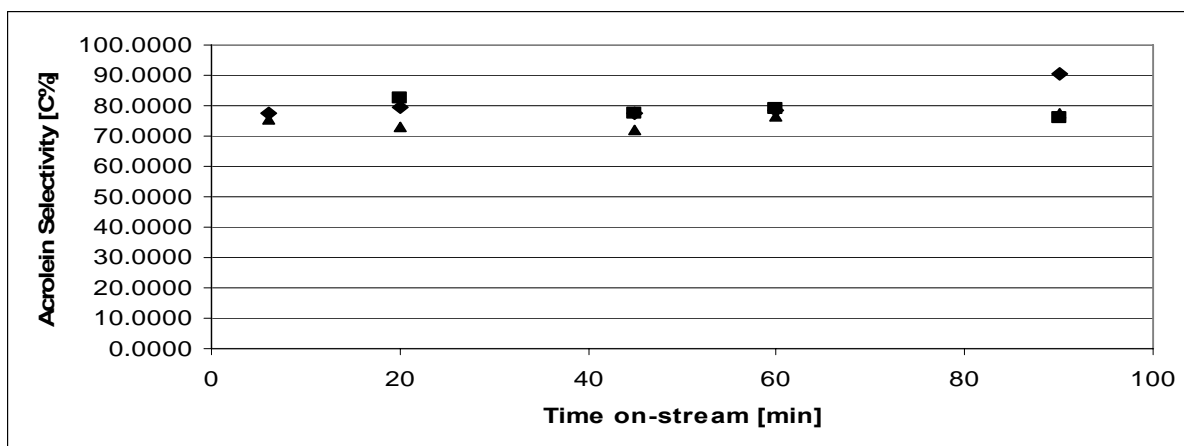


Figure 5-16 Reproducibility of acrolein selectivity with time on-stream (350°C, WHSV = 3 g<sub>Propene</sub>/(g<sub>cat</sub>·h), Propene/Oxygen/Helium = 1/2/7 and P<sub>Total</sub> = 1,45 bar)

The reproducibility of the acrolein selectivity for the experiments is demonstrated in Figure 5-16. The mean acrolein selectivity was calculated as  $78,1 \pm 2,5\%$  for a 95% confidence level. Since there was no apparent pattern for the different repeats in Figure 5-16 it can also be assumed that the acrolein selectivity was reproducible with an experimental error of 3,3%.

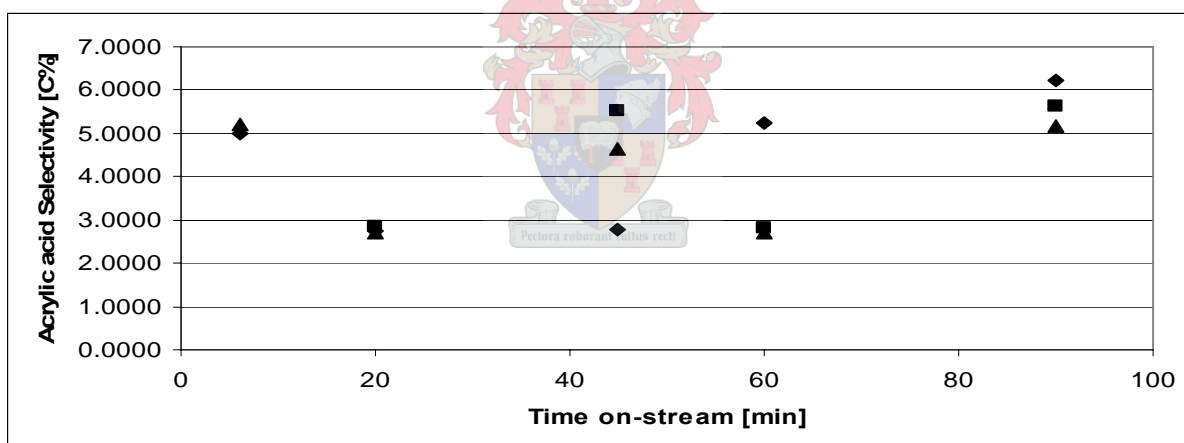


Figure 5-17 Reproducibility of acrylic acid selectivity with time on-stream (350°C, WHSV = 3 g<sub>Propene</sub>/(g<sub>cat</sub>·h), Propene/Oxygen/Helium = 1/2/7 and P<sub>Total</sub> = 1,45 bar)

Since the acrolein selectivity and the propene conversion were reproducible it could be assumed that the acrylic acid and the carbon dioxide selectivity were also reproducible. The mean acrylic acid selectivity was calculated as  $4,2 \pm 0,8\%$  for a 95% confidence level. From this the error in the acrylic acid selectivity was calculated as 18,4%. This error can be ascribed to the small quantities of acrylic acid that formed, which could not be measured accurately by the GC.

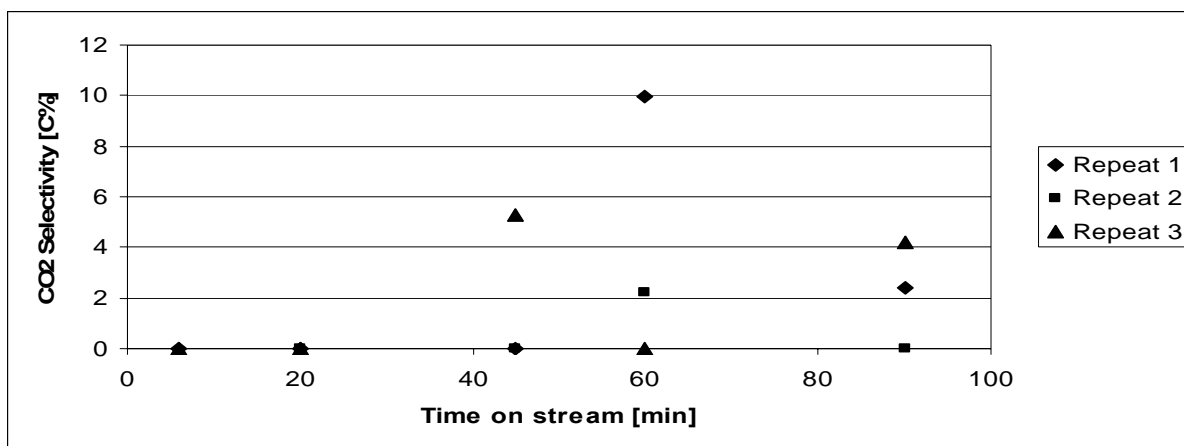


Figure 5-18 Reproducibility of carbon dioxide selectivity with time on-stream (350°C, WHSV = 3  $\text{g}_{\text{Propene}}/(\text{g}_{\text{cat}}\cdot\text{h})$ , Propene/Oxygen/Helium = 1/2/7 and  $P_{\text{Total}}=1,45$  bar)

Figure 5-18 shows that the data of the carbon dioxide selectivity had poor reproducibility. The mean value for the carbon dioxide selectivity was calculated as  $1,4 \pm 1,6\%$ . This indicated that the error for the carbon dioxide selectivity was 113,4%. The poor reproducibility of carbon dioxide selectivity might be the result of the sampling method. It might be that carbon dioxide molecules have been introduced into the ampoules while they were sealed of with a flame. This explains why carbon dioxide forms at unpredictable times. To overcome this obstacle of carbon dioxide in the ampoules it is suggested for future work to purchase an on-line CO/CO<sub>2</sub> analyser to determine the amount of carbon dioxide and carbon monoxide in the product stream.

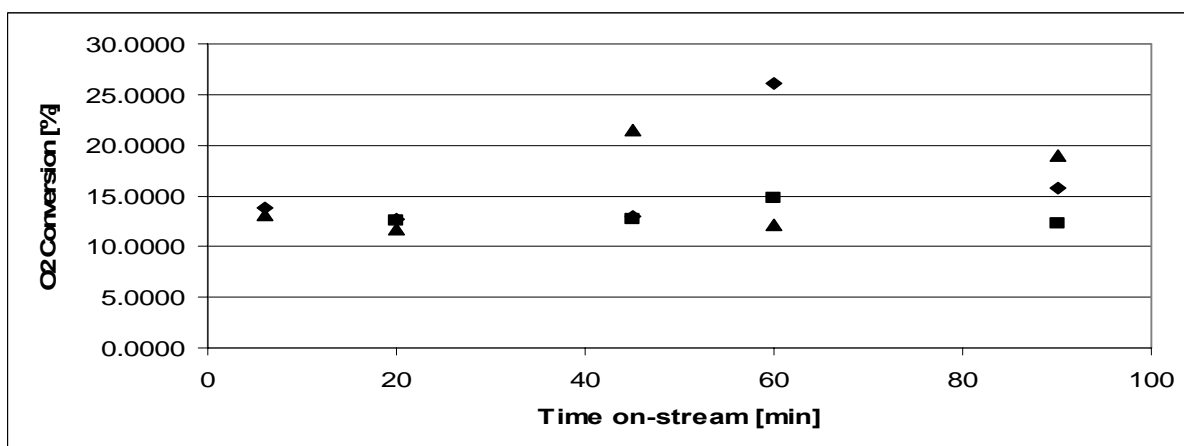


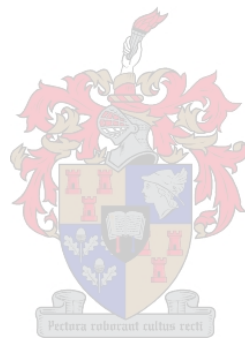
Figure 5-19 Reproducibility of oxygen conversion with time on-stream (350°C, WHSV = 3  $\text{g}_{\text{Propene}}/(\text{g}_{\text{cat}}\cdot\text{h})$ , Propene/Oxygen/Helium = 1/2/7 and  $P_{\text{Total}}=1,45$  bar)

The mean oxygen conversion was calculated as  $15.1 \pm 2,4\%$  for a 95% confidence level. From this the percentage experimental error of the oxygen conversion was calculated as

## Chapter 5 Selective oxidation of propene

16,2%. Since the gaseous oxygen could not be detected with the GC, the oxygen conversion was calculated from a mass balance which resulted in the large experimental error.

The poor repeatability of the product had no effect on the modelling in the following sections since only the propene conversion was used for the modelling.





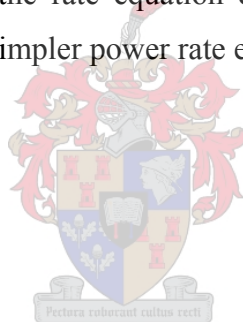
## Chapter 6 Modelling of experimental data

Kinetic modelling can give one useful insight into the inner workings of a catalytic system that can be used to develop or to improve the existing catalysts. The following kinetic modelling was done to gain a better understanding of the reoxidation process, in the low temperature region where the reoxidation of  $\alpha$ -bismuth molybdate is reported to be reaction rate limiting during the selective oxidation of propene to acrolein [Keulks *et al.* 1980].

### 6.1 Power rate law for propene conversion

It is well known that propene reacts with oxygen over  $\alpha$ -bismuth molybdate according to the Mars-van Krevelen mechanism (Keulks *et al.*, 1980; Fansuri 2005). However, depending on the rate limitation of the reaction, the rate equation derived from the Mars-van Krevelen mechanism can be simplified to the simpler power rate equation (equation 6-1), as was seen in section 2.5.1.

$$-r_{propene} = kP_P^n P_{O_2}^m \quad (6-1)$$



The rate constant,  $k$  in equation 6-1, is dependent on the temperature but independent of the concentrations, while  $n$  and  $m$  represent the reaction order of the reaction towards propene and gaseous oxygen partial pressures respectively. To determine the constants  $k$ ,  $n$  and  $m$  (for equation 6-1) from the integral reactor experimental data (appendix E), the packed bed reactor design equation (6-2) [Fogler, 1999] had to be substituted into equation 6-1.

$$-r_{propene} = F_{P,0} \frac{dX}{dW} \quad (6-2)$$

In equation 6-2,  $X$  is the propene conversion,  $F_{P,0}$  the molar flow rate of the propene feed and  $W$  the weight of the catalyst used. Combining equations 6-1 and 6-2, the following expression can be derived:

## Chapter 6 Modelling of experimental data

$$\frac{dX}{dW} = \frac{kP_{P,0}^n (1-X)^n P_{P,0}^m (\theta_{O_2} - \beta X)^m}{F_{P,0}} \quad (6-3)$$

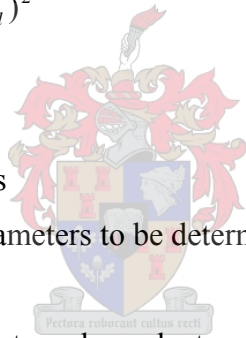
With  $\theta_{O_2}$  being the oxygen to propene feed ratio and  $\beta$  a stoichiometric value.

The value of  $X$  for equation 6-3 can be determined as a function of the mass of catalyst for the different reactions with the fourth order Runge Kutta method. This fourth order Runge Kutta method can be seen in appendix F. The optimum values for  $k$ ,  $m$  and  $n$  were determined from the experimental data by combining the fourth order Runge Kutta method with the least squares equation (equation 6-4 a) and then using the solver function of MS Excel. The solver function was used to determine the values of  $k$ ,  $m$  and  $n$  that fitted the model to the experimental data with the least squares. The variance of the model was determined with equation 6-4 b.

$$s^2 = \sum (X_{\text{Predicted}} - X_{\text{Experimental}})^2 \quad (6-4 \text{ a})$$

$$\delta^2 = \frac{s^2}{N - K} \quad (6-4 \text{ b})$$

N = number of runs  
K = number of parameters to be determined



Since the rate constant ( $k$ ) is temperature dependent, as described by the Arrhenius equation (equation 6-5), the minimization of the least squares with solver had to be performed separately for the data gathered at the three different temperatures.

$$k = A.e^{\frac{-Ea}{R.T}} \quad (6-5)$$

A = frequency factor,  $h^{-1}$   
Ea = Activation energy, J/mol  
R = Universal gas constant, 8,314 J/(mol.K)  
T = Temperature, K

The model predicted for the different temperatures versus the experimental data are displayed in Figure 6-1.

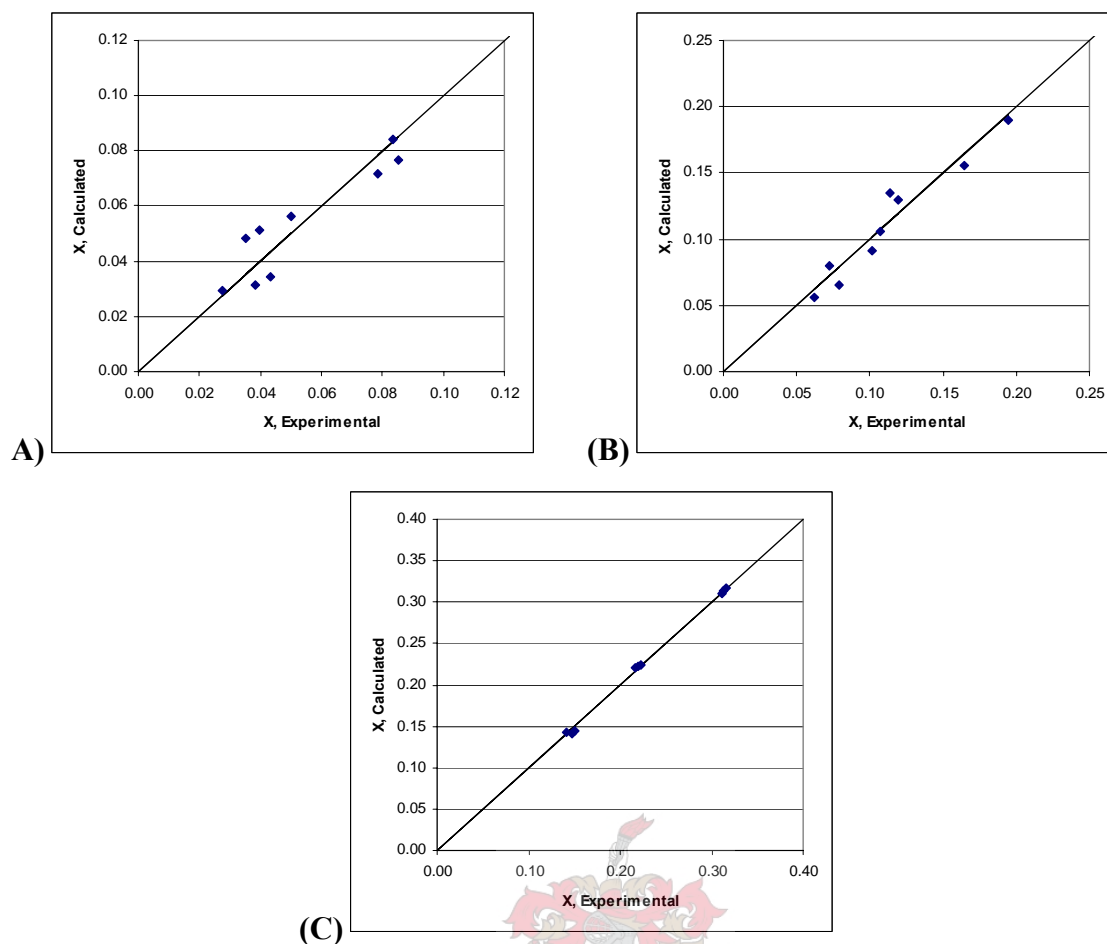


**Figure 6-1** The values for propene conversion (X) predicted with the optimum k, m and n determined for the model versus the experimental values for (A) 325°C, (B) 350°C and (C) 375°C

The optimum values for k, m, n and the model variance determined with the method described above can be seen in Table 6-1. Since no reaction orders for propene conversion were reported for pure  $\alpha$ -Bismuth molybdate in the literature these values had to be compared with that reported by Redlinghöfer *et al.* [2003] for a multicomponent industrial  $\alpha$ -Bismuth molybdate. In section 2.5.2 it can be seen that Redlinghöfer *et al.* [2003] showed that the reaction order for propene jumped from 0 to 1 while the reaction order for oxygen decreased for a temperature rise from 350 to 360°C. The components added to the multicomponent bismuth molybdate catalyst changed the reaction mechanism and therefore this can not be directly compared with pure  $\alpha$ -Bismuth molybdate, but can serve as an indication of the reaction orders of a similar catalyst. In Table 6-1 a similar jump is seen in the reaction order of propene although the jump was more gradual. This jump in the propene reaction order and the decrease of the oxygen reaction order for the propene conversion is an indication that the reaction shifted from reoxidation to reduction rate limiting for a temperature increase from 350 to 375°C.

**Table 6-1 Rate constants and reaction orders for propene and oxygen calculated for  $\alpha$ -Bi<sub>2</sub>Mo<sub>3</sub>O<sub>12</sub>**

Temperature [°C]	k	n	m	$\delta^2$
325	0.09	0.00	0.23	$8,37 \times 10^{-4}$
350	0.78	0.48	0.51	$1,45 \times 10^{-4}$
375	2.24	1.00	0.03	$1,55 \times 10^{-5}$

In Table 6-1 it can be seen the reaction orders for propene (n) were lower than that of the oxygen (m) at 325°C which indicated that the reaction was reoxidation rate limiting at this temperature. It was also seen that at 350°C the cross over from reoxidation rate limiting to reduction rate limiting had already started. The reaction order of oxygen increased from 325 to 350°C and then decreased from 350 to 375°C. Redlinghöfer *et al* [2003] showed similar oxygen reaction order behaviour for an industrial multicomponent bismuth molybdate in Table 2-3. It can also be seen that the reaction is already reduction rate limiting at 375°C and did not start at 410°C as reported by Keulks *et al* [1980]. Keulks *et al.* [1980] calculated the transition temperature of 410°C based on the acrolein formation by looking at the Arrhenius plot. They then decided, based on personal judgement, which points in the transition region lay in the reoxidation rate limiting region and which points lay in the reduction rate limiting region. It is also interesting to see that the reaction orders of oxygen for acrolein and carbon dioxide formation they calculated were smaller than that of propene at 375°C (section 2.5.2), which was an indication that the reaction was already reduction rate limiting at 375°C. It can thus be concluded that the reduction rate limiting region starts at a lower temperature than the 410°C reported by Keulks *et al* [1980].

To confirm if the rate constant, k, values that were determined with the method described above were in the right order of magnitude, the experimental data were used to calculate k from the average rates of reaction. The average rates of propene conversion were determined with the differential reactor design equation 6-6 and can be seen in Appendix E.

$$-r_{\text{Propene, Average}} = \frac{F_{P,0} X}{W} \quad (6-6)$$

With: W = Weight of catalyst, g  
 $F_{\text{Propene},0}$  = Feed rate of propene, mmol/min  
X = Conversion of propene

The average k values that were calculated from the average rate of reactions were all in a range between: 0,065-0,130 min<sup>-1</sup> for 325°C; 0,654-0,950 min<sup>-1</sup> for 350°C and 0,958-2,189

## Chapter 6 Modelling of experimental data

$\text{min}^{-1}$  for  $375^\circ\text{C}$ . By comparing these values with the values of  $k$  in Table 6-1 it can be concluded that the optimum values for  $k$ , calculated with MS solver correspond well to those calculated assuming that the reactor was differential and were therefore in an order of magnitude that was physically possible. Therefore, an Arrhenius plot could be done to determine the activation energy for the propene conversion during the selective oxidation of propene to acrolein with  $\alpha$ -Bismuth molybdate.

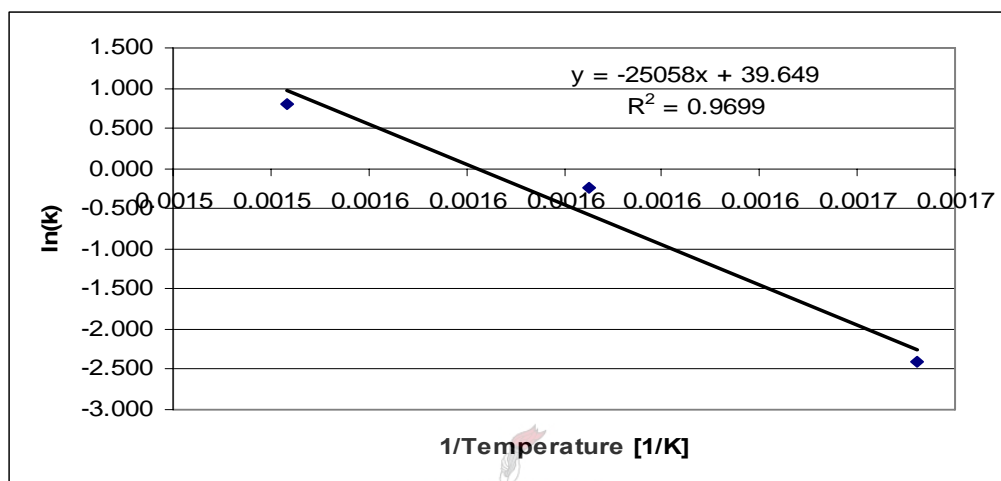


**Figure 6-2 Arrhenius plot for low temperature region ( $<375^\circ\text{C}$ ) of the selective oxidation of propene to acrolein over  $\alpha$ -Bismuth molybdate**

Since the reaction orders in Table 6-1 indicated that the reaction was not reoxidation rate limiting at  $375^\circ\text{C}$  the activation energy calculated with the Arrhenius plot (Figure 6-2) was called the activation energy of the low temperature region and not that of the reoxidation rate limiting region. The activation energy for propene conversion was calculated as  $208 \text{ kJ/mol}$ . This was in the same order of magnitude as the activation energy for acrolein formation that was calculated as a value between  $180$  and  $220 \text{ kJ/mol}$  by Keulks *et al.* [1980]. Even though the fit of the Arrhenius plot was good it might seem as if the point in the middle indicates a systematic development (Two different slopes) which is another indication of a change in the reaction mechanism in this region. To confirm this, more experimental data at different temperatures are necessary.

## 6.2 Reoxidation of $\alpha$ -Bismuth molybdate during the selective oxidation of propene to acrolein

A lot of work on the reaction mechanism of propene over  $\alpha$ -Bismuth molybdate has been done, as has been discussed in section 2.2.2. In Figure 2.2 it can be seen that there are different opinions about the reaction mechanism of the reduction of the catalyst that are still receiving attention. However, the reaction mechanism of the reoxidation of the catalyst has not been investigated that intensively and several questions still need to be answered. One question that needs to be answered is how species E, in the well known SOHIO process proposed by Grasselli [Hanna 2004] (Figure 2-8), is reoxidized to species A. To determine the exact species in the reoxidation process (From E to A in Figure 2-8) spectroscopic methods would have to be used. However, spectroscopic facilities were not available and therefore the reoxidation process was investigated with kinetic information. It is also known that electrophilic oxygen species are responsible for the non-selective oxidation products that form, but the exact mechanism how this occurs has not been demonstrated.

### 6.2.1 Electron transfer mechanism during catalyst reoxidation

A reaction mechanism (electron flow diagram) (Figure 6-3) has been formulated in this study based on ideas from the literature review to try and explain how the catalyst is reoxidized and how the non-selective oxidation products form as a result of this reoxidation process. In the literature review it was seen that the partial oxidation of propene to acrolein occurs with a redox mechanism where the catalyst is reoxidized at one site and reduced at another and therefore electrons have to be conducted like electricity through the catalyst lattice from the one site to the other. It was seen in section 2.3.1.4 that an electron transfer from the catalyst to the dioxygen molecule must occur to form nucleophilic and electrophilic oxygen species. The exact spot on the catalyst where the first electron is transferred to the dioxygen molecule (Step 1 in Figure 6-3) is not known and therefore a general reoxidation mechanism has been formulated based on a general unknown site. For the nucleophilic oxygen species to be incorporated into the catalyst structure a vacant site (site where oxygen has been removed from the catalyst lattice) is needed and therefore the electron transfer will be most likely to occur at such an oxygen vacancy. There are three possible ways for the oxygen to adsorb to the catalyst site where the electron transfer must occur:

## Chapter 6 Modelling of experimental data

- 1) The oxygen shares orbitals with a bismuth atom at the vacancy
- 2) The oxygen shares orbitals with a molybdenum atom at the vacancy
- 3) The oxygen shares orbitals with both the bismuth and the molybdenum atoms at the vacancy

To determine which one of these possibilities actually occurs, spectroscopic facilities would be needed and should be investigated in the future. The proposed mechanism (Figure 6-3) below is valid for any one of these adsorption possibilities with the only complication occurring in Step 2 as will be explained below.

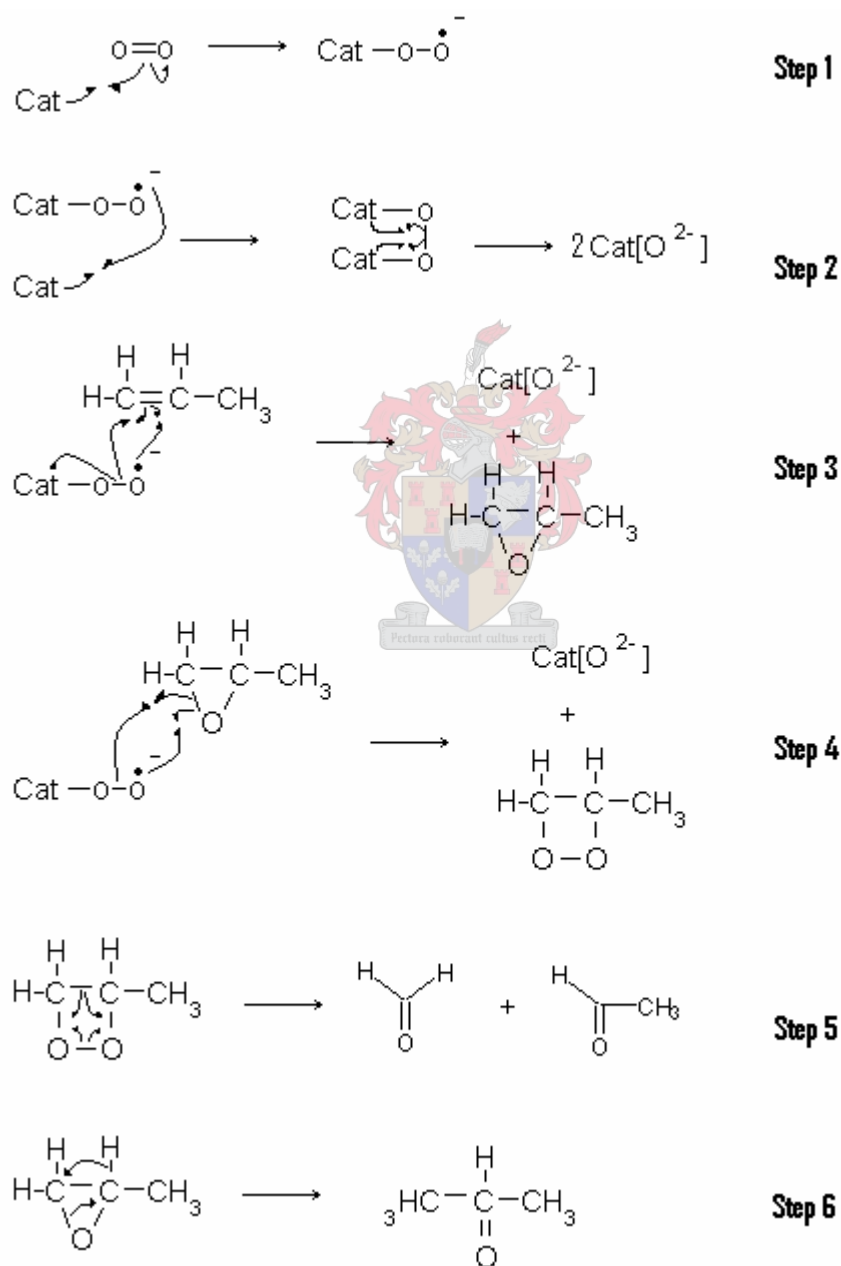


Figure 6-3 Proposed reoxidation scheme and side product formation

## Chapter 6 Modelling of experimental data

In the mechanism it is proposed that when the first electron is transferred to the dioxygen molecule two of the electrons in the double bond of the dioxygen have to move to the oxygen atom furthest away from the catalyst resulting in the ionic species in Step 1. This ionic species is very reactive and will react with the catalyst surface and take up another electron resulting in a dioxygen bridge on the catalyst surface. This is where the complication occurs mentioned above with the absorption of the dioxygen molecule at the reaction site. The question arises if the second bond in the dioxygen bridge forms inside the same oxygen vacancy site or with an adjoining oxygen vacancy site. Since only one nucleophilic oxygen can be incorporated into one oxygen vacancy it will be assumed that this dioxygen bridge will occur across two oxygen vacancies at two identical spots. It is further proposed that Step 2 is finished when two more electrons flow from the catalyst to the dioxygen species resulting in a split in the oxygen bridge to form two nucleophilic oxygen species on the catalyst surface.

It is further proposed that the ionic species in Step 1 is also responsible for the formation of carbon dioxide. In Step 3 it can be seen that one oxygen atom can be inserted into a propene molecule resulting in one nucleophilic oxygen on the catalyst surface and a very unstable oxyhydrocarbon. This oxyhydrocarbon can react with the catalyst ionic species from Step 1 (Step 4) and spontaneously decompose into formaldehyde and acetaldehyde (Step 5), or a hydrogen and oxygen bond shift can occur inside the oxyhydrocarbon (Step 6) to form acetone. It is interesting to note that according to the proposed reaction mechanism the catalyst is reoxidized while the non-selective oxidation products form.

For the experiments that were conducted carbon dioxide was the only side product that was detected. It should be noted that Figure 6-3 does not show how carbon dioxide is formed during the reoxidation process and should be further investigated. A possible reason why no acetone was detected was because Step 6 had steric difficulty to occur. This steric difficulty is the result of the oxygen and hydrogen atoms which are situated on opposite sides of the intermediate oxyhydrocarbon molecule. However, formaldehyde and acetaldehyde were not detected either, because the selectivity of these products was very low, the FID and TCD detectors could not detect them. To verify this model mathematically higher propene conversions must be studied. These higher propene conversions are necessary for the FID and TCD to detect these side products. These intermediates are also very reactive which results in fast reactions to form carbon dioxide.

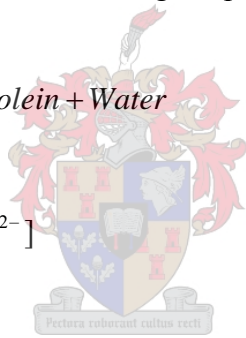


It should also be noted that the proposed mechanism above only shows how the electron transfer occurs from the catalyst to the oxygen to form the electrophilic and nucleophilic oxygen species and not how species E in Figure 2-8 is transformed to species A. It also does not show how the water is produced during the reoxidation process.

### 6.2.2 Rate determining step during reoxidation reaction

To determine which step in the reoxidation rate limiting region is rate limiting new models were derived to investigate the reoxidation of the catalyst in the low temperature region. These models represented the surface oxidized sites ( $A_1$ ) and the surface oxygen vacancy sites ( $E_1$ ) the same way as in the Mars van Krevelen mechanism, while the models also took into account the subsurface oxidized sites ( $A_2$ ) and oxygen vacancies ( $E_2$ ).

The different models were based on the following simplified steps:



Since it is known that the reaction is reoxidation rate limiting at low temperatures ( $<375^\circ\text{C}$ ) the total reduction reaction of the catalyst can be represented by one step (Step 1). The reoxidation of the catalyst surface can be split into four separate reaction steps (Steps 2 to 5). Step 2 represents the orientation and first electron transfer to the gaseous dioxygen molecule. While Step 3 represents the formation of the dioxygen bridge between the two adjoining oxygen vacancies and the final electron transfer to split the oxygen into the two nucleophilic oxygen ions. It is assumed that the nucleophilic oxygen is not formed directly at the correct orientation and that it should diffuse to its correct position to form the reoxidized site  $A_1$  (Step 4). The nucleophilic oxygen species that is still not at its correct position is represented by  $[O^{2-}]$  in the model. Since the oxygen can diffuse in the catalyst bulk the oxidized sites not exposed to the surface ( $A_2$ ) can also reoxidize the vacant sites at the catalyst surface ( $E_1$ ) and

vice versa. This is represented by Step 5 with  $A_1$  being the surface oxidized sites and  $E_2$  being the oxygen vacancies not exposed to the catalyst surface.

To determine which one of the reaction steps is rate limiting, mathematical models needed to be derived from the equations above that could be compared with the experimental data obtained. From Steps 2 to 5 it can be seen that there are basically three steps that can be rate limiting during the reoxidation process and are given below.

- The adsorption of the dioxygen molecule is rate limiting (Step 2)
- The formation of nucleophilic oxygen from electrophilic oxygen is rate limiting (Step 3)
- The diffusion of the nucleophilic oxygen to the desired site is reaction rate limiting (Steps 4 and 5)

It was assumed that Step 3 is not rate limiting because the ionic oxygen species are very reactive and if this reaction was rate limiting, carbon dioxide and not acrolein would be the major product that will form during the reaction. Three models were derived assuming the rate is determined by one step while the rest of the reaction steps are at equilibrium.

### Adsorption of dioxygen molecule is rate limiting

The first model was derived by assuming Step 2 is rate limiting while the rest of the Steps are at equilibrium. It then follows, according to stoichiometry, that the rate of propene can be given as:

$$-r_{\text{Propene}} = -2r_{O_2} = 2k_2[E_1]P_{O_2}^m \quad (6-7)$$

From section 2.5.1 it was seen that the surface oxygen vacancies ( $E_1$ ) can be represented by  $1-\theta$ . With  $\theta$  being the fraction of the catalyst surface that is fully oxidized and is given in section 2.5.1 as equation 2-9. It then follows from substitution that:

$$\begin{aligned} -r_{\text{Propene}} &= 2k_2(1-\theta)P_{O_2}^m \\ \therefore -r_{\text{Propene}} &= 2k_2 \left( 1 - \frac{2k_o P_{O_2}^m}{k_p P_P^n + 2k_o P_{O_2}^m} \right) P_{O_2}^m \end{aligned} \quad (6-8)$$

Equation 6-8 can then be simplified:

$$-r_{\text{Propene}} = \frac{2k_2k_p P_{O_2}^m P_P^n}{k_p P_P^n + 2k_o P_{O_2}^m} \quad (6-9)$$

$$\therefore -r_{\text{Propene}} = \frac{1}{\frac{K_A}{P_{O_2}^m} + \frac{K_B}{P_P^n}}$$

If the adsorption of the dioxygen molecule is the rate limiting step then the experimental data will fit equation 6-9 with  $K_A$  and  $K_B$  being general temperature dependent constants. Since the experimental data that were obtained were from an integral reactor equation 6-9 was substituted into the integral design equation 6-2:

$$\frac{dX}{dW} = \frac{1}{F_{P,0} \left( \frac{K_A}{P_{O_2}^m (\theta_{O_2} - 0,5X)^m} + \frac{K_B}{P_P^n (1-X)^n} \right)} \quad (6-10)$$

### Bulk oxygen diffusion is rate limiting

It was seen in the previous section that the reoxidation process can occur via two different mechanisms: The one mechanism predicts that the oxygen is inserted into the catalyst bulk with the help of two adjoining oxygen vacancies (Dual site reoxidation); while the other mechanism indicates that each nucleophilic oxygen anion is formed at one oxygen vacancy (Single site reoxidation).

#### Bulk oxygen diffusion rate limiting with a dual site reoxidation mechanism

The second model that was derived assumed that the diffusion of the oxygen through the catalyst bulk is the rate limiting step in the reaction, while reoxidation occurs with the dual site reoxidation mechanism. If oxygen bulk diffusion is the rate limiting step then the rate of surface oxidized site formation will be the step that determines the rate of propene conversion. It can then be assumed that if the bulk oxygen diffusion is rate limiting, then the rate of the propene consumption will be the same as the formation of the surface reoxidized sites (equation 6-11). This can be justified because the model is based on the assumption that the rest of the reactions are all at equilibrium.

## Chapter 6 Modelling of experimental data

$$-r_{\text{Propene}} = r_{A_1} = r_{\text{Step4}} + r_{\text{Step5}} \quad (6-11)$$

If the subsurface oxidized sites continuously reoxidize the surface oxygen vacancies the catalyst will deactivate with time. In section 5.2.1 the experimental data showed that the catalyst did not deactivate with time which indicated that the amount of oxygen in the catalyst stayed the same during the reaction. Therefore Step 5 will be at equilibrium, meaning that the forward and backwards rates are the same. It follows that the rate at which total new surface oxidized sites form is only depended on Step 4.

$$\therefore -r_{\text{Propene}} = r_{A_1} = r_4 = k_4[O^{2-}] \quad (6-12)$$

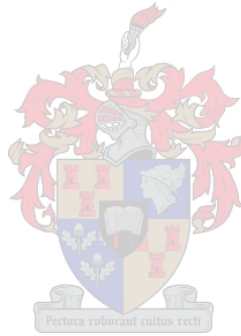
Since the rest of the steps are at equilibrium the following equilibrium constants can be derived:

$$K_1 = \frac{P_{\text{Acrolein}} \cdot [E_1]}{[A_1] \cdot P_p^n}$$

$$K_2 = \frac{[\text{Cat} - O - O^-]}{[E_1] \cdot P_{O_2}^m}$$

$$K_3 = \frac{[O^{2-}]^2}{[E_1][\text{Cat} - O - O^-]}$$

$$K_5 = \frac{[A_2][E_1]}{[A_1][E_2]}$$



By substituting these equilibrium constants into equation 6-12, a model can be obtained to determine the propene consumption rate if the diffusion of oxygen in the catalyst lattice is rate limiting (equation 6-13).

$$-r_{\text{Propene}} = k_4 \sqrt{K_2 K_3 P_{O_2}^m} [E_1]$$

$$\therefore -r_{\text{Propene}} = K_C \sqrt{P_{O_2}^m} (1 - \theta) \quad (6-13)$$

$K_C$  in equation 6-13 is a general temperature constant that includes all the other constants in the equation. By substituting the equation for the surface coverage,  $\theta$ , (equation 2-9) into equation 6-13 this can further be simplified to a general form (equation 6-14) on which the experimental data will fit if the oxygen diffusion is the rate limiting step for a dual site reoxidation mechanism.

$$-r_{Pr\ opene} = \frac{K_D P_P^n \sqrt{P_{O_2}^m}}{P_P^n + K_E P_{O_2}^m} \quad (6-14)$$

In equation 6-14  $K_D$  and  $K_E$  are also general constants that include all the rate and equilibrium constants. Equation 6-14 should be substituted into the differential reactor design equation (equation 6-2) to form equation 6-15, which can be used to see if the experimental data fit this second model.

$$\frac{dX}{dW} = \frac{K_D P_P^n (1-X)^n \sqrt{P_P^m (\theta_{O_2} - 0,5X)^m}}{F_{P,0} \{P_P^n (1-X)^n + K_E P_P^m (\theta_{O_2} - 0,5X)^m\}} \quad (6-15)$$

### Bulk oxygen diffusion rate limiting with a single site reoxidation mechanism

The third model that was derived assumed that the reoxidation process occurs with a single site reoxidation mechanism while the diffusion of the bulk oxygen is rate limiting. The only difference between the third and the second model was to substituting Step 3 with the following step, since no extra oxygen vacancy is needed for the nucleophilic oxygen species to form:



The equilibrium constant for the step will then change to the following equation, while the rest of the equilibrium constants stay the same:

$$K_3 = \frac{[O^{2-}]^2}{[Cat - O - O^-]} \quad (6-16)$$

By substituting these changes into equation 6-12 and combining it with the integral reactor design equation (equation 6-2), the following equation can be derived:

$$\frac{dX}{dW} = \frac{1}{F_{P,0}} \sqrt{\frac{K_F P_P^{n+m} (1-X)^n (\theta_{O_2} - 0,5X)^m}{P_P^n (1-X)^n + K_G P_P^m (\theta_{O_2} - 0,5X)^m}} \quad (6-17)$$

Equation 6-17 will be valid with temperature dependent constants  $K_F$  and  $K_G$  if the bulk oxygen diffusion is rate limiting for a single site reoxidation mechanism.

To determine which one of these models are the correct mechanism, the optimum parameters for each were determined from the experimental data. The optimum parameters were determined the same way, with Solver and the fourth order Runge Kutta method, as was described in section 6.1 for the power rate law. The optimum parameters as well as the variance of the models at each temperature are given in Tables 6-2 and 6-3.

**Table 6-2 Optimum reaction orders for the different reoxidation rate limiting models**

Temperature	Model 1 (Eq 6-10)		Model 2 (Eq 6-15)		Model 3 (Eq 6-17)	
	n	m	n	m	n	m
325°C	1,00	1,00	0,00	0,60	0,00	0,70
350°C	0,70	1,00	0,30	1,00	0,40	1,00
375°C	1,00	0,40	1,00	0,00	1,00	0,40

**Table 6-3 Optimum temperature depended constants and variance ( $\delta^2$ ) for the different reoxidation rate limiting models**

Temperature	Model 1 (Eq 6-10)			Model 2 (Eq 6-15)			Model 3 (Eq 6-17)		
	$K_A$	$K_B$	$\delta^2$	$K_D$	$K_E$	$\delta^2$	$K_F$	$K_G$	$\delta^2$
325°C	1,07	1,60	$7,77 \times 10^{-5}$	0,10	0,03	$7,69 \times 10^{-5}$	0,02	0,76	$7,69 \times 10^{-5}$
350°C	0,80	0,76	$1,38 \times 10^{-4}$	0,30	0,00	$1,57 \times 10^{-4}$	0,09	0,00	$1,57 \times 10^{-4}$
375°C	0,10	0,44	$1,80 \times 10^{-5}$	3,86	1,69	$2,19 \times 10^{-5}$	2,78	4,84	$5,89 \times 10^{-5}$

The reaction mechanism for the selective oxidation of propene to acrolein over  $\alpha$ -Bismuth molybdate was determined by comparing the variance of the optimum models. The model at the specific temperature that had the smallest variance was determined to be the reaction mechanism for that temperature. This criterion to distinguish between different reaction mechanisms had been described by Fogler [1999] and had been applied before by Hurtado *et al* [2004].

From Table 6-3 it can be concluded that reaction kinetics is not the best method to determine the reaction mechanism of the reaction, because the differences between the variance of the different models are very small. But it can only give a good indication of the mechanism and can be used as a foundation for future isotope tracing and spectroscopic experiments.

## Chapter 6 Modelling of experimental data

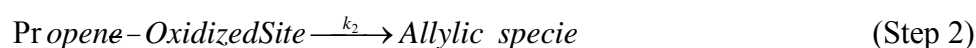
From the variance for the different models at the different temperatures in Table 6-3 it can be seen that it seems as if the reaction mechanism changes with temperature. Models 2 and 3 had the smallest variance at 325°C, but they also had the same variance at 325°C. The fact that they had the same variance made it impossible to distinguish between which reaction mechanism is correct. The variance for Model 1 was very close to that of Models 2 and 3 and no clear distinction could be made between the models. The results could only serve as an indication that Models 2 and 3 were the most likely mechanisms to occur. The conclusion that could be drawn from this was that the bulk oxygen diffusion was most likely to be the rate limiting step at 325°C, but that it could not be determined if the oxygen was inserted with a dual or a single site mechanism.

For 350°C it was seen that model 1 had the smallest variance, which indicated that the first electron transfer from the catalyst to the oxygen molecule was the most likely rate limiting step in the reaction. This might also indicate that the mobility of the oxygen in the lattice had increased enough to overcome bulk oxygen diffusion limitations at 350°C. This agrees with the finding by Libre *et al* [1983] that at higher temperatures oxygen anions diffuse easier through the catalyst bulk. Libre *et al* [1983] explained this faster diffusion of the oxygen by a decrease of the bond strength which is the result of the Bi-O length that increases with an increase in temperature.

From the Power rate law it was seen that at 375°C the reaction was already catalyst reduction rate limiting. Therefore a fourth model was derived assuming the reaction is reduction rate limiting to compare with the result for the reoxidation rate limiting models.

### Reduction rate limiting model

From section 2.2.2 it was seen for the catalyst reduction rate limiting region that the hydrogen abstraction from the propene molecule is the rate limiting step. It was also seen that there are basically just two steps for propene activation up to this rate limiting point: Step 1 is propene coordination on a fully oxidized surface site and Step 2 the abstraction of hydrogen from propene to form an allylic species.



Step 2 is the rate determining step when the reaction is catalyst reduction rate limiting and therefore the rate of propene conversion can be given as:

$$-r_{\text{Pr opene}} = k_2[\text{Pr opene} - \text{OxidizedSite}] \quad (6-18)$$

And it is assumed that step 1 is at equilibrium, because the rate limitation is only dictated by step 2. Therefore the following equilibrium constant for step 1 can be derived:

$$K_1 = \frac{[\text{Pr opene} - \text{OxidizedSite}]}{P_p^n \theta} \quad (6-19)$$

By combining equations 6-18 and 6-19 with the equation for the surface coverage,  $\theta$ , (equation 2-9) the following rate of propene conversion equation was derived:

$$-r_{\text{Pr opene}} = \frac{1}{\frac{K_H}{P_{O_2}^m} + \frac{K_I}{P_P^n}} \quad (6-20)$$

With  $K_H$  and  $K_I$  in equation 6-20 being temperature depending constants. Equation 6-20 is exactly the same form as the Mars-van Krevelen mechanism, but with different constants. Equation 6-20 is also exactly the same as equation 6-9, which indicates that reaction kinetics can not be used to distinguish if the reaction is propene rate limiting or oxygen rate limiting where the limitation is caused by the first electron transfer to the gaseous oxygen molecule.

Equation 6-10 will then also fit the experimental data with a smaller variance than the reoxidation rate limiting models, where the bulk oxygen diffusion is rate limiting, if the propene activation is the rate limiting step. Therefore the optimum reaction order parameters for equation 6-10, in Table 6-2, must be used to determine if the reaction is reduction or reoxidation rate limiting. If the reaction order for propene is higher than the reaction order for oxygen, the reaction is reduction rate limiting; and if the reaction orders are vice versa, the reaction is reoxidation rate limiting.

For 375°C it was seen in Table 6-3 that the variance for model 1 was the smallest with the reaction order for propene (See Table 6-2) larger than that of oxygen. From the variance for



## Chapter 6 Modelling of experimental data

the models in Tables 6-2 and 6-3 it would seem as if the reaction was catalyst reduction rate limiting at 375°C and reoxidation rate limiting at 325 and 350°C. This confirms what was concluded, from the reaction orders of the power rate law, that the reaction was already reduction rate limiting at 375°C.

### 6.3 Differential reactor setup

The parameters  $k$ ,  $m$  and  $n$  determined for the power rate law in section 6.1 were used to evaluate experimental data that Du Preez [2006] obtained for a differential reactor setup. The aim of this evaluation was to compare the differential reactor setup with that of an integral reactor setup. For the differential setup Du Preez split 0,2 g catalyst into three identical reactors that were used for the integral reactor setup. Du Preez did four experiments with this setup with a WHSV of 3  $\text{g}_{\text{Propene}}/(\text{g}_{\text{cat}}\cdot\text{h})$  at 325 and 375°C for oxygen to propene ratios of 1 and 2. This reaction conditions were chosen by Du Preez [2006] to compare with the integral reactor data obtained in this study.

For three differential reactors in series equations 6-21 to 6-23 can be derived to determine the propene conversion in each reactor:

$$X_1 = \frac{\Delta W}{F_{P,0}} k P_{P_1}^n (\theta_{O_2} P_{P_1})^m \quad (6-21)$$

$$X_2 = \frac{\Delta W}{F_{P,0}} \frac{k P_{P_2}^n (\theta_{O_2} P_{P_2})^m}{(1 - X_1)} \quad (6-22)$$

$$X_3 = \frac{\Delta W}{F_{P,0}} \frac{k P_{P_3}^n (\theta_{O_2} P_{P_3})^m}{(1 - X_1)(1 - X_2)} \quad (6-23)$$

With  $\Delta W$  as the amount of catalyst in each reactor and  $P_{P_i}$  being the propene partial pressure in reactor  $i$ . Using these equations with the model parameters from the power rate law (Section 6.1), the theoretical conversions after each reactor were calculated and are displayed versus the experimental conversions in Figures 6-4 to 6-7. Du Preez [2006] compared the differential reactor data with the integral data by calculating the theoretical curve of the propene conversion versus the catalyst weight by substituting the power rate law parameters into a differential equation in Polymath. What his method did not take into account is the fact

Chapter 6 Modelling of experimental data

that there was a pressure drop in the tubes between the differential reactors. Equations 6-21 to 6-23 take these pressure drops into account.

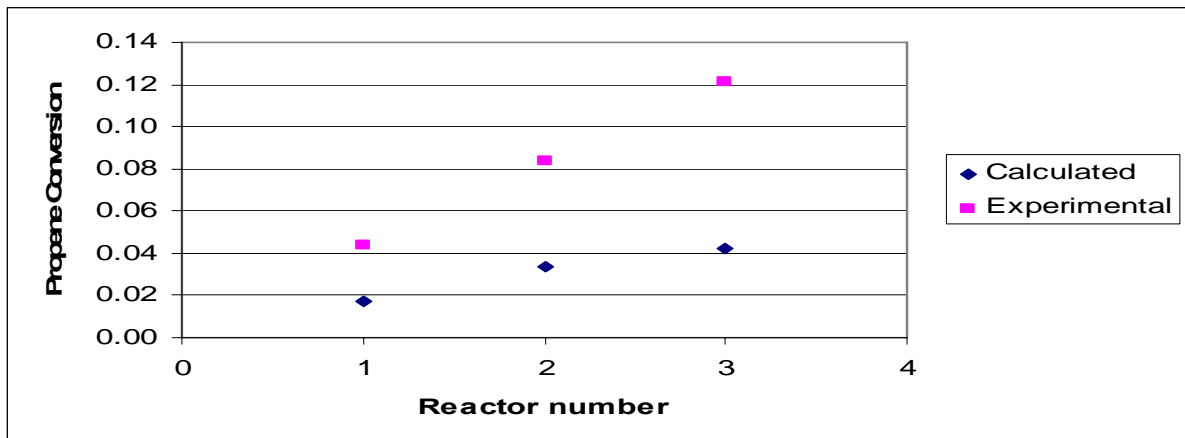


Figure 6-4 Propene conversion of model predicted versus experimental data for differential reactor setup at 325°C for a oxygen to propene ratio of 1.  $WHSV = 3 \text{ g}_{\text{propene}}/(\text{g}_{\text{cat}}\cdot\text{h})$

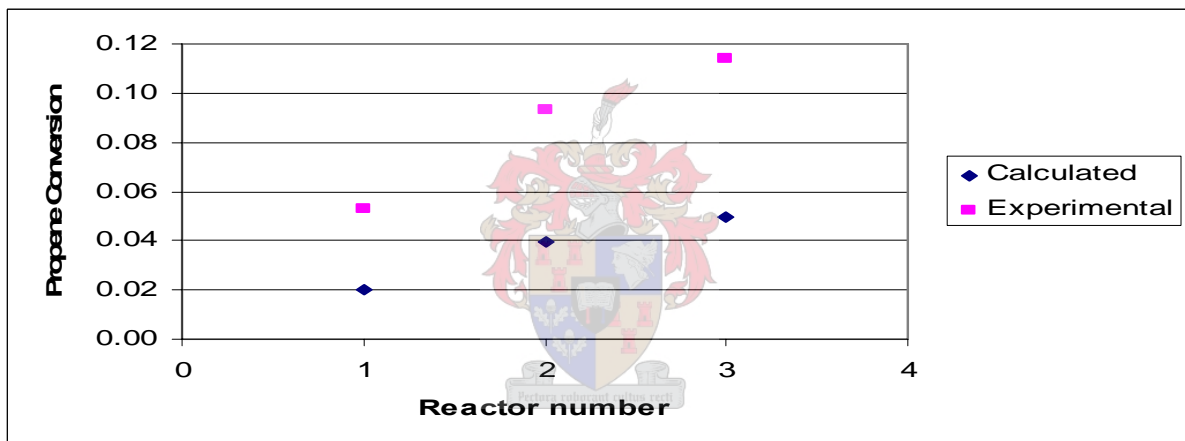


Figure 6-5 Propene conversion of model predicted versus experimental data for differential reactor setup at 325°C for a oxygen to propene ratio of 2.  $WHSV = 3 \text{ g}_{\text{propene}}/(\text{g}_{\text{cat}}\cdot\text{h})$

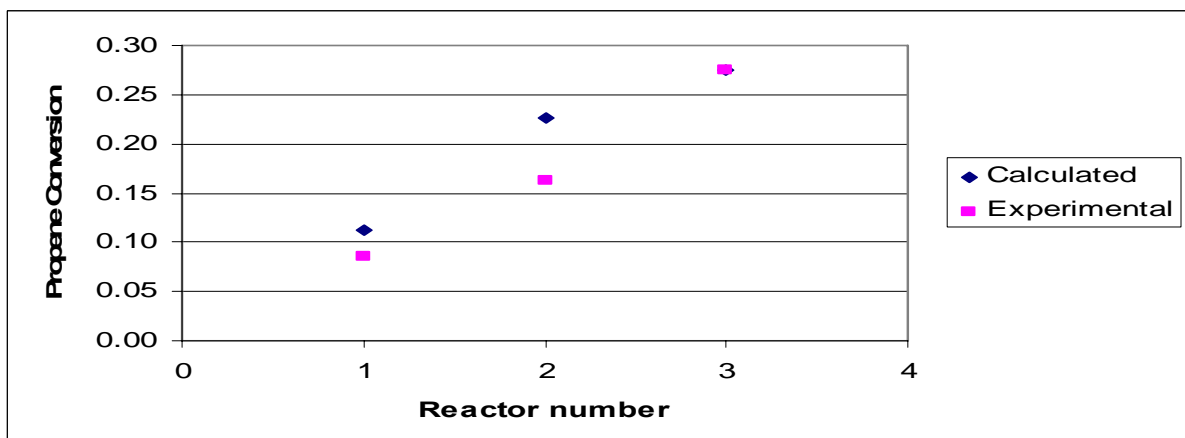


Figure 6-6 Propene conversion of model predicted versus experimental data for differential reactor setup at 375°C for a oxygen to propene ratio of 1.  $WHSV = 3 \text{ g}_{\text{propene}}/(\text{g}_{\text{cat}}\cdot\text{h})$

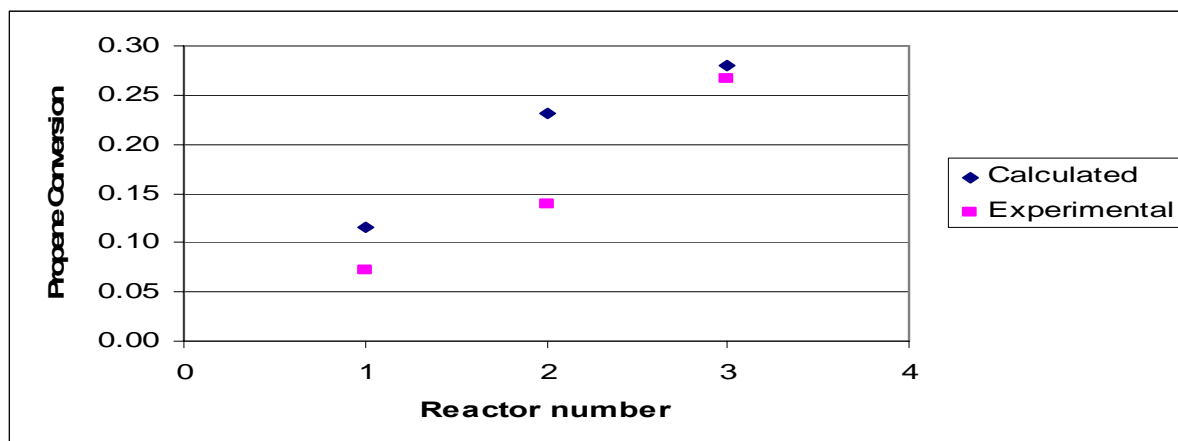


Figure 6-7 Propene conversion of model predicted versus experimental data for differential reactor setup at 375°C for a oxygen to propene ratio of 2.  $WHSV = 3 \text{ g}_{\text{propene}}/(\text{g}_{\text{cat}}\cdot\text{h})$

The four reaction runs gave insufficient data to draw any definite conclusions from the results, but enough to derive some new hypotheses about this setup. In Figures 6-4 and 6-5 it was seen that the experimental values were significantly higher than the values predicted with the model at 325°C. In Figures 6-6 and 6-7 it was seen that the predicted values were slightly smaller than the experimental data, but closer to the experimental values at 375°C.

It is clear from the results that the homogeneous reaction behaviour at 325°C is different from that at 375°C. It was seen that at 325°C (Figures 6-4 and 6-5) the amount of homogeneous reactions increased with increasing reactor size, because the difference between the experimental and predicted conversion increased with an increasing amount of reactors. This was as expected because more reactors and tubing in the reactor setup resulted in an increase of open volume in the system, which will result in more homogeneous reactions. This behaviour was not seen at 375°C where the model predicted the same higher propene conversions than the experimental values. This indicated that at 375°C the homogeneous reactions actually decreased from the amount that occurred during the integral reactor setup. This might be the result of interstage cooling between the differential reactors, because the tubing between the reactors leaves the heating zone between the different reactors (See Figure 3.1). But now the question can be asked why this interstage cooling did have such a big effect at 325°C. This question can not be answered without more experimental work, but it might be the result of the reaction mechanism change that occurs between 325°C and 375°C.

## Chapter 7 Conclusions and recommendations

From the literature review it was concluded that there is a need to produce synthesis gas from methane at low temperatures. It was also seen that  $\alpha$ -Bismuth molybdate might be a mixed metal oxide that is capable of achieving this. However, from experiments it was concluded that the methane is actually inert over  $\alpha$ -Bismuth molybdate at moderate temperatures. From further reading it was also seen that the problem with the partial oxidation of methane at low temperatures is the activation of the methane molecule.

Since the partial oxidation of methane was not feasible over  $\alpha$ -Bismuth molybdate the selective oxidation of propene to acrolein by  $\alpha$ -Bismuth molybdate were investigated. From literature it was seen that no time on-stream experiments had been done for this specific reaction and that several questions regarding the reoxidation still need to be answered. Since the kinetic experiments were so time consuming it was decided to investigate the time on-stream behaviour of the reaction and the reoxidation of the catalyst only in the low temperature region ( $<375^{\circ}\text{C}$ ) where the reaction is reoxidation rate limited.

Experiments showed that the reaction had no external mass transfer limitations at the reaction conditions where the kinetic experiments were conducted. Internal mass transfer studies showed that the reaction rate decreased with a decrease in particle size, which was *visa versa* of what was expected. This confirmed a theory in the literature that states that a certain particle size is required to provide sufficient lattice oxide ions during the redox cycle of the catalyst.

The time on-stream kinetic studies showed that the catalyst stayed active for at least six hours with no change in activity or yield of the different products. It was also seen that the reaction reached steady state almost immediately after the reaction started. These studies were done at a WHSV of  $3 \text{ g}_{\text{Propene}} / (\text{g}_{\text{Catalyst}} \cdot \text{h})$  and the effects of the propene to oxygen feed ratio and temperature were investigated. It was seen that the reaction had similar behaviour at 350 and 375 $^{\circ}\text{C}$ , while the behaviour changed at 325 $^{\circ}\text{C}$ . It was seen that the propene conversion, carbon dioxide yield and oxygen conversion increased with a decrease in the propene to oxygen feed ratio over the whole temperature range. While the acrylic acid selectivity increased and the acrolein selectivity decreased at 325 $^{\circ}\text{C}$  and vice versa at 350 and 375 $^{\circ}\text{C}$ .

## Chapter 7 Conclusions and recommendations

The effect of the WHSV was also studied with different WHSV's of 2, 3 and 5  $\frac{\text{g}_{\text{Propene}}}{(\text{g}_{\text{Catalyst}} \cdot \text{h})}$ . The results showed that the propene and oxygen conversions decrease with an increase of the WHSV. The product yields and reactant conversions were all in the following ranges under the reaction conditions: Propene conversion 4-37%; Oxygen conversion 3-90%; Acrolein yield 60-95%; Acrylic acid yield 3-9%; Carbon dioxide yield 0-18%. Because of the high propene conversion, the reaction data were treated as integral reactor data. The carbon balance for these reaction runs were all between 97 and 103%.

The repeatability of the experiments showed that the catalyst can be regenerated with gaseous oxygen in between runs without a loss in catalyst activity. The propene conversion could be repeated with a difference (error) between the runs of 3,80%. The acrolein yield data had a small error of 3,25%, while the rest of the products had poor repeatability: Carbon dioxide yield error of 113,40%, Acrylic acid yield error of 18,44% and the Oxygen conversion error of 16,18%. The poor repeatability of the product yields can be ascribed to the small quantity of the products that formed at the conditions where the reactions were performed, the poor sensitivity of the TCD, carbon dioxide in the evacuated ampoules and the fact that the oxygen was calculated with a mass balance using these measured products. The poor repeatability had no effect on the modelling of the reaction, because only the propene conversion was used for this purpose.

A mechanism had been proposed of how the electron transfer occurs during the activation of the gaseous dioxygen molecule to explain how nucleophilic oxygen anions are formed during the reoxidation of the catalyst. This mechanism explains how the non-selective oxidation products are formed by the reaction of electrophilic oxygen with propene. It also shows how nucleophilic oxygen anions are formed in the reaction between the electrophilic oxygen and propene.

This mechanism was used to derive models to determine which step is the rate limiting step during the reoxidation process. Using the different models it was determined from the experimental data that the rate limiting step at 325°C was most likely to be bulk oxygen diffusion. However, it could not be distinguished if the oxygen is inserted with a single or a dual site mechanism. It was also determined that the oxygen coordination and first electron transfer from the catalyst to the gaseous oxygen molecule was the most likely rate limiting step at 350°C, while it indicated that the reaction was already reduction rate limiting at 375°C.

## Chapter 7 Conclusions and recommendations

It was also concluded that reaction kinetics is not the best method to determine the definite reaction mechanism, but can give a good indication of the most likely reaction mechanism.

The aim of the study was reached by showing that  $\alpha$ -Bismuth molybdate is not a feasible catalyst for the catalytic partial oxidation of methane at low temperatures and the work also aided in the answering of questions regarding the reoxidation mechanism of the catalyst.

It is recommended, for the catalytic partial oxidation of methane over mixed metals, that the effect of different additives to the catalyst must be investigated. A possible membrane reactor was also described that might be possible to produce synthesis gas at low temperatures, with a conventional partial oxidation catalyst that thermodynamically favours total oxidation reactions at low temperatures.

For the selective oxidation of propene to acrolein over  $\alpha$ -Bismuth molybdate it is recommended that higher propene conversions are investigated. These higher conversions can be used to study the kinetics of the non-selective oxidation products. It is also recommended that spectroscopy studies are done to determine the exact species that are present during the reoxidation of the catalyst. It is further recommended that isotopic labelling and/or spectroscopic methods are used to study the reoxidation process of the selective oxidation of propene to acrolein over  $\alpha$ -Bismuth molybdate instead of reaction kinetics. A study of the reaction on a more controlled particle size distribution is also recommended to get a better understanding of the oxygen diffusion in the catalyst bulk.

The differential reactor setup for the selective oxidation of propene to acrolein over  $\alpha$ -Bismuth molybdate should also be investigated further.

## References

Ayame, A., Uchida, K., Iwataya, M. and Miyamoto, M., **Applied Catalysis A: General** **227 (2002) 7-17**, X-ray photoelectron spectroscopic study on  $\alpha$ - and  $\gamma$ -bismuth molybdate surfaces exposed to hydrogen, propene and oxygen

Al'kaeva, E.M., Andrushkevich, T.V., Ovsitser, O.Yu. and Sokolovskii, V.D., **Catalysis Today** **24 (1995) 357-359**, Influence of bulk oxygen diffusion on the kinetics of partial oxidation over molybdenum-containing catalysts

Basile, A. and Paturzo, L., **Catalysis Today** **67 (2001) 55-64**, An experimental study of multilayered composite palladium membrane reactors for partial oxidation of methane to syngas

Bettahar, M.M., Costentin, G., Savary, L. and Lavalley, J.C, **Applied Catalysis A: General** **145 (1996) 1-48**, On the partial oxidation of propane and propylene on mixed metal oxide catalysts

Bruno, T., Beretta, A., Groppi, G., Roderi, M. and Forzatti, P., **Catalysis Today** **99 (2005) 89-98**, A study of methane partial oxidation in annular reactor: activity of Rh/ $\alpha$ -Al<sub>2</sub>O<sub>3</sub> and Rh/ZrO<sub>2</sub> catalysts

Brückman, K., Haber, J. and Turek, W., **J. Catalysis** **114 (1988) 196-199**, Kinetics of the oxidation of propene on MoO<sub>3</sub> based model catalysts

Cooper, C.A., Hammond, C.R., Hutchings, G.J., Taylor, S.H., Willock, D.J. and Tabata, K., **Catalysis Today** **71 (2001) 3-10**, A combined experimental and theoretical approach to the study of methane activation over oxide catalysts

De Groote, A.M. and Froment, G.F., **Applied Catalysis A: General** **138(1996) 245-264**, Simulation of the Catalytic Partial Oxidation of Methane to Synthesis Gas

Du Preez, L.J., **Final year project 2006**, Partial oxidation of propene to acrolein using a differential reactor setup, University of Stellenbosch

Djaidja, A., Barama, A. and Bettahar, M.M., **Catalysis Today** **61** (2000) 303-307, Oxidative transformation of methane over nickel catalysts supported on rare-earth metal oxides

Ebrahim, H.A. and Jamshidi, E., **Energy Conversion and Management**, Volume 45, Issue 3, February 2004, Pages 345-363, Synthesis gas production by zinc oxide reaction with methane: elimination of greenhouse gas emission from a metallurgical plant

Fansuri, H., Catalytic partial oxidation of propylene to acrolein: The catalyst structure, reaction mechanism and kinetics, **PhD thesis, Curtin University of Technology, 2005**

Fehlings, M., König, D. and Vogel, H., **Chem. Technik** **52** (2000) 90-95, Partialoxidation von Propen an Bi/Mo-Mischoxiden

Fogler, H.S., **Elements of chemical reaction engineering**, Third Edition, Prentice-Hall 1999

Gates, B.C., Katzer J.R. and Schuit G.C.A., **Chemistry of Catalytic Processes**, McGraw-Hill Inc., 1979

Grasselli, R.K, Brazdil, J.F. and Suresh, D.D., **J. Catalysis** **66**, 347-367 (1980<sup>a</sup>), Redox kinetics of bismuth molybdate ammoxidation catalysts

Greenberg, M.D., **Advanced Engineering Mathematics**, second edition, 1998, Prentice-Hall International, Inc.

Guo, C., Zhang, J., Li, W., Zhang, P. and Wang Y., **Catal. Today** **98** (2004) 583-587, Partial oxidation of methane to syngas over BaTi<sub>1-x</sub>Ni<sub>x</sub>O<sub>3</sub> catalysts

Haber, J. and Turek, W., **J Catalysis** **190**, 320-326 (2000), Kinetic studies as a method to differentiate between oxygen species involved in the oxidation of propene

Han, Y., Ueda, W. and Moro-Oka, Y., **Applied Catalysis A: General** **176** (1999) 11-16, Lattice oxide ion-transfer effect demonstrated in the selective oxidation of propene over silica-supported bismuth molybdate catalysts



Hanna, T.A., **Coordination Chem. Reviews** **248** (2004) 429-440, The role of bismuth in the SOHIO process

Hargreaves, J.S.J., Hutchings, G.J., Joyner, R.W. and Taylor, S.H., **Applied Catalysis A: General** **227** (2002) 191-200, A study of the methane-deuterium exchange reaction over a range of metal oxides

Heintz, M. and Pietruszka, B., **Catalysis Today** **89**(2004) 21-25, Plasma catalytic conversion of methane into syngas: the combined effect of discharge activation and catalysis

Hurtado, P., Ordonez, S., Sastre, H. and Diez, F.V., **Applied Catalysis A: Environmental** **51** (2004) 229-238, Development of a Kinetic Model for the Oxidation of Methane over Pd/Al<sub>2</sub>O<sub>3</sub> at dry and wet conditions

Keulks, G.W., Hall, J.L., Daniel, C. and Suzuki, K., **J. Catalysis** **34**, 79-97 (1974), The catalytic oxidation of propylene; IV. Preparation and characterization of  $\alpha$ -Bismuth molybdate

Keulks, G.W. and Krenzke, L.D., **J. Catalysis** **64**, 295-302 (1980), The catalytic oxidation of propylene; VIII. An investigation of the kinetics over Bi<sub>2</sub>Mo<sub>3</sub>O<sub>12</sub>, Bi<sub>2</sub>MoO<sub>6</sub> and Bi<sub>3</sub>FeMo<sub>2</sub>O<sub>12</sub>

Kharton, V.V., Yaremchenko, A.A., Valente, A.A., Sobyanin, V.A., Belyaev, V.D., Semin, G.L., Veniaminov, S.A., Tsipos, E.V., Shaula, A.L., Frade, J.R. and Rocha, J., **Solid State Ionics** **176** (2005) 781-791, Methane oxidation over Fe-, Co-, Ni- and V-containing mixed conductors

Libre, J.M., Barboux, Y., Grzyboska, B., Conflant, P. and Bonnelle, J.P., **Applied Catalysis**, **6** (1983) 315-328, Catalytic oxidation of propene: Surface potential measurements and structural properties of  $\alpha$ -Bi<sub>2</sub>Mo<sub>3</sub>O<sub>12</sub>,  $\alpha$ -Bi<sub>2</sub>O<sub>3</sub> and MoO<sub>3</sub>

Magagula, Z. and Van Steen, E., **Catalyst Today** **49** (1999) 155-160, Time on stream behaviour in the (amm)oxidation of propene/propane over iron antimony oxide: cyclic operation

Mallens, E.P.J., Hoebink, J.H.B.J. and Marin G.B., **J. Catalysis** **167**, 43-56 (1997), The Reaction Mechanism of the Partial Oxidation of Methane to Synthesis Gas: A Transient Kinetic Study over Rhodium and a Comparison with Platinum

Mars, P. and Van Krevelen, D.W., **Chem. Eng. Sci. (Special supplement)** vol. **8**. 1954, Oxidation carried out by means of vanadium oxide catalysts

Mestl, G., Linsmeier, Ch., Gottschall, R., Dieterle, M., Find, J., Herein, D., Jäger, J., Uchida, Y. and Schlögl, **J. Molec. Catal. A:Chemical** **162** (2000) 463-492, Molybdenum Oxide Based Partial Oxidation Catalyst: 1. Thermally Induced Oxygen Deficiency, Elemental and Structural Heterogeneity and the Relation to Catalytic Performance

Monnier, J.R. and Keulks, G.W., **J. of Catalysis** **68**, 51-66 (1981), The Kinetics and Mechanism over  $\beta$ -Bi<sub>2</sub>Mo<sub>2</sub>O<sub>9</sub>

Ohler, N. and Bell, A.T., **J Catalysis** **231** (2005) 115-130, Selective oxidation of methane over MoO<sub>x</sub>/SiO<sub>2</sub>: isolation of the kinetics of reactions occurring in the gas phase and on the surfaces of SiO<sub>2</sub> and MoO<sub>x</sub>

Otsuka, K., Wang, Y., Sunada, E. and Yamanaka, I., **J. Catalysis** **175**, 152-160 (1998), Direct Partial Oxidation of Methane to Synthesis Gas by Cerium Oxide

Redlingshöfer, H., Kröcher, O., Böck, W., Hutchmacher, K. and Emig, G., **Ind. Eng. Chem. Res.** **2002**, **41**, 1445-1453, Catalytic wall reactor as a tool for isothermal investigations in the heterogeneously catalyzed oxidation of propene to acrolein

Redlingshöfer, H., Fischer, A., Weckbecker, C., Hutchmacher, K. and Emig, G., **Ind. Eng. Chem. Res.** **2003**, **42**, 5482-5488, Kinetic modelling of the heterogeneously catalyzed oxidation of propene to acrolein in a catalytic wall reactor

Schiedernoch, R., Tischer, S., Correa, C., and Deutschman, O., **Chem. Eng. Sci.** **58** (2003) 633-642, Experimental and Numerical Study on the Transient Behaviour of Partial Oxidation of Methane in a Catalytic Monolith

Song, C. and Pan, W., **Catalysis Today** **98** (2004) 463-484, Tri-reforming of methane: a novel concept for catalytic production of industrial useful synthesis gas with desired H<sub>2</sub>/CO ratio

Souza, M.M.V.M and Schmal, M., **Applied Catalysis A: General** **281** (2005) 19-24, Autothermal reforming of methane over Pt/ZrO<sub>2</sub>/Al<sub>2</sub>O<sub>3</sub> catalysts

Sun, W.Z., Jin, G.Q. and Guo, X.Y., **Catal. Comm.** **6** (2005) 135-139, Partial oxidation of methane to syngas over Ni/SiC catalysts

Theron, J.N., The Oxidative Reforming of Methane To Synthesis Gas on a Commercial Steam Reforming Catalyst, **Chem. Eng., PhD Thesis, University of Cape Town, 1997**

Tsyganok, A.I., Inaba, M., Tsunoda, T., Suzukie, K., Takehira, K. and Hayakawa, T., **Applied Catalysis A: General** **275** (2004) 149-155, Combined partial oxidation and dry reforming of methane to synthesis gas over noble metals supported on Mg-Al mixed oxides

Van Hoof, J.H.C., **Chemistry and Chemical Engineering of Catalytic Processes, 1980, 512-521**, The Oxidation and Ammoxidation of Propene

Van Vuuren, P., Selective Oxidation of Propene to Acrolein on  $\alpha$ -Bi<sub>2</sub>Mo<sub>3</sub>O<sub>12</sub> Nano-particles, **Chem. Eng., MScEng Thesis, University of Stellenbosch, 2004**

Viparelli, P., Villa, P., Basile, F., Trifore, F., Vaccari, A., Nanni, P. and Viviani, M., **Applied Catalysis A: General** **280** (2005) 225-232, Catalyst based on BaZrO<sub>3</sub> with different elements incorporated in the structure II. BaZr(1-x)Rh<sub>x</sub>O<sub>3</sub> systems for the production of syngas by partial oxidation of methane

Wang, W., Stagg-Williams, S.M., Noronha, F.B., Mattos, L.V. and Passos, F.B., **Catalysis Today** **98**(2004) 553-563, Partial oxidation and combined reforming of methane on Ce-promoted catalysts

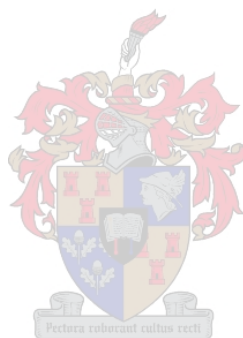
Wu, T., Yan, Q. and Wan, H., **J. Mol., Catal. A: Chemical** **226**(2005) 41-48, Partial Oxidation of Methane to Hydrogen and Carbon Monoxide over a Ni/TiO<sub>2</sub> Catalyst

Xu, D., Li, W., Ge, Q and Xu, H., **Fuel Proc. Tech. 86 (2005) 995-1006**, A novel process for converting coalmine-drained methane gas to syngas over nickel-magnesia solid solution catalysts

Yanina, S.V. and Smit, R.L., **J. Catalysis 213 (2003) 151-162**, The Morphological Evolution of the  $\text{Bi}_2\text{Mo}_3\text{O}_{12}$  (010) Surface in Air- $\text{H}_2\text{O}$  Atmosphere

Zhang, Q., He, D., Han, Z., Zhang, X. and Zhu, Q., **Fuel 81 (2002) 1599-1603**, Controlled partial oxidation of methane to methanol/formaldehyde over Mo-V-Cr-Bi-Si oxide catalysts

Zhu, J., Van Ommen, J.G. and Lefferts, L., **J. Catalysis 225 (2004) 388-397**, Reaction scheme of partial oxidation of methane to synthesis gas over yttrium-stabilized zirconia



## Appendix A: Calibrations of Mass flow controllers (MFC)

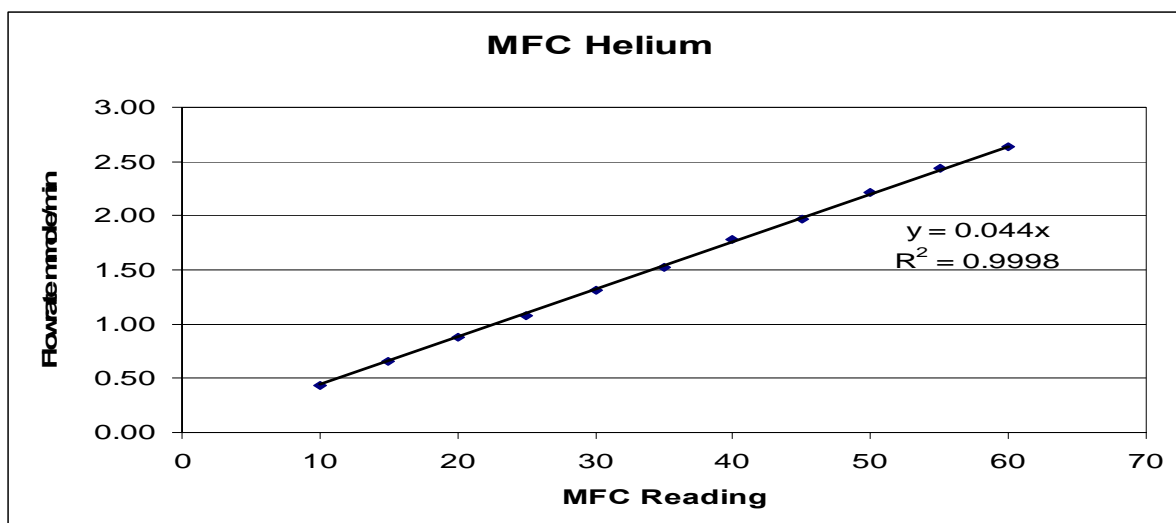


Figure 8-0-1 Calibration data for helium mass flow controller

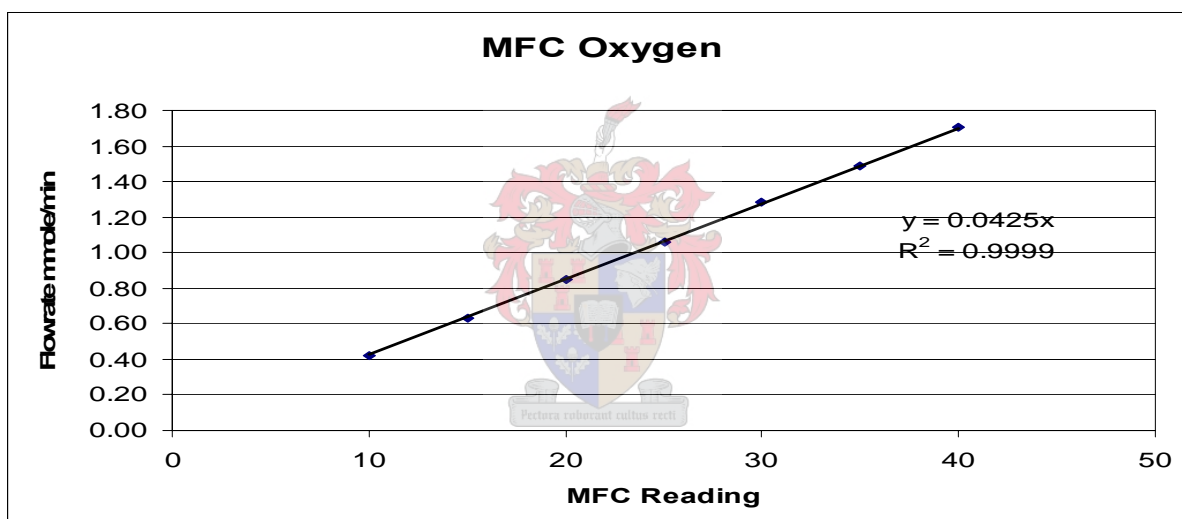


Figure 8-0-2 Calibration data for oxygen mass flow controller

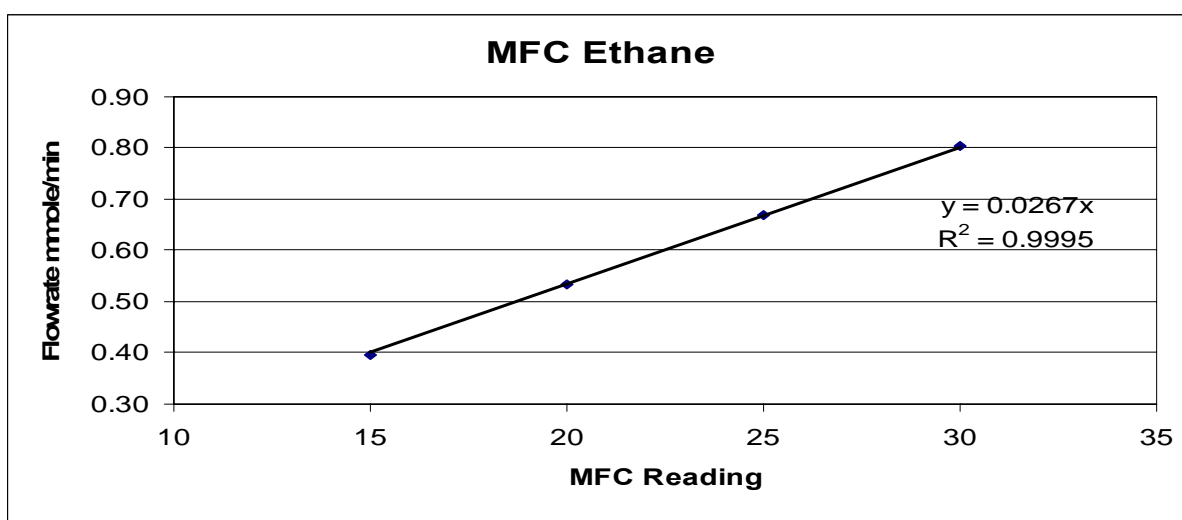


Figure 8-0-3 Calibration data for ethane mass flow controller

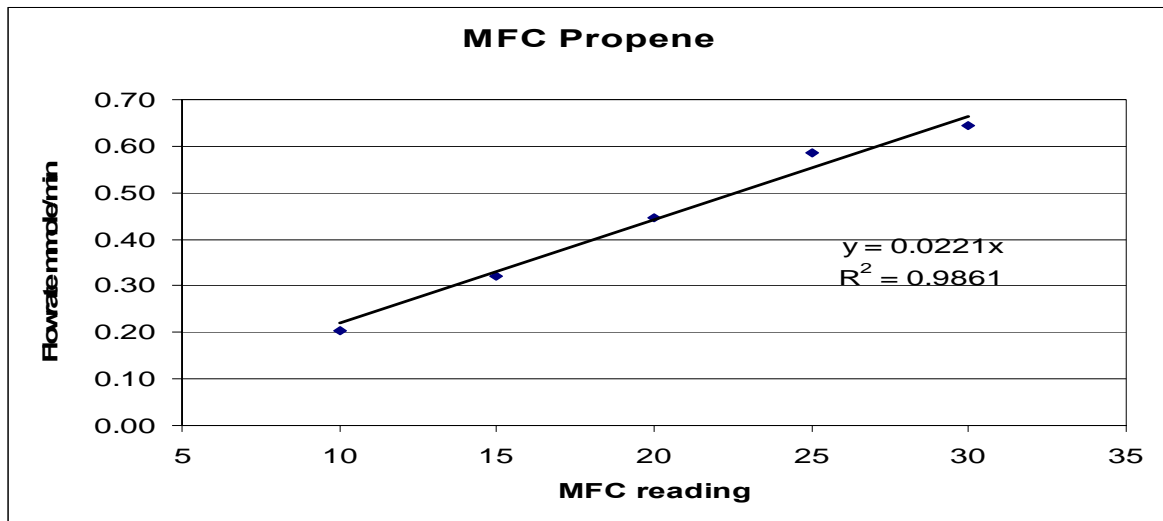


Figure 8-0-4 Calibration data for propene mass flow controller

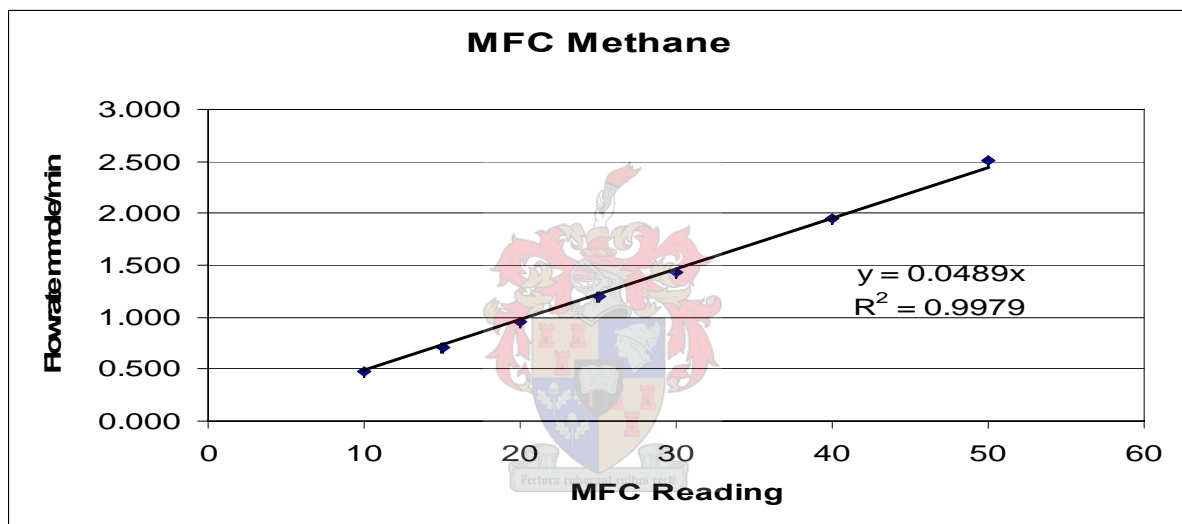


Figure 8-0-5 Calibration data for methane mass flow controller

## Appendix B: Response factor for carbon dioxide

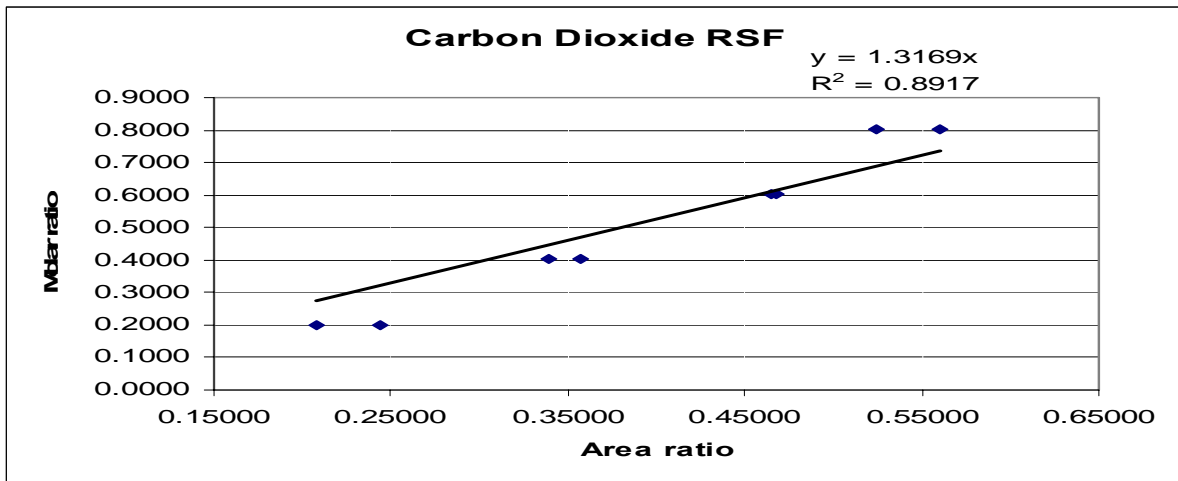


Figure 8-6 Experimental data to determine the carbon dioxide response factor

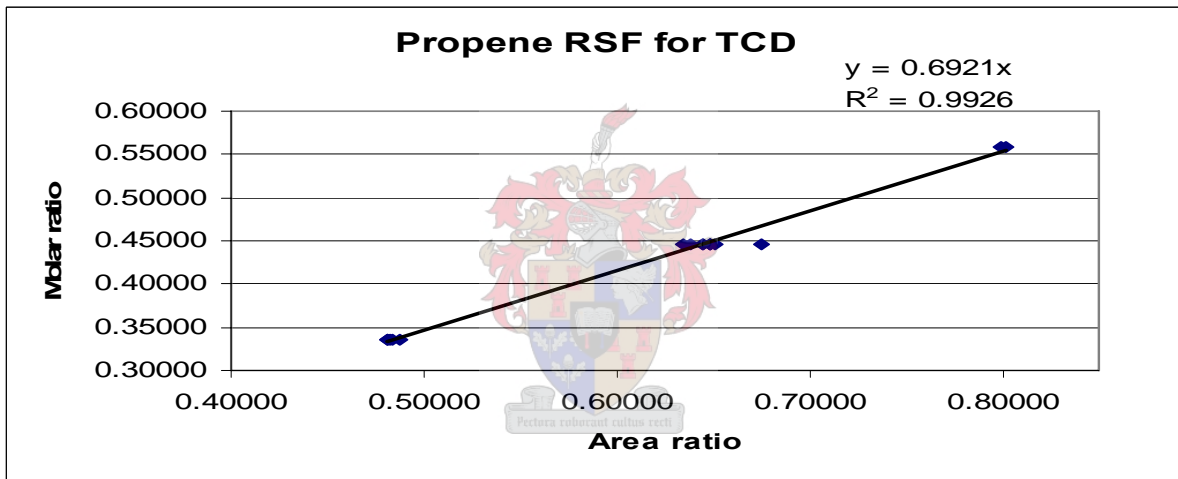


Figure 8-7 Experimental data to determine the Propene response factor for the TCD

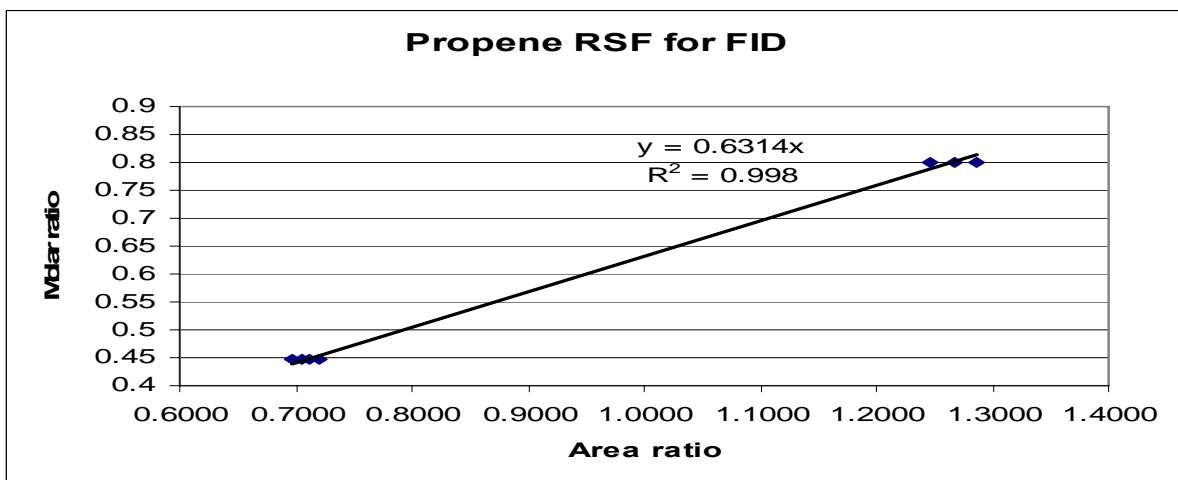


Figure 8-8 Experimental data to determine the Propene response factor for the FID

## Appendix C: Operating the Oven

The first step for a reaction run was to switch on the oven in which the reactor was suspended and the heating wire that heated the product stream. It should be noted that the temperatures measured by the thermocouples inside the oven was out by a certain factor. A calibration was done to determine this factor and can be seen in Figure 8-9. Since the oven temperature cycle in the oven was too big when the oven was set on automatic temperature control ( $\pm 10^{\circ}\text{C}$ ) the oven was controlled manually. This ensured that the temperature was controlled with in  $\pm 2^{\circ}\text{C}$ .

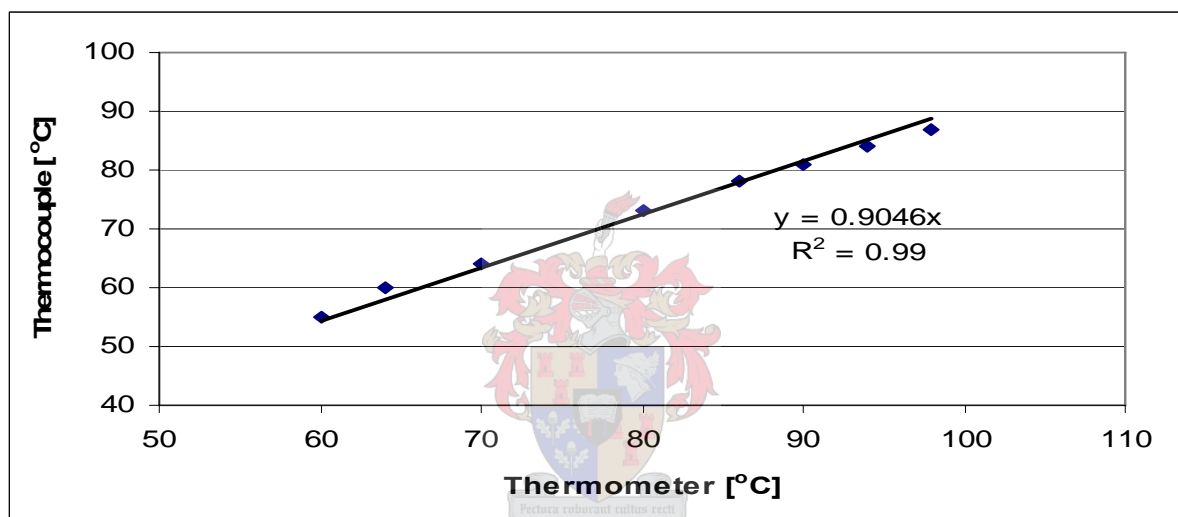


Figure 8-9 Thermocouple calibration chart for the reactor rig oven (With Thermometer being the real temperature)



## Appendix D: Residence Time Distribution (RTD) GC Output

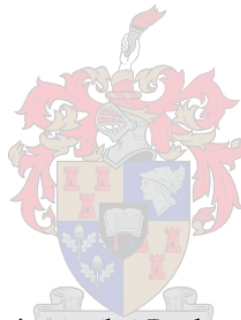
It can be determined if the flow through a reactor is plug flow by studying the residence time distribution function of the reactor [Fogler, 1999]. For a step input the residence-time distribution function  $E(t)$  can be determined with the following equation:

$$E(t) = \frac{d}{dt} \left[ \frac{C(t)}{C_0} \right]_{step} \quad (D-1)$$

The mean residence time can be determined with equation D-2 and the variance can be determined with equation D-3.

$$t_m = \int_0^{\infty} tE(t)dt \quad (D-2)$$

$$\delta^2 = \int_0^{\infty} (t - t_m)^2 E(t)dt \quad (D-3)$$



Using the residence time and the variance the Peclet number ( $Pe_r$ ) can be determined with equation D-4, which can be used to determine the dispersion in a reactor.

$$\frac{\delta^2}{t_m^2} = \frac{2}{Pe_r} - \frac{2}{Pe_r^2} (1 - e^{-Pe_r}) \quad (D-4)$$

One divided by the Peclet number gives an indication of the dispersion in the reactor. The smaller this number, the more plug flow is the flow through the reactor bed.

The experimental data for the residence time distribution are displayed in Figures 8-10 to 8-15. The experiments were done by connecting the reactor exit directly with the TCD of the GC, which recorded the propene output of the reactor. For each run four step inputs were made after 30, 120, 210 and 300 seconds, two by turning the propene open and two by turning the propene shut. It can be seen in the figures that every time the propene was turned open (30 and 210 seconds) the mass flow controllers compromised the step input resulting in an

## Appendices

extra peak. For this reason only the step inputs at 120 and 300 seconds (Propene shut down) were used to calculate the Peclet numbers for the different flow conditions in the reactors.

Figures 8-14 and 8-15 showed that the residence time in the reactor rig tubing at 60 ml/s was 5,6 seconds and at 75 ml/s it was 4,8 seconds. These times were subtracted from the step inputs for the different flow rates.

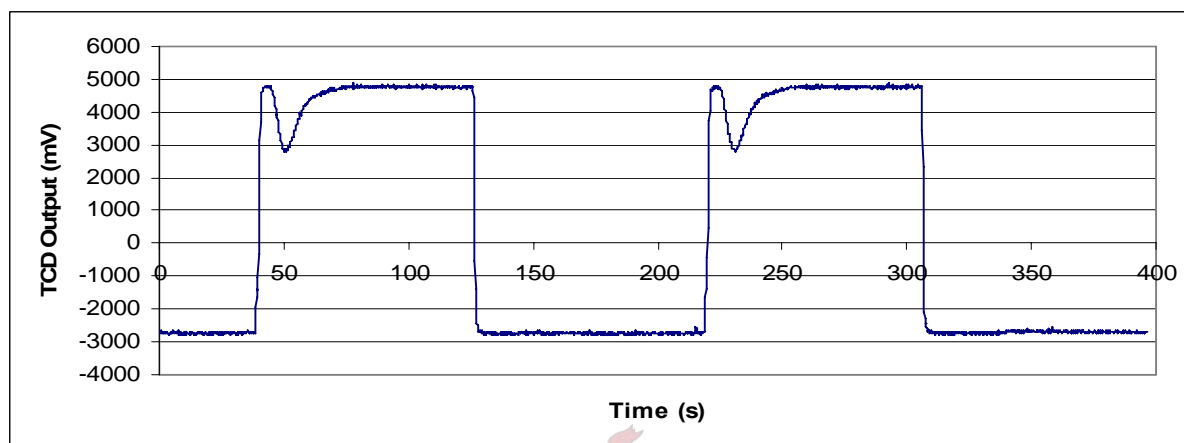


Figure 8-10 TCD output for Propene step input through glass reactor (Flow rate = 60 ml/s; T = 27°C)

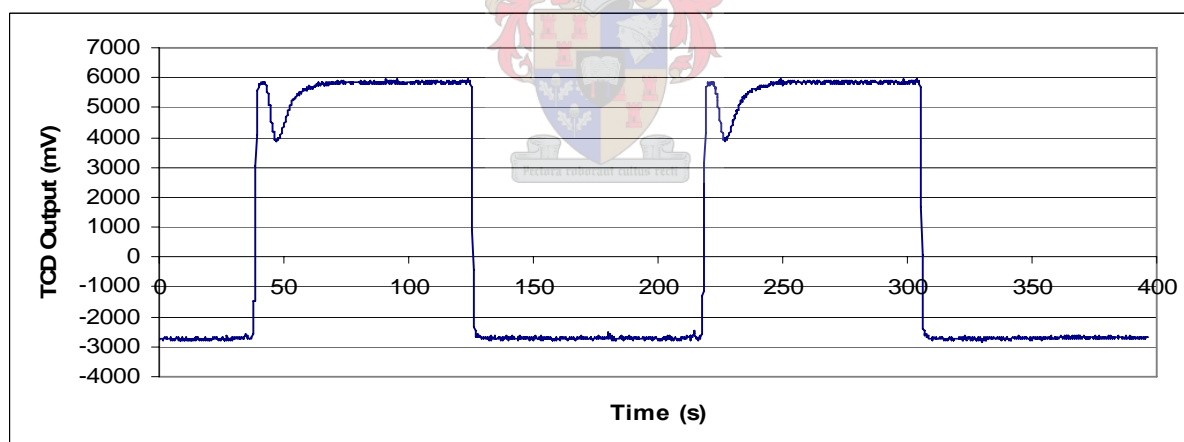


Figure 8-11 TCD output for Propene step input through glass reactor (Flow rate = 75 ml/s; T = 27°C)

## Appendices

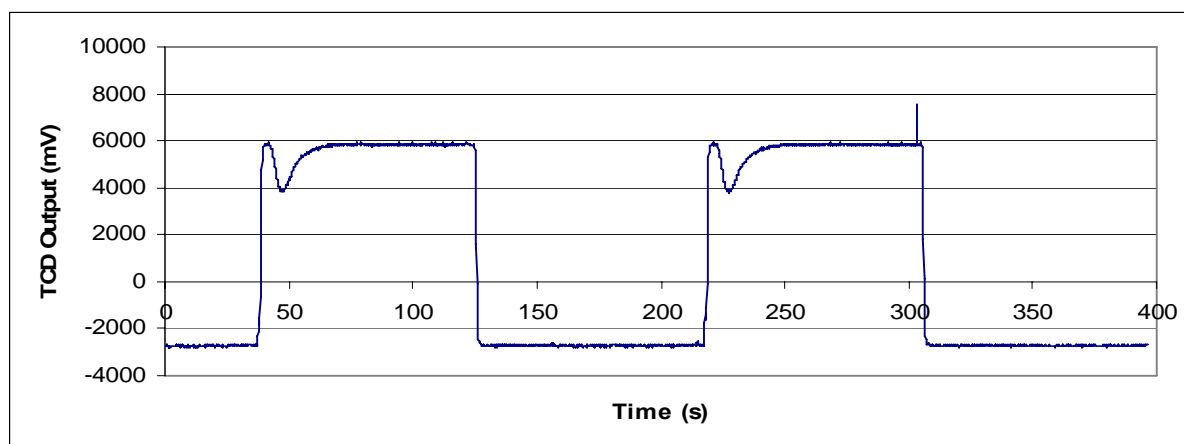


Figure 8-0-12 TCD output for Propene step input through glass reactor (Flow rate = 75 ml/s; T = 400°C)

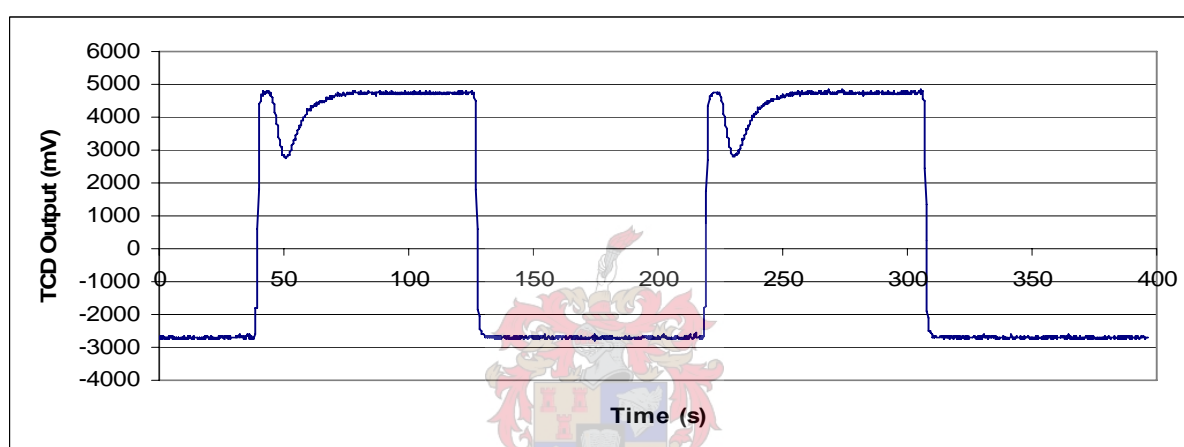


Figure 8-13 TCD output for Propene step input through glass reactor (Flow rate = 60 ml/s; T = 400°C)

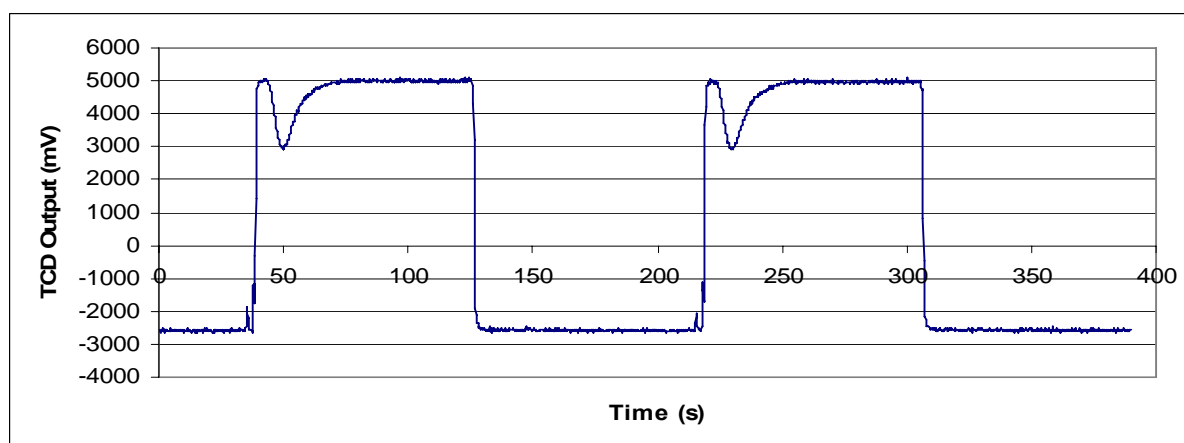


Figure 8-0-14 TCD output for Propene step input without a reactor (Flow rate = 60 ml/s; T = 27°C)

## Appendices

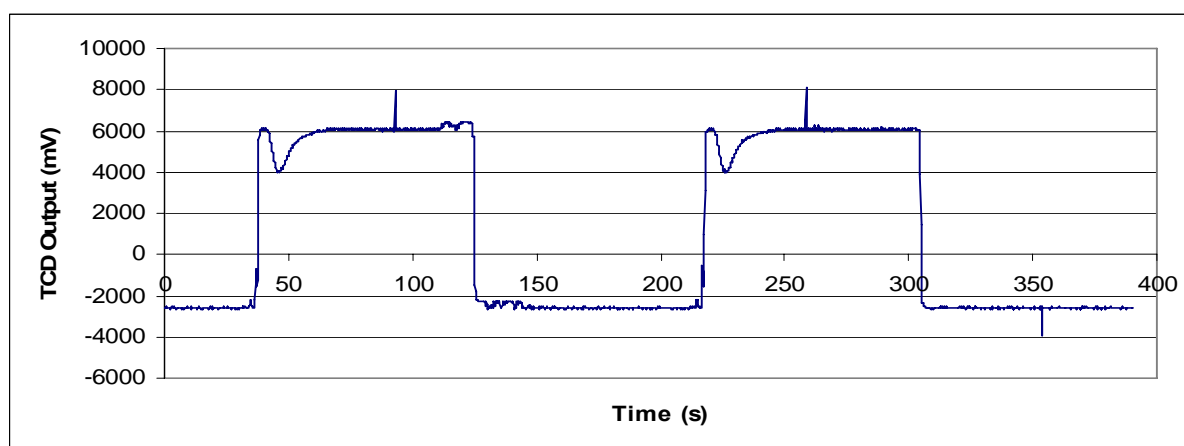
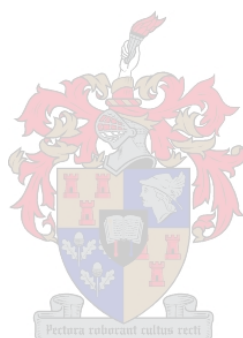


Figure 8-15 TCD output for Propene step input without a reactor (Flow rate = 75 ml/s; T = 27°C)



## Appendix E: Data used for modelling

**Table 8-1 Average propene conversions from experimental data split into three temperature zones before subtraction of homogenous conversions**

WHSV	O/P Ratio	325°C Region	350°C Region	375°C Region
		Propene Conversion	Propene Conversion	Propene Conversion
2	1	9.406	14.203	35.798
2	1,333	10.059	19.254	35.925
2	2	9.865	22.231	36.151
3	1	5.079	12.978	26.310
3	1,333	5.523	13.546	26.600
3	2	6.567	14.747	26.940
5	1	4.277	8.972	19.381
5	1,333	5.361	10.715	18.830
5	2	5.884	10.040	19.616

**Table 8-2 Average rate constants calculated from average rate of propene conversions**

Oxygen/Propene ratio	Average $-r_{\text{propene}}$	m	n	k
-	mmol <sub>propene</sub> /(g <sub>cat</sub> ·min)	-	-	min <sup>-1</sup>
325°C				
1.000	0.042	0	0.22	0.065
1.333	0.047	0	0.22	0.073
2.000	0.060	0	0.22	0.092
1.000	0.063	0	0.22	0.096
1.333	0.068	0	0.22	0.105
2.000	0.066	0	0.22	0.102
1.000	0.053	0	0.22	0.082
1.333	0.075	0	0.22	0.115
2.000	0.085	0	0.22	0.130
350°C				
1.000	0.121	0.5	0.5	0.868
1.333	0.128	0.5	0.5	0.793
2.000	0.142	0.5	0.5	0.720
1.000	0.091	0.5	0.5	0.654
1.333	0.131	0.5	0.5	0.829
2.000	0.154	0.5	0.5	0.803
1.000	0.121	0.5	0.5	0.852
1.333	0.155	0.5	0.5	0.950
2.000	0.141	0.5	0.5	0.706
375°C				
1.000	0.258	1	0.03	1.997
1.333	0.261	1	0.03	1.498
2.000	0.265	1	0.03	1.000
1.000	0.248	1	0.03	1.973
1.333	0.249	1	0.03	1.456
2.000	0.250	1	0.03	0.958
1.000	0.288	1	0.03	2.189
1.333	0.277	1	0.03	1.564
2.000	0.292	1	0.03	1.091

## Appendix F: Fourth-order Runge-Kutta method

The differential equation F-1 can be solved numerically using the fourth order Runge-Kutta method (Equations F-2 to F-6) [Greenberg 1998]:

$$\frac{dy}{dx} = f(x, y) \quad (\text{F-1})$$

$$y_{n+1} = y_n + \frac{1}{6}(k_1 + 2k_2 + 2k_3 + k_4) \quad (\text{F-2})$$

$$k_1 = hf(x_n, y_n) \quad (\text{F-3})$$

$$k_2 = hf\left(x_n + \frac{h}{2}, y_n + \frac{h}{2}k_1\right) \quad (\text{F-4})$$

$$k_3 = hf\left(x_n + \frac{h}{2}, y_n + \frac{h}{2}k_2\right) \quad (\text{F-5})$$

$$k_4 = hf\left(x_{n+1}, y_n + k_3\right) \quad (\text{F-6})$$

With h being the step size



## Appendix G: GC Data of Reaction Runs

Table 8-3 Original FID and TCD GC data of external mass transfer experiments of Table 3-4

Run 26				Run 27			
TCD				TCD			
Sample no.	Time min	Area Propene [%]	Area Ethane [%]	Sample no.	Time min	Area Propene [%]	Area Ethane [%]
1	by pass	20.5	31.6	1	by pass	23.8	29.7
2	5	17	35.5	2	5	21	29.8
3	10	20.6	35	3	10	22.7	30.2
4	20	19.6	33.3	4	20	22.5	30.2
5	40	20.6	35.3	5	40	failed	
6	60	20.1	33.9	6	60	22.5	29.8
7	90	20.9	35	7	90	22.8	31.2

Run 29			
TCD			
Sample no.	Time min	Area Propene [%]	Area Ethane [%]
1	by pass	18.8	38.6
2	5	17.1	38.5
3	10	16.6	37.1
4	45	17.9	40.3
5	60	17.2	38.2
6	90	17.3	39.5

Table 8-4 FID and TCD GC data of internal mass transfer experiments of Table 3-5

Run 30				Run 31			
TCD				TCD			
Sample no.	Time min	Area Propene [%]	Area Ethane [%]	Sample no.	Time min	Area Propene [%]	Area Ethane [%]
1	by pass	18.6	38.7	1	by pass	18.7	38.9
2	10	18.2	40.2	2	10	17.9	39.9
3	40	17.9	39.1	3	40	17.5	40.2
4	60	18.4	40.5	4	60	17.9	39.4
5	90	17.8	39.6	5	90	18.0	40.0

Run 32				Run 33			
TCD				TCD			
Sample no.	Time min	Area Propene [%]	Area Ethane [%]	Sample no.	Time min	Area Propene [%]	Area Ethane [%]
1	by pass	17.9	37.1	1	by pass	18.5	38.2
2	10	17.1	37.8	2	10	17.5	38.7
3	40	17.0	37.5	3	40	17.0	37.9
4	60	17.1	38.3	4	60	17.2	38.1
5	90	17.3	37.8	5	90	17.6	38.8

Appendices

Table 8-5 Original FID and TCD GC data of reaction number 1 in Table 3-6

Run 38

TCD					FID					
Sample no.	Time min	Area Propene [%]	Area Ethane [%]	Area CO2 [%]	Sample no.	Time min	Area Propene [%]	Area Ethane [%]	Area Acro [%]	Area AA [%]
1	By Pass	22.2	35.1		1	By Pass	40.80	58.60		
2	2	23.2	38.9	0.0	2	2	38.80	59.20	1.20	0.10
3	4	22.1	37.2	0.0	3	4	35.20	52.70	0.90	0.10
4	6	20.8	34.9	0.0	4	6	39.10	59.50	1.10	0.10
5	8	22.2	37.3	0.0	5	8	39.10	59.00	1.00	0.10
6	10	21.6	36.0	0.1	6	10	37.20	56.40	1.00	0.10
7	12	21.3	36.3	0.7	7	12	Failed			
8	15	22.5	38.0	0.0	8	15	38.00	57.80	1.10	0.10
9	17	Failed			9	17	39.20	59.80	1.00	0.00
10	20	22.5	37.7	0.0	10	20	39.10	59.70	1.00	0.10
11	35	20.6	34.3	0.1	11	35	38.80	58.80	1.00	0.10
12	45	21.8	36.9	0.0	12	45	39.20	59.40	1.00	0.00
13	60	22.1	36.6	0.0	13	60	38.90	58.70	1.00	0.10
14	90	22.5	37.5	0.0	14	90	39.20	59.30	0.90	0.00

Table 8-6 Original FID and TCD GC data of reaction number 2 in Table 3-6

Run 46

TCD					FID					
Sample no.	Time min	Area Propene [%]	Area Ethane [%]	Area CO2 [%]	Sample no.	Time min	Area Propene [%]	Area Ethane [%]	Area Acro [%]	Area AA [%]
1	By Pass	20.5	32.5		1	By Pass	40.70	59.10		
2	2	18.1	33.6	0.0	2	2	39.10	59.60	1.00	0.00
3	4	18.7	31.8	0.1	3	4	38.70	59.50	1.10	0.10
4	6	17.6	32.3	0.0	4	6	38.40	58.60	1.10	0.10
5	8	19.4	33.7	0.0	5	8	39.10	59.60	1.00	0.10
6	10	19.6	32.7	0.0	6	10	38.70	59.20	1.00	0.10
7	12	19.2	32.6	0.0	7	12	38.90	59.80	1.00	0.10
8	15	18.3	32.9	0.0	8	15	39.10	59.80	0.90	0.00
9	17	19.6	33.4	0.0	9	17	38.90	59.30	1.00	0.10
10	20	19.5	32.8	0.1	10	20	39.00	59.40	1.10	0.20
11	35	16.7	30.4	0.0	11	35	38.90	59.90	0.80	0.10
12	45	19.5	33.2	0.0	12	45	39.10	59.80	1.00	0.00
13	60	19.6	33.6	0.0	13	60	38.80	59.90	1.10	0.10
14	90	18.5	31.5	0.0	14	90	38.70	59.40	1.00	0.10



Appendices

Table 8-7 Original FID and TCD GC data of reaction number 3 in Table 3-6

Run 42

TCD					FID					
Sample no.	Time min	Area Propene [%]	Area Ethane [%]	Area CO2 [%]	Sample no.	Time min	Area Propene [%]	Area Ethane [%]	Area Acro [%]	Area AA [%]
1	By Pass	19.1	31.3		1	By Pass	40.50	58.60		
2	2	16.4	31.7	0.2	2	2	37.90	59.00	1.40	0.10
3	4	18.0	31.0	0.0	3	4	38.80	59.60	1.40	0.10
4	6	17.7	30.5	0.0	4	6	38.50	59.50	1.40	0.10
5	8	17.6	30.6	0.0	5	8	38.50	59.80	1.30	0.10
6	10	16.8	31.9	0.0	6	10	38.40	59.40	1.40	0.10
7	12	17.8	30.6	0.0	7	12	38.60	59.70	1.40	0.10
8	15	17.6	30.3	0.0	8	15	38.50	59.60	1.30	0.10
9	17	17.6	30.5	0.0	9	17	38.50	59.70	1.30	0.10
10	20	18.3	31.3	0.0	10	20	38.90	59.50	1.40	0.10
11	35	17.9	30.8	0.0	11	35	38.50	59.80	1.40	0.10
12	45	Failed			12	45	Failed			
13	60	17.3	30.2	0.0	13	60	38.50	59.90	1.40	0.10
14	90	17.8	31.2	0.0	14	90	38.30	59.60	1.30	0.10

Table 8-8 Original FID and TCD GC data of reaction number 4 in Table 3-6

Run 44

TCD					FID					
Sample no.	Time min	Area Propene [%]	Area Ethane [%]	Area CO2 [%]	Sample no.	Time min	Area Propene [%]	Area Ethane [%]	Area Acro [%]	Area AA [%]
1	By Pass	21.6	34.4		1	By Pass	40.90	58.50		
2	2	18.4	34.4	0.0	2	2	36.20	60.10	3.00	0.20
3	4	19.6	36.6	0.0	3	4	36.30	60.50	2.90	0.20
4	6	18.8	35.2	0.0	4	6	35.90	60.50	3.10	0.30
5	8	18.8	34.9	0.3	5	8	36.60	59.70	3.00	0.00
6	10	19.1	35.5	0.2	6	10	36.10	60.10	3.20	0.10
7	12	19.0	35.4	0.1	7	12	36.30	60.20	3.00	0.20
8	15	18.8	34.7	0.2	8	15	36.40	60.40	2.90	0.10
9	17	19.5	36.2	0.0	9	17	36.40	60.60	2.80	0.00
10	20	19.3	36.0	0.0	10	20	36.10	60.50	3.00	0.10
11	35	18.9	34.8	1.5	11	35	36.40	60.50	2.70	0.20
12	45	19.7	36.0	0.4	12	45	36.80	59.90	2.80	0.20
13	60	19.7	36.0	0.2	13	60	36.90	60.10	2.60	0.10
14	90	19.8	36.4	0.0	14	90	36.40	60.30	2.90	0.10

Appendices

Table 8-9 Original FID and TCD GC data of reaction number 5 in Table 3-6

Run 47

TCD					FID					
Sample no.	Time min	Area Propene [%]	Area Ethane [%]	Area CO2 [%]	Sample no.	Time min	Area Propene [%]	Area Ethane [%]	Area Acro [%]	Area AA [%]
1	By Pass	20.5	32.5		1	By Pass	40.70	59.10		
2	2	17.5	33.4	0.0	2	2	36.00	60.50	3.10	0.10
3	4	17.3	33.2	0.0	3	4	35.60	60.80	2.90	0.30
4	6	Failed			4	6	Failed			
5	8	18.6	34.9	0.0	5	8	35.90	60.70	3.00	0.20
6	10	18.7	35.5	0.0	6	10	35.90	60.80	2.90	0.20
7	12	17.5	35.1	0.0	7	12	35.60	60.80	3.00	0.20
8	15	18.7	35.0	0.0	8	15	36.00	60.90	2.60	0.10
9	17	Failed			9	17	Failed			
10	20	17.7	35.0	0.0	10	20	36.20	60.70	2.90	0.10
11	35	18.1	36.3	0.3	11	35	36.00	60.30	3.00	0.20
12	45	18.6	35.0	0.0	12	45	36.10	60.80	2.80	0.20
13	60	17.0	34.0	0.1	13	60	35.90	60.30	2.80	0.10
14	90	17.6	33.0	0.0	14	90	36.20	60.80	2.70	0.20

Table 8-10 Original FID and TCD GC data of reaction number 6 in Table 3-6

Run 36

TCD					FID					
Sample no.	Time min	Area Propene [%]	Area Ethane [%]	Area CO2 [%]	Sample no.	Time min	Area Propene [%]	Area Ethane [%]	Area Acro [%]	Area AA [%]
1	By Pass	21.0	33.5		1	By Pass	41.00	58.20		
2	2	18.8	34.6	0.0	2	2	36.10	60.30	3.30	0.20
3	4	18.3	34.4	0.4	3	4	36.00	59.90	3.20	0.00
4	6	18.2	34.2	0.4	4	6	35.90	60.00	3.30	0.30
5	8	18.4	34.4	0.0	5	8	36.10	60.20	3.20	0.30
6	10	18.5	34.0	0.4	6	10	36.00	60.10	3.30	0.20
7	12	17.7	33.2	0.4	7	12	35.80	60.00	3.10	0.30
8	15	18.1	33.4	1.3	8	15	36.10	60.20	3.00	0.20
9	17	Failed			9	17	Failed			
10	20	17.7	33.1	0.5	10	20	35.60	60.40	3.00	0.20
11	35	18.9	34.9	0.3	11	35	36.20	60.50	2.90	0.20
12	45	18.3	34.2	0.4	12	45	36.10	60.10	3.00	0.20
13	60	18.0	33.1	0.4	13	60	36.30	60.50	2.90	0.20
14	90	18.6	34.5	1.0	14	90	36.20	60.40	3.10	0.10

Appendices

Table 8-11 Original FID and TCD GC data of reaction number 7 in Table 3-6

Run 43

TCD					FID					
Sample no.	Time min	Area Propene [%]	Area Ethane [%]	Area CO2 [%]	Sample no.	Time min	Area Propene [%]	Area Ethane [%]	Area Acro [%]	Area AA [%]
1	By Pass	20.7	32.9		1	By Pass	40.80	58.70	0.00	0.00
2	2	16.8	36.6	0.7	2	2	31.90	61.70	5.90	0.30
3	4	16.3	35.8	1.1	3	4	31.40	61.90	6.20	0.30
4	6	16.7	36.5	0.2	4	6	30.90	61.50	6.00	0.20
5	8	16.8	37.2	0.9	5	8	31.10	62.30	6.10	0.40
6	10	Failed			6	10	Failed			
7	12	16.1	35.9	1.0	7	12	31.10	62.00	6.20	0.30
8	15	16.1	35.8	0.7	8	15	31.40	61.70	6.10	0.30
9	17	16.4	35.7	1.9	9	17	31.30	61.80	6.10	0.30
10	20	15.1	33.8	0.7	10	20	31.60	61.60	6.10	0.20
11	35	17.1	37.0	0.9	11	35	31.70	61.80	6.00	0.30
12	45	16.3	35.3	0.8	12	45	31.70	61.40	6.00	0.30
13	60	16.4	36.5	0.9	13	60	31.50	62.00	6.00	0.20
14	90	16.4	35.9	1.9	14	90	31.60	61.80	5.90	0.30

Table 8-12 Original FID and TCD GC data of reaction number 8 in Table 3-6

Run 45

TCD					FID					
Sample no.	Time min	Area Propene [%]	Area Ethane [%]	Area CO2 [%]	Sample no.	Time min	Area Propene [%]	Area Ethane [%]	Area Acro [%]	Area AA [%]
1	By Pass	20.7	33.1		1	By Pass	40.70	58.60		
2	2	15.7	34.8	1.0	2	2	31.80	62.00	5.60	0.30
3	4	16.1	35.3	1.2	3	4	31.60	62.70	4.30	0.20
4	6	14.9	35.2	0.7	4	6	31.30	61.10	5.90	0.20
5	8	15.6	34.1	0.5	5	8	31.50	61.90	5.80	0.30
6	10	16.4	36.7	1.0	6	10	31.50	62.40	5.80	0.20
7	12	15.8	35.0	0.9	7	12	31.10	61.80	5.60	0.50
8	15	16.4	36.4	0.9	8	15	31.50	62.20	5.70	0.30
9	17	15.3	36.5	1.0	9	17	31.30	62.40	5.70	0.30
10	20	16.3	36.1	0.8	10	20	31.90	61.90	5.80	0.20
11	35	15.8	35.9	0.7	11	35	26.80	53.40	4.80	0.40
12	45	16.5	35.8	1.1	12	45	31.80	61.80	5.80	0.30
13	60	16.1	34.7	0.9	13	60	31.70	61.30	5.30	0.30
14	90	15.4	34.5	1.0	14	90	31.30	61.90	5.80	0.20

Appendices

Table 8-13 Original FID and TCD GC data of reaction number 9 in Table 3-6

Run 37

TCD					FID					
Sample no.	Time min	Area Propene [%]	Area Ethane [%]	Area CO2 [%]	Sample no.	Time min	Area Propene [%]	Area Ethane [%]	Area Acro [%]	Area AA [%]
1	By Pass	21.9	33.7		1	By Pass	41.40	58.20		
2	2	15.0	32.4	1.3	2	2	31.80	61.80	5.80	0.40
3	4	16.2	35.8	1.6	3	4	31.40	61.90	6.00	0.40
4	6	Failed			4	6	Failed			
5	8	17.0	37.6	1.3	5	8	31.40	62.30	5.90	0.30
6	10	15.6	36.6	1.2	6	10	31.30	61.60	6.10	0.30
7	12	16.4	36.1	1.4	7	12	31.50	61.90	5.90	0.30
8	15	17.0	37.3	1.5	8	15	31.50	61.90	5.90	0.40
9	17	16.6	36.4	1.5	9	17	31.50	62.10	5.80	0.30
10	20	17.4	37.0	1.3	10	20	31.40	61.80	5.90	0.30
11	35	16.4	35.3	1.3	11	35	32.10	61.50	5.40	0.30
12	45	16.4	35.8	1.4	12	45	32.30	61.80	5.50	0.30
13	60	16.2	35.4	1.3	13	60	31.90	62.10	5.70	0.30
14	90	16.5	35.8	1.3	14	90	31.90	61.90	5.70	0.30

Table 8-0-14 Original FID and TCD GC data of reaction number 1 in Table 3-7

Run 51

TCD					FID					
Sample no.	Time min	Area Propene [%]	Area Ethane [%]	Area CO2 [%]	Sample no.	Time min	Area Propene [%]	Area Ethane [%]	Area Acro [%]	Area AA [%]
1	By Pass	20.0	31.9		1	By Pass	40.9	58.7		
2	30	18.8	33.4	0.0	2	30	37.7	59.8	2.0	0.1
3	35	18.7	33.9	0.0	3	35	37.6	60.1	2.0	0.2
4	30	20.5	36.6	0.2	4	30	37.4	60.1	2.0	0.2
5	35	19.9	36.3	0.0	5	35	37.8	59.9	2.0	0.1
6	30	20.0	37.4	0.0	6	30	38.0	60.2	1.6	0.1
7	35	Failed			7	35	Failed			

Table 8-15 Original FID and TCD GC data of reaction number 2 in Table 3-7

Run 54

TCD					FID					
Sample no.	Time min	Area Propene [%]	Area Ethane [%]	Area CO2 [%]	Sample no.	Time min	Area Propene [%]	Area Ethane [%]	Area Acro [%]	Area AA [%]
1	By Pass	20.9	33.4		1	By Pass	40.9	58.8		
2	30	19.8	33.5	0.0	2	30	39.0	59.5	1.0	0.1
3	35	19.8	33.5	0.0	3	35	39.1	59.8	0.9	0.1
4	30	20.2	36	0.0	4	30	39.4	59.8	0.8	0.0
5	35	21.8	36.3	0.0	5	35	39.2	59.6	0.9	0.1
6	30	22.4	37.2	0.0	6	30	39.4	59.5	0.7	0.1
7	35	22.5	37.5	0.0	7	35	39.7	59.3	0.7	0.1

Appendices

Table 8-16 Original FID and TCD GC data of reaction number 3 in Table 3-7

Run 50

TCD					FID					
Sample no.	Time min	Area Propene [%]	Area Ethane [%]	Area CO2 [%]	Sample no.	Time min	Area Propene [%]	Area Ethane [%]	Area Acro [%]	Area AA [%]
1	By Pass	20.7	33.0		1	By Pass	40.6	59.1		
2	30	14.5	30.5	0.2	2	30	32.9	62.1	4.6	0.3
3	35	15.3	31.5	0.3	3	35	33.4	62.0	4.2	0.3
4	30	16.7	34.3	0.0	4	30	33.5	62.0	4.3	0.2
5	35	17.3	33.9	0.5	5	35	34.6	60.8	4.2	0.2
6	30	18.6	34.7	0.1	6	30	35.6	60.4	3.6	0.2
7	35	16.4	32.9	0.0	7	35	35.6	60.4	3.8	0.1

Table 8-17 Original FID and TCD GC data of reaction number 4 in Table 3-7

Run 55

TCD					FID					
Sample no.	Time min	Area Propene [%]	Area Ethane [%]	Area CO2 [%]	Sample no.	Time min	Area Propene [%]	Area Ethane [%]	Area Acro [%]	Area AA [%]
1	By Pass	20.8	33.1		1	By Pass	40.8	59.0		
2	30	18.0	33.5	0.0	2	30	37.5	60.3	1.8	0.1
3	35	18.8	33.3	0.4	3	35	37.4	60.1	1.9	0.1
4	30	18.9	35.1	0.3	4	30	37.2	60.2	2.1	0.1
5	35	19.6	34.9	0.4	5	35	37.2	60.3	2.0	0.1
6	30	21.0	36.6	0.1	6	30	37.8	59.9	1.8	0.1
7	35	19.9	36.1	0.3	7	35	37.8	60.2	1.8	0.1

Table 8-18 Original FID and TCD GC data of reaction number 5 in Table 3-7

Run 52

TCD					FID					
Sample no.	Time min	Area Propene [%]	Area Ethane [%]	Area CO2 [%]	Sample no.	Time min	Area Propene [%]	Area Ethane [%]	Area Acro [%]	Area AA [%]
1	By Pass	20.6	32.8		1	By Pass	40.9	59.0		
2	30	15.0	38.0	1.6	2	30	28.1	63.8	7.5	0.4
3	35	14.8	38.0	1.8	3	35	28.2	63.4	7.5	0.5
4	30	15.4	38.4	3.2	4	30	27.6	62.1	7.8	0.3
5	35	15.4	39.0	1.6	5	35	28.1	63.3	8.1	0.3
6	30	15.7	41.9	1.2	6	30	28.2	63.1	8.2	0.3
7	35	16.3	40.8	1.7	7	35	28.1	63.4	8.0	0.3

Appendices

Table 8-19 Original FID and TCD GC data of reaction number 6 in Table 3-7

Run 53

TCD					FID					
Sample no.	Time min	Area Propene [%]	Area Ethane [%]	Area CO2 [%]	Sample no.	Time min	Area Propene [%]	Area Ethane [%]	Area Acro [%]	Area AA [%]
1	By Pass	21.7	35.1		1	By Pass	40.7	59.1		
2	30	17.7	35.4	1.2	2	30	34.1	61.4	3.8	0.2
3	35	18.3	36.1	1.3	3	35	34.1	61.8	3.8	0.2
4	30	19.9	39.4	1.0	4	30	34.4	61.5	3.7	0.2
5	35	19.7	37.9	1.2	5	35	34.3	61.4	3.9	0.2
6	30	19.2	38.3	1.1	6	30	Failed			
7	35	19.7	38.9	1.1	7	35	34.2	61.6	3.9	0.2

Table 8-20 Original FID and TCD GC data of reproduced reaction

Run 49

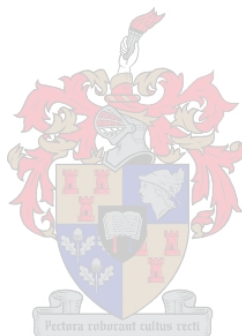
TCD					FID					
Sample no.	Time min	Area Propene [%]	Area Ethane [%]	Area CO2 [%]	Sample no.	Time min	Area Propene [%]	Area Ethane [%]	Area Acro [%]	Area AA [%]
1	By pass	20.9	36.1		1	By Pass	40.7	58.9		
2	6	17.8	34.0	0.0	2	6	35.9	60.8	2.9	0.2
3	20	18.4	34.7	0.0	3	20	36.2	60.9	2.7	0.1
4	45	17.8	35.2	0.3	4	45	35.3	61	3.1	0.2
5	60	18.2	34.5	0.0	5	60	36.1	60.7	2.8	0.1
6	90	17.3	32.8	0.2	6	90	35.7	60.6	3	0.2

Run 48

TCD					FID					
Sample no.	Time min	Area Propene [%]	Area Ethane [%]	Area CO2 [%]	Sample no.	Time min	Area Propene [%]	Area Ethane [%]	Area Acro [%]	Area AA [%]
1	By pass	20.9	33.8		1	By pass	39.5	57.8		
2	6	15.7	32.3	0	2	6	35.4	61.1	3.1	0.2
3	20	18.3	35.5	0	3	20	35.2	60	2.9	0.1
4	45	17.4	35.4	0	4	45	33.2	57	2.8	0.1
5	60	17.4	35.1	0.5	5	60	35.6	61	3	0.2
6	90	18.9	34.8	0.1	6	90	36.1	60.3	2.9	0.2

## Appendix H: Nomenclature

A	Preexponential factor of Arrhenius plot	mmol/(min.bar <sup>x</sup> )
C <sub>reactant</sub>	Concentration of reactant	mol/dm <sup>3</sup>
DAB	Diffusivity	dm <sup>2</sup> /s
E <sub>a</sub>	Activation energy	J/mol
f <sub>o,i</sub>	Area correction factor for organic compound i	
F <sub>P,0</sub>	Propene feed flow rate	mmol/min
K <sub>A</sub> -K <sub>1</sub>	General temperature dependant constants for different reaction models	
K <sub>1</sub> -K <sub>5</sub>	Reaction equilibrium constants	
k	Rate constant for power rate law	mmol/(min.bar <sup>x</sup> )
k <sub>O</sub>	Rate constant for oxygen conversion	mmol/(min.bar <sup>x</sup> )
k <sub>P</sub>	Rate constant for propene conversion	mmol/(min.bar <sup>x</sup> )
k <sub>1</sub> -k <sub>6</sub>	Rate constants for different reaction steps during the partial oxidation reaction	
m	Oxygen reaction order	
N <sub>ci</sub>	Number of carbon in molecule	
N <sub>C(O)</sub>	Number of carbon connected to 1 oxygen with 1 single bond	
N <sub>C(No O)</sub>	Number of carbon not connected to oxygen	
n	Propene reaction order	
n <sub>acrolein</sub>	Mol of acrolein	mol
n <sub>ethane</sub>	Mol of ethane	mol
n <sub>propene</sub>	Mol of propene	mol
n <sub>H<sub>2</sub>O</sub>	Mol of water	mol
n <sub>O<sub>2</sub></sub>	Mol of Oxygen	mol
P <sub>O<sub>2</sub></sub>	Oxygen partial pressure	bar
P <sub>P</sub>	Propene partial pressure	bar
P <sub>P,0</sub>	Propene feed partial pressure	bar
P <sub>Total</sub>	Total pressure	bar
Pe <sub>r</sub>	Peclet number	
R	Universal gas constant	8,314 J/(mol.K)
r <sub>O<sub>2</sub></sub>	Rate of oxygen consumption	mmol/min
r <sub>P</sub>	Rate of propene consumption	mmol/min
s	Least squares	
T	Temperature	K
t <sub>m</sub>	Mean residence time	s
W	Mass of catalyst	g
W <sub>reactant</sub>	Molar flux of reactant	mol/(dm <sup>2</sup> .s)
X	Propene conversion	
z	Boundary layer thickness	dm
	β	Stoichiometric factor
	δ <sup>2</sup>	Variance
	θ	Fraction of oxidized surface sites
	θ <sub>O<sub>2</sub></sub>	Oxygen to propene feed ratio



## Appendix I: List of Abbreviations

BET	Brunauer, Emmett and Teller
FID	Flame ionization detector
GC	Gas chromatograph
RSF	Response factor
RTD	Residence time distribution
TCD	Thermal conductivity detector
WHSV	Weight hourly space velocity, $\text{g}_{\text{Propene}}/(\text{g}_{\text{Cat}} \cdot \text{h})$
XRD	X-ray diffraction

